Leibniz Association

LEIBNIZ RESEARCH CENTRE FOR WORKING ENVIRONMENT AND HUMAN FACTORS

Transcriptomics-based developmental toxicity and cardiotoxicity assessment using induced pluripotent stem cells

Dissertation

zur Erlangung des akademischen Grades des Doktors der Naturwissenschaften (Dr. rer. nat.) an der Fakultät für Chemie und Chemische Biologie der Technischen Universität Dortmund

vorgelegt von
Anna Cherianidou, M.Sc.

Dortmund, Juni 2023

1. Gutachter: Prof. Dr. Jan G. Hengstler
2. Gutachter: Prof. Dr. Agapios Sachinidis

Eidesstattliche Versicherung (Affidavit)

Cherianidou, Anna
Name, Vorname
(Surname, first name)

208552
Matrikel-Nr.
(Enrolment number)

Belehrung:

Wer vorsätzlich gegen eine die Täuschung über Prüfungsleistungen betreffende Regelung einer Hochschulprüfungsordnung verstößt, handelt ordnungswidrig. Die Ordnungswidrigkeit kann mit einer Geldbuße von bis zu 50.000,00 € geahndet werden. Zuständige Verwaltungsbehörde für die Verfolgung und Ahndung von Ordnungswidrigkeiten ist der Kanzler/die Kanzlerin der Technischen Universität Dortmund. Im Falle eines mehrfachen oder sonstigen schwerwiegenden Täuschungsversuches kann der Prüfling zudem exmatrikuliert werden, § 63 Abs. 5 Hochschulgesetz NRW.

Die Abgabe einer falschen Versicherung an Eides statt ist strafbar.

Wer vorsätzlich eine falsche Versicherung an Eides statt abgibt, kann mit einer Freiheitsstrafe bis zu drei Jahren oder mit Geldstrafe bestraft werden, § 156 StGB. Die fahrlässige Abgabe einer falschen Versicherung an Eides statt kann mit einer Freiheitsstrafe bis zu einem Jahr oder Geldstrafe bestraft werden, § 161 StGB.

Die oben stehende Belehrung habe ich zur Kenntnis genommen:

Official notification:

Any person who intentionally breaches any regulation of university examination regulations relating to deception in examination performance is acting improperly. This offence can be punished with a fine of up to EUR 50,000.00. The competent administrative authority for the pursuit and prosecution of offences of this type is the chancellor of the TU Dortmund University. In the case of multiple or other serious attempts at deception, the candidate can also be unenrolled, Section 63, paragraph 5 of the Universities Act of North Rhine-Westphalia.

The submission of a false affidavit is punishable.

Any person who intentionally submits a false affidavit can be punished with a prison sentence of up to three years or a fine, Section 156 of the Criminal Code. The negligent submission of a false affidavit can be punished with a prison sentence of up to one year or a fine, Section 161 of the Criminal Code.

I have taken note of the above official notification.

Dortmund, 29.06.2023
Ort, Datum
(Place, date)

Unterschrift
(Signature)

Titel der Dissertation:
(Title of the thesis):

Transcriptomics-based developmental toxicity and cardiotoxicity assessment using induced pluripotent stem cells

Ich versichere hiermit an Eides statt, dass ich die vorliegende Dissertation mit dem Titel selbstständig und ohne unzulässige fremde Hilfe angefertigt habe. Ich habe keine anderen als die angegebenen Quellen und Hilfsmittel benutzt sowie wörtliche und sinngemäße Zitate kenntlich gemacht.
Die Arbeit hat in gegenwärtiger oder in einer anderen Fassung weder der TU Dortmund noch einer anderen Hochschule im Zusammenhang mit einer staatlichen oder akademischen Prüfung vorgelegen.

I hereby swear that I have completed the present dissertation independently and without inadmissible external support. I have not used any sources or tools other than those indicated and have identified literal and analogous quotations.

The thesis in its current version or another version has not been presented to the TU Dortmund University or another university in connection with a state or academic examination.*

*Please be aware that solely the German version of the affidavit ("Eidesstattliche Versicherung") for the PhD thesis is the official and legally binding version.

Dortmund, 29.06.2023
Ort, Datum
(Place, date)

Unterschrift
(Signature)

Contents

Summary

Developmental toxicity is a major concern in the field of toxicology, requiring the development of in vitro tests that can effectively identify substances with developmental toxic effects in relation to human exposure. In this regard, the present PhD study established the hiPSC-based in vitro test. Traditional approaches to assessing embryotoxicity have relied on animal studies, which are often complex, expensive, and time-consuming. Furthermore, the results may not directly apply to humans due to species differences.

In this doctoral research, an innovative approach was pursued to overcome these challenges by developing a novel in vitro test system capable of evaluating both developmental teratogenicity and cardiotoxicity. The UKK2 protocol, in combination with human induced pluripotent stem cells (hiPSCs), transcriptomics, and an accurately selected panel of substances based on their in vivo concentrations, was employed. Specifically, this thesis investigated the differentiation of hiPSCs into various germ layers and subsequently into cardiomyocytes, both in the presence and absence of different substances known to have embryotoxic effects. Additionally, gene expression analyses were conducted using isolated RNA, utilizing whole-genome microarrays to identify distinctive gene signatures associated with early embryotoxicity or cardiotoxicity.

In the initial phase of the thesis, the effectiveness of the UKK2 test system was assessed in the presence and absence of 23 teratogens and 16 non-teratogens at both the maximal plasma concentration (C_{max}) and the 20-fold C_{max} concentration. Following a 24-hour incubation period for germ layer induction along with the test compounds, the analysis focused on examining total RNA using whole-genome transcriptome microarrays. A classifier was established by considering the 1000 probe sets (PS) that exhibited the highest variability across all samples and evaluating the cytotoxic effects associated with different compounds. This classifier demonstrated a high level of accuracy, ranging between 90% to 92%, enabling the prediction of teratogens using the UKK2 test systems.

In the subsequent phase of this thesis, an extension of the UKK2 protocol, known as UKK-CTT, was employed to evaluate developmental cardiotoxicity. Utilizing Isotretinoin as a -gold standard- due to its complete inhibition of cardiac differentiation, a gene signature was identified and established using transcriptomics data to predict the inhibitory potential of teratogens and non-teratogens in the cardiomyogenesis process. Furthermore, the ”Developmental Cardiotoxicity Index” (CDI31g) was established, effectively distinguishing between compounds that do or do not impact the differentiation of hiPSCs into functional cardiomyocytes. To enhance the prediction of UKK-CTT, a phenotypical anchoring point was incorporated into the test system, including assessing α-cardiac actinin 2 structure and the pattern of cardiomyocyte beating.

The future of human-based in vitro models for developmental toxicity screening appears promising, as the

studies demonstrated thus far. These models have shown potential in the preclinical phase of drug testing and improving human teratogenicity prediction. Advancements in hPSC-based models, such as incorporating tissue morphogenesis and refining organoid models, will contribute to more accurate assessments of drug-induced developmental toxicity. The development and application of the UKK2 test system and UKK-CTT in hPSC-based models have provided valuable insights into drug-induced developmental toxicity during cardiac organogenesis. These insights improve our understanding of critical embryonic development phases and lay the groundwork for targeted interventions and enhanced drug safety during these vulnerable periods.

Zusammenfassung

Die Embryo-Entwicklungstoxizität ist ein wichtiges Anliegen der Toxikologie. Es erfordert die Entwicklung von In-vitro-Tests, mit denen embryotoxische Substanzen nach Exposition des Menschen sich identifizieren lassen. Herkömmliche Ansätze zur Bewertung der Embryotoxizität stützen sich auf Tierversuche, die oft sehr komplex, teuer und zeitaufwändig sind. Darüber hinaus sind möglicherweise aufgrund von Speziesunterschieden nicht alle Befunde direkt auf den Menschen übertragbar.

Um diese Herausforderungen zu überwinden wurde im Rahmen der vorliegenden Doktorarbeit ein neuartiges In-vitro-Testsystem entwickelt, wodurch eine sowohl eine potenzielle Embryotoxizität als auch eine Kardiotoxizität bewertet werden können. Das sogenannte –Universitätsklinikum Köln (UKK)2-Testsystem wurde mittels humaner induzierten pluripotenten Stammzellen (hiPSCs), Transkriptom-Analysen und mittels einer Reihe von ausgewählten Substanzen entwickelt. Die teratogene und nicht teratogene Substanzen wurden in Konzentrationen eingesetzt, welche die in vivo-Konzentrationen entsprachen. Für diesen Zweck wurde eine gezielte Differenzierung von hiPSCs in verschiedene Keimblättern und anschließend in Kardiomyozyten sowohl in Gegenwart als auch in Abwesenheit von verschiedenen Substanzen mit und ohne nachgewiesener embryotoxischer Wirkung durchgeführt. Darüber hinaus wurden Genexpressionsanalysen mit isolierter RNA unter Verwendung von DNA-Microarrays durchgeführt, um charakteristisch für Embryotoxizität oder Kardiotoxizität Gensignaturen zu identifizieren.

In der ersten Phase der Arbeit wurde die Wirksamkeit des UKK2-Testsystems in Gegenwart und Abwesenheit von 23 Teratogenen- und 16 Nicht-Teratogenen-Substanzen sowohl bei der maximalen Plasmakonzentration (C_{max}) als auch bei der 20-fachen C_{max}-Konzentration untersucht. Nach einer 24-stündigen Inkubationszeit erfolgte die Induktion der Keimblätter, da die Analyse der Gesamt-RNA mittels der DNA-Mikroarrays zu Nachwies von spezifischen Keimblätter-Gensignaturen zeigte. Unter Berücksichtigung der
1000 differentiell exprimierten Genen, die in allen Proben die größte Variabilität aufwiesen, und unter Berücksichtigung der zytotoxischen Wirkungen der verschiedenen Verbindungen wurde ein prädiktiver Klassifikator erstellt. Dieser Klassifikator zeigte eine hohe Genauigkeit, die zwischen 90% und 92% lag, und dadurch ermöglichte er die Vorhersage von Teratogenen- und Nicht-Teratogenen Substanzen.

Als nächstes wurde das UKK2-Testsystem zu dem sogenannten UKK-Kardiotoxizitätstest (UKK-CTT) zur Testung der Substanzen entwickelt, welche den Prozess der Kardiomyogenese hemmen. Unter Verwendung von Isotretinoin als –Goldstandard-, welches die Differenzierung von hiPSCs zu Kardiomyozyten (Kardiomyogenese) vollständig hemmte, wurde eine Gensignatur mit Hilfe von Transkriptomanalysen identifiziert, welche geeignet ist Teratogene von Nicht-Teratogenen-Substanzen zu unterscheiden. darüber hinaus wurde der ”Developmental Cardiotoxicity Index” (CDI31g) erstellt, wodurch effektiv zwischen Substanzen unterschieden werden

kann, die den Prozess der Kardiomyogenese in differenzierten hiPSCs beeinträchtigen. Um die Vorhersage von UKK-CTT zu verbessern, wurde ein phänotypischer Ankerpunkt in das Testsystem etabliert, der die kardialen Aktinfilamente-Struktur und die schlagende Aktivität der Kardiomyozyten berücksichtigt.

Die Befunde meiner Dissertation zeigen, dass die human-relevanten hiPSC-basierten in-vitro-Testsysteme für das Screening von Substanzen in der präklinischen Phase der Arzneimittelentwiklung vielversprechend sind, um embryotoxische Substanzen/Pharmaka beim Menschen nachzuweisen. Die Entwicklung und Anwendung des UKK2-Testsystems und des UKK-CTT mittels von hiPSC-basierten. Modellen führten zu wertvollen Erkenntnisse in Bezug auf die Mechanismen der Entwicklungstoxizität und Kardiotoxizität. Diese Erkenntnisse bilden eine solide Grundlage für eine sichere Arzneimittelentwicklung in der präklinischen Phase.

Abbreviations & units

µg	microgram
µL, mL, L	microliter, millilitre, litre
µM, mM	micromolar, milimolar
AUC	Area Under Curve
BMP	Bone Morphogenic Protein
cDNA	complementary Deoxyribonucleic Acid
C_{max}	Therapeutic plasma/blood concentration
CMMC	Center for Molecular Medicine Cologne
CMs	Cardiomyocytes
CO_2	Carbon dioxide
cRNA	Complementary Ribonucleic Acid
Ct	Cycle threshold
DHODH	Dihydroorotate Dehydrogenase
Di	Developmental index
DMEM	Dulbecco's Modified Eagle Medium: Nutrient mixture
DMSO	Dimethyl Sulfoxide
DNA	Deoxyribonucleic Acid
DNase	Deoxyribonuclease
DoD	Day of Differentiation
Dp	Developmental potency
DPBS	Dulbecco's Phosphate-Buffered Saline
EBs	Embryoid Bodies
ECVAM	European Centre for the Validation of Alternative Methods
eGFP	enhanced Green Fluorescent Protein
FC	Fold-Change
FDA	Food and Drug Administration
FDR	False Discovery Rate
FN	False Negative
FP	False Positive
fRMA	frozen Robust Multiarray Analysis
g	gravity (a unit for centrifugation)
GAPDH	Glyceraldehyde 3-Phosphate Dehydrogenase

GO	Gene Ontology
GSK3	Glycogen synthase kinase 3
h	hours
HDACi	Histone Deacetylase inhibitor
hESC	human Embryonic Stem Cell
hiPSC	human induced Pluripotent Stem Cell
hPSC-CMs	human Pluripotent Stem Cells-derived Cardiomyocytes
hPSCs	human Pluripotent Stem Cells
ICH	International Council of Harmonization
iPSC	Induced Pluripotent Stem Cell
IVT	In Vitro Transcription
KEGG	Kyoto Encyclopedia of Genes and Genomes
LOOCV	Leave-One-Out-Cross-Validation
mEST	mouse Embryonic Stem Cell Test
min	minute
miRNA	micro Ribonucleic Acid
mRNA	messenger Ribonucleic Acid
N2 tank	Nitrogen tank
OECD	Economic Co-operation and Development
PCA	Principal Component Analysis
PCR	Poly Chain Reaction
PPPC	Predicted Probability for Positive Class
qRT-PCR	quantitative Real Time Polymerase Chain Reaction
RAR	Retinoic Acid Receptor
RNA	Ribonucleic Acid
RNase	Ribonuclease
ROCKi	Rho-Kinase inhibitor
ROS	Reactive Oxygen-Species
rpm	rounds per minute
RT	Reverse Transcription
rt	room temperature
RXR	Retinoid X Receptor
SD	Standard Deviation
sec	seconds
SEM	Standard Error of Mean
SPS	Significant Probe Set
TGA	Therapeutic Goods Administration
TN	True Negative
TP	True Positive

Publication in this thesis

1) Cherianidou A, Seidel F, Kappenberg F, Dreser N, Blum J, Waldmann T, Blüthgen N, Meisig J, Madjar K, Henry M, Rotshteyn T, Marchan R, Edlund K, Leist M, Rahnenführer J, Sachinidis A, Hengstler JG. **Classification of Developmental Toxicants in a Human iPSC Transcriptomics-Based Test. Chem Res Toxicol.** 2022 May 16;35(5):760-773. doi: 10.1021/acs. chemrestox.1c00392. Epub 2022 Apr 13. PMID: 35416653; PMCID: PMC9377669.

Cited in this thesis on page no.: 21-22, 40-44, 63, 67-69

1 Introduction

1.1 Developmental toxicity & teratogenicity

In the past century, causes of congenital malformations were attributed to genetic or infectious causes. However, the tragic thalidomide incident in the late 1950s and early 1960s brought attention to xenobiotics, or foreign substances that could also cause birth defects. This incident raised awareness among the scientific community and the general public regarding the potential risks of exposing developing embryos to external substances [1]. Further epidemiological studies confirmed that in-utero exposure to various xenobiotics, including drugs, environmental contaminants, metabolic byproducts, and metals, can lead to teratogenesis. As a result, a growing need exists to advance our understanding of the underlying mechanisms involved in normal and abnormal development in toxicologic pathology [2, 3].

Developmental toxicity includes a wide array of negative consequences on the embryo's normal development, occurring both prenatally and postnatally. These effects can be attributed to parental drug exposure before conception, during pregnancy, or until sexual maturity. The outcomes of developmental toxicity consist of early embryonic mortality, structural anomalies, impaired growth, and functional deficits [4].

Teratogenicity is the field of study that focuses on the development of congenital malformations. The term originates from the Greek word "teras," meaning "monster," historically used to describe babies born with severe malformations and considered omens. A teratogen is an agent that can disrupt the development of the embryo or fetus. Teratogens can be categorized as physical agents, metabolic conditions, maternal infections, chemicals, and drugs. Significant milestones in the history of teratogenicity include the induction of embryonic lethality in cats through X-rays in 1905 and the observation of limb disorders in pigs caused by a lipid diet in 1921. Crucial data regarding human teratogenicity emerged at different periods. For instance, microcephaly induced by X-rays was reported in 1929, virus-induced malformations in 1941, drug-induced malformations (such as aminopterin) in 1952, environmental chemical-induced malformations (such as methylmercury) in 1959, and thalidomide-induced human malformations in 1961[5].

Various environmental chemicals, drugs, and infectious agents are known to cause teratogenic effects. Maternal infections, including Toxoplasma gondii, Treponema pallidum, Rubella, Cytome-

galovirus, and Herpes simplex, can lead to spontaneous abortions or fetal congenital malformations such as hearing loss, brain damage, necrotic eye damage, heart defects, and an increased risk of developing type I diabetes [6]. Teratogenic drugs can be further classified into categories such as anticonvulsants (valproic acid, phenytoin, trimethadione, carbamazepine), ACE inhibitors (benazepril, captopril, enalapril, fosinopril, lisinopril, quinapril, ramipril), antibiotics (tetracycline, doxycycline, streptomycin), antidepressants (lithium chloride), anticancer drugs (methotrexate, aminopterin), and others (diethylstilbestrol, thalidomide, alcohol, isotretinoin).

During pregnancy, the fetus goes through three distinct stages: blastocyst formation (0 to 16 days of gestation), organogenesis (17 to 60 days), histogenesis and functional maturation (61 days until full term) [7]. Exposure to teratogens during the organogenesis stage can lead to structural malformations. It has been observed that there are specific sensitive time windows during which exposure to teratogens can result in particular malformations. The most critical period for developing significant morphological abnormalities is between the 3rd and 8th weeks of pregnancy (**Figure 1**). Exposure to teratogens after the 8th week of pregnancy is more likely to cause minor morphological abnormalities but remains sensitive to functional anomalies associated with the central nervous system.

During the first two weeks of pregnancy, the response to teratogens follows an ”all or none” pattern, meaning it either leads to embryo death or has no effect. Exposure to teratogens during the embryonic period (3 to 8 weeks of pregnancy) is responsible for developing congenital malformations. Moreover, specific windows within the embryonic period are susceptible to teratogens and are associated with specific malformations.

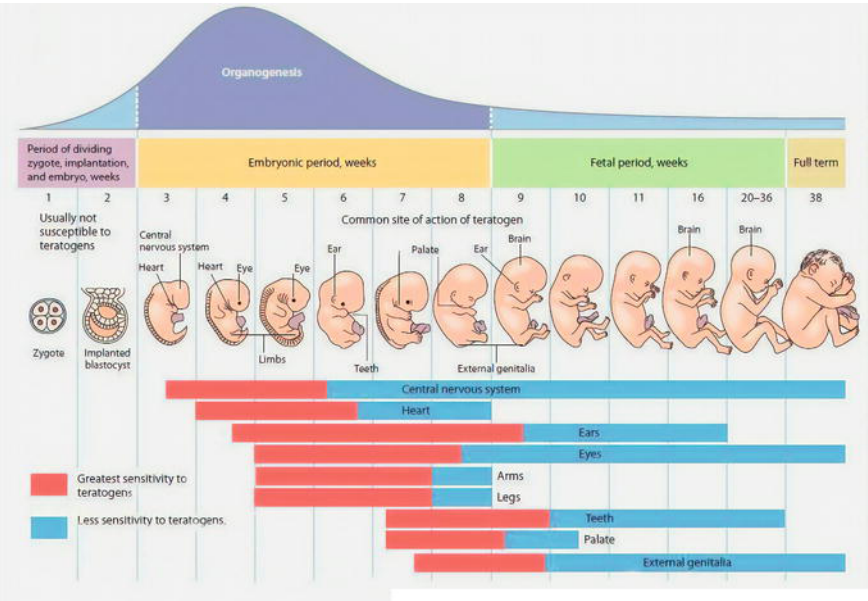

Figure 1: Summary of human embryonic development and the critical period during which teratogens are most likely to cause teratogenic effects. Source [8].

A prominent example demonstrating the sensitive window in humans is exposure to thalidomide. Depending on the time period of exposure during pregnancy, thalidomide can lead to different types of abnormalities. Exposure during the first 20 days of pregnancy results in external ear defects, exposure during 21 to 28 days leads to thumb hypoplasia, exposure during 24 to 31 days causes upper limb defects, exposure during 27 to 33 days results in lower limb defects, and direction during 32 to 36 days of pregnancy leads to triphalangism [9]. This illustrates that the timing of teratogen exposure during pregnancy significantly impacts the resulting congenital malformations.

Other factors, such as the pharmacokinetic status of drugs in mothers, the dosage of exposure, and genetic susceptibility also play significant roles in teratogenic outcomes [10]. According to the first principle of teratology, the cause of congenital malformations is attributed to the interaction between genetic and environmental factors. Genetic susceptibility encompasses maternal and embryonic genetic mutations contributing to developing congenital defects. Studies involving gene mutations in animal models have helped establish links between genetic mutations and congenital phenotypes [11]. Overall, environmental factors, drugs/chemicals, radiation, maternal infections, and genetic factors collectively contribute to the developmental defects observed in humans. While these agents partially reproduce developmental defects in different species of laboratory animals, regulatory authorities have proposed human health risk assessment guidelines based on data obtained from in vitro and in vivo studies.

1.2 The physiology of retinoic acid in health and disease

Retinoic acid (RA), derived from vitamin A, is a vital molecule with essential physiological functions throughout the life cycle [12]. In adulthood, vitamin A plays a crucial role in vision, skin renewal, spermatogenesis, and immune system functioning [13-16]. During prenatal development, it regulates the formation of the vertebrate body plan. Concentration-dependent effects of RA are observed, with both deficiency and excessive intake leading to severe health consequences in embryos, children, and adults. Insufficient levels can impair vision, cause anemia, and weaken immunity, while overdosing may result in symptoms like headaches, nausea, and skeletal abnormalities [17, 18]. To prevent adverse effects, recommended vitamin A intakes range from 300-400 μg/day for children to 700-900 μg/day for women and men, with a maximum limit of 3000 μg/day [19]. Retinoic acid and related retinoids find extensive pharmaceutical use, addressing conditions such as cancer, skin disorders, and multiple sclerosis [20, 21].

1.3 The role of retinoic acid in the process of embryonic development

Retinol's role as a vitamin was discovered early in the twentieth century [22]. However, it wasn't until much later that its critical function in embryonic development was revealed, prompted by the observation of malformations caused by high doses of retinol. We now understand that the embryo's retinoic acid levels are tightly regulated through a complex interplay of synthesizing and metabolizing enzymes. After entering the cellular environment, retinol engages in a molecular association with intracellular retinol binding proteins [23]. Subsequently, it undergoes enzymatic processing facilitated by short-chain dehydrogenase/reductase, specifically RDH10, resulting in the conversion to retinaldehyde [24]. Retinaldehyde, in turn, can be reversibly transformed back into retinol through the action of DHRS3, enabling its storage and contributing to the maintenance of retinoic acid homeostasis [25]. The oxidation of retinaldehyde to RA is primarily catalyzed by retinaldehyde dehydrogenases (RALDH1–3) [26]. RALDH2, among the various RALDH enzymes, serves as the primary source of RA during embryonic development and is closely associated with active RA signalling [27]. Cellular RA binding proteins, CRABP, facilitate the uptake of RA, guiding its delivery to the nucleus for the regulation of gene expression or to CYP26 enzymes (CYP26A1, CYP26B1, and CYP26C1) for degradation [12].

The central functions of retinoic acid (RA) in embryogenesis primarily arise from its essential role in gene regulation. RA is a ligand for retinoic acid receptors (RARs) and retinoic acid X receptors (RXRs), which belong to the steroid hormone superfamily of transcription factors. These receptors function as heterodimers and exhibit relative redundancy. Interestingly, the local concentration of RA, determined by the balance between its synthesis and metabolism rather than receptor availability, appears to be crucial for its activity. RA also competes with other signalling molecules involved in pattern formation during vertebrate embryo development [28, 29]. These findings indicate that maintaining a precise balance in the availability of retinoic acid plays a fundamental role in normal development.

1.4 The adverse effects of retinoids on embryonic development

The association between fetal malformations and vitamin A deficiency was first documented in the 1930s and 1940s [30-32]. Moreover, the majority of our understanding regarding the effects of maternal vitamin A deficiency and its influence on fetal development has been derived from studies conducted in animal models.

Offspring of rats deficient in vitamin A have exhibited a variety of abnormalities affecting multiple organs, including the heart [33, 34]. Similarly, In humans, individuals carrying mutations in STRA6 and RALDH2, resulting in retinoic acid (RA) deficiency, have been reported to exhibit congenital heart defects [35, 36]. Notably, an excessive intake of vitamin A during pregnancy has also been associated with heart defects and other malformations, demonstrating its teratogenic potential [37, 38].

In the 1980s, it was discovered that synthetic retinoids, including those used to treat skin conditions, also exhibited teratogenic properties [39, 40]. Studies on isotretinoin (13-cis-RA) confirmed its human teratogenicity, with observed malformations resembling those caused by vitamin A overdose [41]. Craniofacial anomalies and thymic hypoplasia were particularly notable, indicating neural crest cell migration deficiencies into these developing tissues [42, 43]. Numerous structurally analogous retinoids were subsequently developed, with varying potencies in inhibiting chondrogenesis in vitro assays, which proved helpful in predicting their relative teratogenic potential in vivo [44]. In conclusion, the documented association between maternal vitamin A deficiency, synthetic retinoids, and teratogenic effects highlights the critical role of vitamin A in normal fetal development, emphasizing the need for careful regulation of vitamin A intake during pregnancy.

1.5 The influence of retinoids on cardiac development

Heart development relies on the essential role of retinoic acid (RA) [45], which plays a crucial role plays a crucial role in various aspects of heart development, including heart looping, development of posterior chambers, and differentiation of ventricular cardiomyocytes. Regulating RA levels in the heart depends on the local activity of enzymes involved in its synthesis and metabolism. Specifically, the expression of Raldh2, an enzyme involved in RA synthesis, is observed in cardiac progenitors at late-bud stages and later in the sinoatrial and atrial tissues [46-48] [48]. Deficiency of the enzyme Raldh2 leads to abnormalities in the anteroposterior patterning of the primitive heart [47] and affects markers associated with the second heart field, such as Isl1, Tbx1, Fgf8, and Fgf10. The balance between RA synthesis by Raldh2 and degradation by CYP26 enzymes, such as Cyp26a1 and Cyp26b1, is critical for regulating RA availability and distribution in the developing heart [28, 48]. Disruption of Raldh2 in zebrafish leads to the formation of enlarged hearts due to increased Nkx2.5-expressing cardiac progenitor cells [49]. The expression of Raldh2 is controlled by a complex involving Hox, Pbx1, and Meis1, and deficiencies in these factors result in similar cardiac phenotypes [50]. Loss of Cyp26 enzymes in zebrafish and mice results in smaller atria, looping defects, and outflow tract abnormalities [51]. RA signalling changes also affect progenitor cells' contribution to heart development by expressing Hoxa1, Hoxa3, and Hoxb1 [52]. Alterations in the balance of RA significantly impact the expression of various cardiac genes, including Tbx3, Tbx5, Fgf8, Nppa, and Gata4 [53]. Thus, maintaining the proper ratio of RA is critical for heart development, and disruptions in this balance lead to altered expression of RA-regulated genes, ultimately resulting in structural malformations.

1.6 Regulatory guidelines for testing of new drugs and chemicals

Regulatory guidelines for testing new drugs and chemicals play a vital role in assessing their potential toxicity and ensuring the safety of human health and the environment. Recently, there has been a growing emphasis on developing and utilizing in vitro toxicity testing methods within these guidelines [54]. Understanding the regulatory framework for in vitro testing is crucial for a thesis. In vitro toxicity testing involves using cell-based systems, isolated tissues, or reconstructed human tissue models to evaluate the toxic effects of drugs and chemicals. These methods offer several advantages, including reduced reliance on animal testing, cost-effectiveness, and the ability to assess a wide range of endpoints in a controlled laboratory environment [55]. Regulatory guidelines provide specific recommendations and requirements for in vitro toxicity testing. They outline the methodologies, test systems, and endpoints that should be considered to ensure a comprehensive evaluation. For example, guidelines may specify using well-established cell lines, primary cells, or advanced 3D tissue models to mimic the physiological conditions relevant to the target organ or system. The guidelines also emphasize the importance of selecting appropriate endpoints to assess toxicity accurately. These endpoints may include cell viability, cytotoxicity, genotoxicity, oxidative stress, inflammation, and specific molecular toxicity markers. The choice of endpoints depends on the anticipated mode of action and the particular concerns associated with the drug or chemical being tested [56].

Furthermore, regulatory guidelines often require the validation of in vitro methods to ensure their reliability and reproducibility. This involves demonstrating that the selected test systems and endpoints can accurately predict toxic effects observed in animal or human studies. Validation studies include comparing the results obtained from in vitro tests with data from in vivo studies to establish the predictivity and relevance of the in vitro models. Guidelines may also guide data interpretation and decision-making processes to facilitate the integration of in vitro toxicity testing within regulatory frameworks. They outline the criteria for evaluating and classifying the toxicity potential of a substance based on the observed effects in the in vitro tests. This information assists regulatory authorities in making informed decisions regarding the approval, labelling, and risk management of new drugs and chemicals [57].

Pharmaceutical drugs aimed at treating women of childbearing potential require reproductive toxicity testing according to the ICH guideline S5 (R2) [58]. This involves in vivo tests using rodent and non-rodent species to identify potential hazards. The guidelines address the limitations of rodent species in predicting teratogenicity. The testing process includes six phases to monitor effects from premating to sexual maturity and birth, covering adverse effects on reproductive systems and newborn development. OECD guidelines recommend various tests for evaluating chemicals. However, the need for large animal numbers, high costs, and long durations prompts the search for an alternative in vitro methods for developmental toxicity testing [59]. Taken together, integrating in vitro

toxicity testing within regulatory frameworks is essential for evaluating the safety of drugs and chemicals, reducing reliance on animal testing, and ensuring informed decision-making processes.

1.7 In vitro humanized models for evaluating developmental toxicity

In recent years, there has been an increasing focus on developing alternative in vitro human models to investigate the potential teratogenic effects of drugs during embryonic development. These models provide valuable opportunities to complement traditional animal-based developmental toxicity studies. By simulating critical aspects of human embryonic development in vitro, hPSC-based models can potentially provide valuable insights into drug-induced developmental toxicity. Most recent research has focused on evaluating the effects of drug exposure during specific stages of embryonic development, such as the development of blastoids resembling human blastocysts [60, 61] and gastruloids replicating crucial processes like gastrulation [62]. Organoids, which mimic organ development, have also been utilized to study adverse effects on organogenesis [63]. These in vitro models offer advantages in terms of scalability, compatibility with toxicological screens, and potential for predicting toxicity, although further studies are needed to explore their full potential [64].

Among the advanced models are the 2D and 3D human pluripotent stem cell (hPSC) models, which have been developed to target specifically drug-induced cardiac developmental toxicity [65]. While 2D platforms offer simplicity and accuracy in predicting teratogenicity, they lack the ability to capture morphological defects. Consequently, there is a growing interest in using 3D models, such as cardiac organoids, to replicate tissue morphogenesis better. Although still in early development, 3D cardiac organoids have shown promise in assessing developmental cardiac toxicity [66], validating teratogenicity for selected drugs and providing insights into specific heart regions and cell populations [67].

Thus, the use of in vitro human models provides valuable insights into drug-induced developmental toxicity during embryonic development, particularly in cardiac toxicity. While 2D models are also accurate, 3D cardiac organoids show promise in capturing morphological defects and assessing toxicity in specific heart regions and cell populations.

1.8 In vitro generation of functional cardiomyocytes from human induced Pluripotent Stem Cells (hiPSCs)

The differentiation potential of human induced pluripotent stem cells (hiPSCs) is well-established, with the ability to differentiate into cells representing all three germ layers in vitro. Several scientific

teams have successfully developed lineage-specific differentiation protocols, yielding high yields of the desired cell populations [68-70]. One notable study by Christine Mummery and colleagues focused on differentiating human embryonic stem cells (hESCs) into functional cardiomyocytes. The resulting cardiomyocytes expressed cardiac structural markers such as α-actinin, MLC-2a, and MLC-2v, and exhibited action potentials characteristic of ventricular, atrial, and nodal-like cells [62]. Although the study did not produce cardiomyocytes in large numbers, it provided valuable insights into the involvement of growth factors and proteins, including endoderm-secreted factors, BMPs, activin A, FGFs, and Wnt/β-catenin repressors, in cardiac differentiation.

In recent years, several scientists, including our research group, have reported on the role of canonical Wnt and transforming growth factor β (TGFβ) pathways in mediating cardiac differentiation [71]. Our group has optimized the cardiac differentiation protocol by modulating the Wnt/β-catenin signalling pathway. Initially, we activated the pathway using Wnt ligands (CHIR), and then, after 48 hours, we blocked the Wnt pathway using inhibitors such as IWP2 and others. This optimized approach has proven effective in efficiently generating cardiac cells from human pluripotent stem cells [72].

These advancements in understanding the signalling pathways and optimizing differentiation protocols have led to generating specific cell types, such as cardiomyocytes, from hiPSCs. These differentiated cells hold great potential for disease modelling, drug screening, and regenerative medicine applications. Continued research in this field will further enhance our understanding of cardiac differentiation mechanisms and contribute to developing novel therapeutic approaches for cardiovascular diseases.

1.9 Transcriptomics and -omic approaches for enhancing developmental hazard detection and endpoint assessment

Applying the embryonic stem cell test (EST) in regulatory testing requires improvements in endpoint scoring, test duration, predictivity, and the applicability domain for developmental hazard detection. To address these challenges, a proposed approach focuses on early changes in gene expression profiles through transcriptomic profiling. Utilizing Affymetrix chips, researchers have identified a ”differentiation track” of gene expression that effectively distinguishes between diverse developmental toxicants. This finding can potentially enhance predictivity and expand the applicability domain of the ECVAM-validated modified EST (mEST) [73].

Another promising avenue is exploring the cardiogenic effects of 309 ToxCast chemicals with a comprehensive set of in vitro assays [74]. Statistical analysis revealed significant associations be-

tween 26 chemicals and the mEST response. Correlation analysis with multiplex reporter assays uncovered increased bioactivity of critical developmental regulators and decreased embryonic stem cell differentiation. Genetic regulators within reactive oxygen species signalling pathways were also correlated with reduced ESC differentiation, suggesting potential modes of action contributing to cardiogenic disruption. Shinde et al. (2017) [75] introduced two novel transcriptome-based indices, namely ”developmental potency” (Dp) and ”developmental index” (Di), in their study that employed the UKK and UKN1 test systems with human pluripotent stem cells (hPSCs). These indices were developed to assess teratogenicity by analyzing gene expression changes in hPSCs.

In pursuing more accurate and predictive teratogenic assays, -omic based approaches, including transcriptomics and proteomics, offer alternative methodologies for developing precise endpoints. Leveraging the distinct expression patterns of thousands of genes during differentiation, these -omic techniques enable the comprehensive detection of mRNA or protein markers specific to critical developmental periods [76]. Transcriptomic analyses have also assessed the transcriptional responses of differentiating human embryonic stem cells (hESCs) to various teratogens. Notably, low concentrations of cytosine arabinoside induced ectodermal markers while inhibiting mesodermal characteristics, indicating dysregulation in processes related to neuronal differentiation, mesoderm development, and axonal guidance [76]. Similarly, ethanol exposure increased endodermal differentiation markers, while retinoic acid treatment and thalidomide exposure affected neural and mesodermal processes, respectively [77].

Complementary -omic approaches, such as integrating transcriptomic and proteomic data, have proven successful in studying the effects of teratogens on gene and protein expression in embryoid bodies (EBs) [78]. For example, thalidomide-treated EBs showed a loss of POU5F1 regulatory proteins and overexpression of neuronal development-related proteins, highlighting the importance of -omic integration for a comprehensive understanding [78]. The availability of diverse data sets will facilitate future studies, enabling optimization and standardization of prospective teratogenic assays. The utilization of -omic approaches holds tremendous potential for providing deeper insights into the effects of teratogens on both gene and protein expression during embryonic development readout.

1.10 Aims of the present study

This thesis aims to develop a novel in vitro test system for assessing developmental teratogenicity and cardiotoxicity to replace animal experiments. The primary objective of this research is to create an innovative assay capable of accurately detecting teratogens in vitro, which may gain recognition from regulatory authorities as a reliable test system for risk assessment in the future. To achieve this goal, we utilized the UKK2 protocol in combination with human induced pluripotent stem cells (hiPSCs), transcriptomics, and a carefully selected group of substances, based on their in vivo concentrations. Specifically, in this thesis, we investigated the differentiation of hiPSCs into various germ

layers and subsequently into cardiomyocytes, both in the presence and absence of different embryotoxic substances. Additionally, we performed gene expression studies using isolated RNA, employing whole genome microarrays to identify specific early embryotoxic or cardiotoxic gene signatures.

The first part of the thesis focuses on developmental embryotoxicity, explicitly targeting the initial day of the differentiation protocol (day1), which allowed the observation of representatives from all three germ layers. Through the implementation of this innovative system, it was demonstrated how the new approach significantly improved upon the existing UKK testing system [75]. Through the implementation of UKK2, we successfully substituted hESCs with hiPSCs. Additionally, this system offered the advantage of requiring only a 24-hour incubation period with the test compounds and collecting the sample for analysis. The construction of two classifiers became possible by including 39 carefully screened test compounds, covering a broad spectrum of diverse molecular mechanisms, including well-known teratogens and non-teratogens.

In the second part of this thesis, an extension of the UKK2 protocol was implemented, employing a 14-day procedure that involved phasic activation of the β-catenin/Wnt pathway, the co-called UKK-CTT, to assess developmental cardiotoxicity. To accomplish this objective, transcriptional profiling was conducted at three distinct time points: day1 (mesoderm formation), day4 (early cardiac mesoderm), and day14 (beating cardiomyocytes). Building upon the setup established in Part 1, four compounds were selected based on their in vivo plasma peak concentrations. Thalidomide, Valproic acid, and Isotretinoin, known teratogens, were chosen alongside Buspirone, classified as a negative compound. Notably, Isotretinoin served as a gold standard due to its complete inhibition of cardiac differentiation, contrasting with other test compound-teratogens that impede but do not entirely hinder the progression towards cardiomyocytes. Thus, in this second part we aimed to identify and establish a gene signature to predict the inhibitory potential of teratogens and non-teratogens in the process of cardiomyogenesis by utilizing the transcriptomics data. Additionally, we sought to incorporate a phenotypical anchoring point (cardiac α-actinin structure) within the test system to enhance our ability to predict developmental cardiotoxicity.

2 Material and methods

2.1 Material

2.1.1 Cell culture material

Table 1: Cell types

Cell Types	Description
iPS (IMR90)-4	Human induced pluripotent stem cell from Lung Fibroblasts (IMR90) (female)
Tuesday	Human induced pluripotent stem cell from dermal fibroblast (male)

Table 2: List of cell culture media and reagents

Component	Catalog Number	Company
DMEM/F12 - glutamax	31331028	Gibco
RPMI 1640 Medium GlutaMAX™	61870010	Gibco
DPBS (w/o Ca^{2+}/Mg^{2+})	14190094	Gibco
B-27® Supplement, minus insulin	A1895601	Gibco
CTS™ TrypLE™ Select Enzyme	A1285901	Thermo Fisher Scientific
StemMACS iPS-Brew XF, 50 × Supplement	130104368	Miltenyi
StemMACS™ iPS-Brew XF	130104368	Miltenyi
mFreSR™ cryopreservation medium	05853	STEM CELL Technologies
TrypLE™ Express Enzyme	31331028	Gibco
Corning® Matrigel®	354230	Corning
Pen/Strep	15140122	Gibco
StemPro® EZPassage™ Disposable Stem Cell Passaging Tool	23181-010	Invitrogen

2.1.2 Chemicals and solutions and reagents

Table 3: List of compounds

Product	Catalog Number	Company
3,3',5-Triiodo-L-thyronine sodium salt	T6397	Sigma Aldrich
5,5-Diphenylhydantoin sodium salt	sc-214337	Santa Cruz
9-cis retinoic acid	14587	Cayman
Acitretin	PHR1523	Merck
Actinomycin D	BVT-0089	Adipogen Life Sciences
Ampicillin anhydrous	A9393	Sigma Aldrich
Ascorbic acid	A0278	Sigma Aldrich
Atorvastatin Calcium	PHR1422	Sigma Aldrich
Buspirone hydrochloride	B7148	Sigma Aldrich
Carbamazepine	C4024	Merck
Cefotiam dihydrochloride	1098005	Sigma Aldrich
Chlorpheniramine maleate salt	C3025	Sigma Aldrich
Clomiphene citrate salt	C6272	Sigma Aldrich
CHIR (99021)	442310	R&D
Dextromethorphan HBr	PHR1018	Sigma Aldrich
Diethylpyrocarbonate treated (DEPC) water	750024	Thermo Fisher Scientific
Dimethyl sulfoxide (DMSO)	A994.1	Carl Roth
Diphenhydramine	sc-204729	Santa Cruz Biotechnoolgy
Doxorubicin hydrochloride	D2975000	Sigma Aldrich
Doxylamine succinate	D3775	Sigma Aldrich
DPBS, calcium, magnesium	14040091	ThermoFisher Scientific
DPBS, no calcium, no magnesium	14190094	ThermoFisher Scientific
Entinostat (MS-275)	Cay13284	Cayman Chemicals
Ethanol, 70% denatured	2202	ChemSolute
Ethanol, absolute	100983	Merck
Famotidine	F6889	Sigma Aldrich
Favipiravir	HY14768	Hycultec
Finasteride	14938	Cayman Chemical
Folic acid	F7876	Sigma Aldrich
Isotretinoin	PHR1188	Sigma Aldrich
IWP	10536	Sigma Aldrich
Leflunomide	PHR1378	Merck
Levothyroxine	PHR1613	Sigma Aldrich
Lithium chloride	L4408	Sigma Aldrich

Magnesium chloride anhydrous	8147330500	Merck
Medroxyprogesterone	24908	Cayman Chemical
Methicillin sodium salt monohydrate	1410002	Sigma Aldrich
Methotrexate	PHR1396	Sigma Aldrich
Methylmercury	33368	Sigma Aldrich
Misoprostol	13820	Cayman Chemical
Panobinostat	Cay13280	Cayman Chemicals
Paroxetine hydrochloride	PHR1804	Sigma Aldrich
Ranitidine hydrochloride	R101-1G	Sigma Aldrich
Retinol	17772	Merck
Rock Inhibitor (Y-27632)	688001	Calbiochem
Sucralose	PHR1342	Sigma Aldrich
Teriflunomide (A-771726)	HY15405	Hycultec
Thalidomide	T144	Sigma Aldrich
Trichostatin A	T1952	Sigma Aldrich
Valproic acid	PHR1061	Sigma Aldrich
Vinblastine sulfate salt	V1377	Sigma Aldrich
Vismodegib	HY10440	Hycultec
Vorinostat (SAHA)	Cay10009929	Cayman Chemicals

Table 4: List of molecular reagents

Molecular biology Kits	**Catalog Number**	**Company**
TRIzol® Reagent	15596026	Invitrogen
DNase I	AM2222	Invitrogen
PCR Purification Kit	K0701	Thermo Fisher Scientific
SuperScript® VILO cDNA Synthesis Kit	11754250	Invitrogen
SYBR® Green qPCR	11733038	Invitrogen

Table 5: List of primers (All primers were purchased from Sigma Aldrich)

Primers for qRT-PCR	Sequence
HS_KDR_Forward_Primer	GGCCCAATAATCAGAGTGGCA
HS_KDR_Reverse_Primer	CCAGTGTCATTTCCGATCACTTT
HS_ETS1_Forward_Primer	GATAGTTGTGATCGCCTCACC
HS_ETS1_Reverse_Primer	GTCCTCTGAGTCGAAGCTGTC
HS_HHEX_Forward_Primer	ACGCCCTTTTACATCGAGGAC
HS_HHEX_Reverse_Primer	CGTGTAGTCGTTCACCGTC
HS_MEIS2_Forward_Primer	GAAAAGGTCCACGAACTGTGC
HS_MEIS2_Reverse_Primer	CTTTCATCAATGACGAGGTCGAT
HS_RBM20_Forward_Primer	GCAGCCATACCCAGTACCC
HS_RBM20_Reverse_Primer	CATTACCCCAGTGAAAGGATGC
HS_BAMBI_Forward_Primer	AGCACGACAGACATCTGCC
HS_BAMBI_Reverse_Primer	CGGAACCACAACTCTTTGGAAG
HS_CDX4_Forward_Primer	CCGATGCCAGCCTCCAATTT
HS_CDX4_Reverse_Primer	CTGTGCCCATTGTACTAGACG
HS_HOXA3_Forward_Primer	ATGCAAAAAGCGACCTACTACG
HS_HOXA3_Reverse_Primer	TACGGCTGCTGATTGGCATTA
HS_ISL1_Forward_Primer	GCGGAGTGTAATCAGTATTTGGA
HS_ISL1_Reverse_Primer	GCATTTGATCCCGTACAACCT
HS_SHISA3_Forward_Primer	CAGGGCAACTACCACGAGG
HS_SHISA3_Reverse_Primer	GAGAAAGGGGACGTAGACAGG
HS_SMAD6_Forward_Primer	CCTCCCTACTCTCGGCTGTC
HS_SMAD6_Reverse_Primer	GGTAGCCTCCGTTTCAGTGTA
HS_SOX17_Forward_Primer	GTGGACCGCACGGAATTTG
HS_SOX17_Reverse_Primer	GGAGATTCACACCGGAGTCA

Table 6: List of microarray, instruments, kits and reagents

Item	Catalog Number	Company
3 IVT Express Kit	901229	Affymetrix, Thermo Fisher Scientific
GeneChip Fluidics Station 450	00-0079	Affymetrix, Thermo Fisher Scientific
GeneChip Hybridization Oven 645	00-0331	Affymetrix, Thermo Fisher Scientific
GeneChip hybridization, wash and stain kit	900720	Affymetrix, Thermo Fisher Scientific
GeneChip Scanner 3000 7G WholeGenome Association System	00-0362	Affymetrix, Thermo Fisher Scientific
Human Genome U133 Plus 2.0 arrays	900466	Affymetrix, Thermo Fisher Scientific

2.1.3 Consumables and instruments

Table 7: List of plastic and glass consumables

Item	Catalog Number	Company
1 ml pipettes	86.1251.001	SARSTEDT AG & CO
1.5 ml Microcentrifuge Tubes	MCT150-C	Axygen
10 microliter filtered tips	07-602-7300	Nerbe plus
10 ml pipettes	1110508	Labomedic
100 microliter filtered tips	07-642-7300	Nerbe plus
1000 microliter filtered tips	07-692-7300	Nerbe plus
15 ml tubes	1110502	Labomedics
1ml sterile syringe	300013	BD plastipak
2 ml pipettes	86.1252.001	SARSTEDT AG & CO,
20 microliter filtered tips	07-622-7300	Nerbe plus
200 microliter filtered tips	07-662-7300	Nerbe plus
25 ml pipettes	1110611	Labomedic
5 ml pipettes	1110507	Labomedic
50 ml tubes	1110503	Labomedic
6 cm petri dishes	353004	Corning Inc
6-well cell culture plates	353046	Corning Inc
MicroAMP fast optical 96-well plate	4346906	Applied Biosystems,
MircroAmp optical adhesive film	4311971	Applied Biosystems,
Stainless steel sterile needle 20 gauge	301300	BD microlance
StemPro® EZPassage™ Disposable Stem Cell Passaging Tool	23181-010	Invitrogen
Sterile cell scraper	99002	Techno Plastic Products AG (TPP)

Table 8: List of instruments

Instument	**Provider**
Avanti Centrifuge G-52 I	Beckman Coulter
Cell Culture Hood	Herasafe,Hera sure
Centrifuge 5412 (refrigerated)	Eppendorf, Thermo
Cryo tank	Chronos
EVOS Cell Imaging Systems	Invitrogen
Fluorescence microscope Zeis	Axiovert 200 fluorescence microscope, Zeis
Incubator	Heraeus240,Thermo
Incubator shaker	InfrasHT
Inverted Microscope I	Ziess
Inverted Microscope II	Olympus
Micro Centrifuge	Gilson,Biozyme
Nanodrop Spectrophotometer	Mol bio lab
PCR Thrermocycler L1000	BioRad
Real-Time PCR System (One-Step) 7500fast	Life Technology
Ultrasonic water bath (2200)	Branson
Vortex	Phonix
Water Bath	GFL

2.2 Methods

2.2.1 Coating the plates

To facilitate cell adhesion and promote proper growth conditions, the cell culture plates underwent a matrigel matrix coating process. Before the cells were transferred to the plates, thawed aliquots of 150 μL at 4°C were mixed with 12 mL of pre-chilled DMEM/F12 + GlutaMAX medium. Subsequently, the mixture was incubated for 30 minutes inside a cell culture incubator operating at 37 °C and 5 % CO_2. Before cell plating, the matrigel was carefully aspirated from the plates to ensure optimal cell attachment.

2.2.2 Thawing, passaging, and freezing the cells

The process of thawing frozen hiPSCs began by placing the vials containing the cells in a water bath of 37 °C for 3 to 4 minutes. Subsequently, StemMACS™ iPS-Brew XF basal medium, pre-warmed and supplemented with 10 mL of StemMACS iPS-Brew XF 50X supplement, was cautiously added drop by drop to the vial. The cells were then transferred to a 15 mL tube containing 5 mL of prepared media. The cell suspension was centrifuged at room temperature (rt) at a speed of 1000 rpm for 5 minutes. Following this the supernatant was aspirated, and the cell pellet was re-suspended in cell culture media supplemented with a ROCK inhibitor (10 μM, Y27632). The resulting mixture was evenly distributed onto plates previously coated with matrigel. After a 24-hour incubation period, the cells were attached, and the medium was subsequently replaced with cell culture media without ROCK inhibitor.

The pluripotent cells were passaged when they reached approximately 85% confluency, employing either the classical colony-cutting method or single-cell splitting. In the case of colony cutting, once the plates reached confluency, differentiated colonies were carefully removed using a 1 mL pipette under a stereomicroscope. The plate was then washed once with PBS buffer and fresh media was added. The undifferentiated colonies were excised using a syringe needle, collected in a Falcon tube, and centrifuged at 200 x g for 5 minutes. The resulting colony or cell pellet was re-suspended in fresh media and evenly distributed onto plates previously coated with matrigel. Alternatively, when the cells reached 80% confluency for single-cell passaging, they were detached from the plates by adding a cell dissociation reagent CTS™ TrypLE™ Select Enzyme and incubating for 2 to 3 minutes. The detached cells were collected in a Falcon tube and centrifuged at 1000 rpm at rt for 5 minutes. The subsequent steps were carried out as described in the previous method. For the freezing, the cell pellet obtained as previously described was re-suspended in ice-cold freezing media in a 1:1 ratio and transferred into vials. The medium and cells were gently mixed, and the vials were then placed in a freezer set at -80 °C. The vials remained in the freezer for one day before being transferred and stored in a liquid nitrogen tank.

For the freezing, the cell pellet obtained as previously described was re-suspended in ice-cold freezing media in a 1:1 ratio and transferred into vials. The medium and cells were gently mixed, and the vials were then placed in a freezer set at -80 °C. The vials remained in the freezer for one day before being transferred and stored in a liquid nitrogen tank.

2.2.3 Differentiation of hiPSCs towards germ layers and further to cardiomyocytes

To initiate the differentiation process of hiPSC, cells in their pluripotent state were dissociated using CTS™ TrypLE™ Select Enzyme. Subsequently, 600,000 cells per well were seeded on Matrigel-coated 6-well plates. StemMACS™ iPS-Brew XF medium including 10 μM ROCK inhibitor in the culture medium. The following day, the medium was changed to StemMACS™ iPS-Brew XF medium without the addition of ROCK inhibitor.

On day0, the induction of differentiation was initiated by adding 10 μM of the Wnt activator small molecule CHIR to RPMI 1640 GlutaMAX™ medium. B-27™ Supplement without insulin from Thermo Fisher Scientific, Germany, was also included in the medium. At the same time, the cells were incubated (5 % CO_2, 37 °C) with the test compounds at a 1-fold C_{max} and a DMSO concentration of 0.1 % as DMSO-control. Following CHIR exposure, the medium was changed to basal RPMI/B-27-insulin medium, and the cells were maintained for an additional 24 hours. On day2, RPMI/B-27-insulin medium supplemented with 10 μM of the small molecule WNT inhibitor IWP2 was added to the cells. This medium was maintained for 48 hours, from day2 to day4. Subsequently, the cells were maintained in basal RPMI/B-27-insulin medium, and spontaneously beating clusters started to become visible from day9 onwards. After exposure to CHIR, RNA extraction was performed on the cells at three time points: 1 hour, 24 hours, and 48 hours (24 hours of CHIR exposure). RNA extraction for the compound-treated conditions and the corresponding DMSO controls was conducted on day1, day4, and day14. Three biological replicates were generated for each tested condition to ensure reliable results.

2.2.4 Test compounds, teratogenicity information and plasma peack concetrations

The test compounds used in the study were obtained from Sigma-Aldrich (refer to Materials 2.2.1, **Table 3**). To ensure their availability and suitability for the experiments, the compounds were dissolved and stored at concentrations 20,000-fold C_{max}. These solutions were prepared using 100 % DMSO as the solvent, except in cases where the compounds were soluble in distilled water. The concentrations of the teratogens and non-teratogens tested in the study, along with their corresponding C_{max} values and information on teratogenicity, are provided in **Table 9** in the Results section.

2.2.5 RNA extraction and cDNA synthesis

RNA was extracted using Trizol reagent in accordance with the manufacturer's instructions. Subsequent RNA purification steps were conducted using the RNeasy Mini Kit, following the provided manual instructions. Following the homogenization of the samples, phase separation of the lysates was achieved using chloroform. The resulting lysates were then centrifuged, and the RNA was precipitated using ice-cold ethanol. The RNA purification process continued with washing the samples on spin columns, removing impurities, and ultimately the elution of RNA in water. The RNA samples underwent treatment with DnaseI to remove any genomic DNA contamination. The concentration of total RNA was determined using a UV-Vis spectrophotometer, specifically the nanodrop2000c model. 1 μg or 500 ng of total RNA was used for cDNA synthesis, employing the Vilo SuperScript cDNA synthesis kit following the manufacturer's recommended protocol. The composition of the reaction mixture was prepared according to the manufacturers' protocol. Initially, the reaction mixture was incubated at 25°C for 10 minutes. After this initial step, cDNA synthesis was performed for 60 minutes at 42 °C. The synthesis reaction was then terminated by incubating at 85 °C for 5 minutes. The resulting cDNA was stored at -20 °C until it was utilized for qRT-PCR assays.

2.2.6 Real-Time Polymerase Chain Reaction (qRT- PCR)

In all PCR reactions, GAPDH was utilized as the internal control. The primers, purchased from Sigma-Aldrich, were diluted to a working concentration of 5 mM, with 5 μM of forward and reverse primers. The specific primer sequences can be found in the Materials section 2.1.2 (**Table 5**). Each PCR reaction consisted of 10 μL of SYBR Green PCR master mix 1 μL of the primers, and 3 μL of cDNA template, resulting in a final reaction volume of 20 μL. The ABI-7500 Fast PCR system was employed for the analysis. The cycling conditions for amplifying the target sequences were as follows: an initial denaturation step at 50 °C for 2 minutes, followed by an initial denaturation at 95 °C for 2 minutes. This was followed by 40 cycles of denaturation at 95 °C for 30 seconds and annealing at 60 °C for 30 seconds. The Dissociation Stage consisted of three steps: denaturation at 95 °C for 15 seconds, annealing at 60 °C for 1 minute and final denaturation at 95 °C for 15 seconds. A melting curve analysis was performed to verify the amplification of a single PCR product.

The mRNA levels were determined using the cycle threshold (Ct) method to calculate relative fold change by comparing endogenous controls and ground controls. For all PCR reactions we used biological triplicates.

2.2.7 Fluorescent imaging and video analyzer

To analyze the beating activity and the sarcomere contractive activity of the CMs on day14 we used the software Video Analyzer (1.9) as described in Acharya et. al 2022 [79]. The videos and fluorescent live images ware taken using EVOS Cell Imaging Systems (CMMC, Cologne).

2.3 Statistical analysis of gene expression data

2.3.1 Gene arrays

Genome-wide expression levels were assessed using Affymetrix's "GeneChip® Human Genome U133 Plus 2.0" arrays. The samples were processed using Affymetrix's "GeneChip® 3' IVT PLUS Reagent Kit," following the provided instructions. Initially, the RNA was transcribed into double-stranded cDNA, which was then utilized to synthesize and amplify single-stranded complementary RNA (cRNA) through in vitro transcription (IVT), employing T7 RNA polymerase [81]. The resulting cRNA was labeled with biotin, subsequently purified, fragmented, and hybridized to the array, which contained approximately 1,300,000 unique oligonucleotides. Following hybridization, the array underwent a series of washing, staining, and scanning steps. During scanning, the fluorescent signals emitted by the stained cRNA-oligonucleotide hybrids were captured, representing the expression levels of 54,675 probe sets, corresponding to approximately 39,000 human genes.

2.3.2 Statistical analysis of gene expression data, principal component analysis, volcano plots

The analyses were performed using the statistical software R, version 4.2.2, along with additional R-packages. Each combination of compound and day involved three independent biological replicates, and Affymetrix gene arrays were used to measure gene expression levels. The analysis was conducted by Prof. J. Rahnenführer and Dr. F. Kappenberg.

To pre-process the Affymetrix CEL-files, the frozen robust multi-array average (fRMA) algorithm was applied, which includes background correction, normalization, and summarization steps. This process generated expression values for 54,675 probe sets (PS). The software R, version 4.2.2 and R-packages affy, frma, and hgu133plus2frmavecs were employed for this purpose.

Principal component analysis (PCA) was carried out based on the pre-processed expression values. Plots were generated using either all 54,675 PS or the top 1000 or 500 PS selected based on their variance across all samples. Both scenarios, involving all samples (all compounds, all days) and samples specific to individual days, were considered.

Differential expression analysis between samples treated with different compounds and DMSO was performed using the R-package limma [82] [83] .The limma approach, an empirical Bayes method, considered all PS to adjust the variance estimates. The resulting moderated t-test, referred to as the "limma t-test," provided p-values that were adjusted for multiple testing using the Benjamini-Hochberg procedure [84]. The gene list for each compound included fold-change (FC), log2 fold-change, unadjusted and adjusted p-values from the limma t-test, as well as mean values on the original or log2 scale for DMSO samples and the respective compound. Volcano plots were used to display

the results, with log2 FC on the x-axis and -log10 of the unadjusted p-value on the y-axis for each PS. PS with an adjusted p-value smaller than 0.05 and an absolute log2 FC larger than log2(2)=1 were considered significant PS (SPS).

Venn diagrams were constructed to compare sets of SPS for the test compounds, including all SPS, upregulated SPS, and downregulated SPS. Only SPS with gene annotations were considered. For each specific part of the Venn diagrams corresponding to Isotretinoin, the top 50 genes were determined. SPS were sorted based on adjusted p-values, and the top 50 SPS with gene annotations were selected for upregulated and downregulated SPS separately. Heatmaps were used to display normalized expression values of these top genes. Furthermore, the Isotretinoin-specific SPS for each day were individually analyzed for enriched Gene Ontology (GO) groups and KEGG pathways, separately for upregulated and downregulated SPS.

For the KEGG pathway analysis, SPS were assigned to their respective KEGG pathways. Fisher's exact test was applied to statistically assess whether there were more differentially expressed PS assigned to specific pathways than expected by chance. The R package clusterProfiler was utilized for KEGG pathway analyses.

In addition to R, the TAC4.1 Affymetrix tool was used to process CEL-files and obtain the gene list for downstream analysis. A log2 fold change of +/-2 was used as the cutoff. These genes were further processed using online tools such as Metascape [85] to enrich the Gene Ontology lists. Additional Venn diagrams were generated using the online platform VENNY 2.1.

2.3.3 Classifier „Cytotox 1000" and „Cytotox SPS" (This part is from our publication Cherianidou et. al 2021[86])

Two classification procedures were used in our analysis: the Number of Significant Probe Sets (SPS) procedure and the Penalized Logistic Regression with Leave-One-Out Cross Validation (Top-1000) procedure.

The SPS procedure involved obtaining an initial classification of compounds based solely on the number of significant probe sets. A probe set was considered significant if both the FDR-adjusted p-value from the LIMMA t-test was smaller than 0.05 and the absolute value of the fold change (FC) was larger than 2. The number of SPS for each compound at a specific concentration was determined and used for the classification procedure. The accuracy of different threshold values for the number of SPS was analyzed, with conditions above the threshold classified as test-positive and conditions below it classified as test-negative. The threshold that yielded the highest accuracy was identified. Measures such as sensitivity, specificity, accuracy, and the area under the receiver operator characteristic curve (AUC) were calculated to assess the quality of the classification procedures.

The Top-1000 procedure utilized penalized logistic regression and normalized gene expression values. A leave-one-out cross-validation approach was used, where in each iteration, samples corresponding to one compound were left out of the dataset. The difference between test compound-exposed samples and corresponding controls were calculated, and the empirical variance of the difference was determined for each probe set. A logistic regression-based classifier was trained on the 1000 probe sets with the highest variance and evaluated on the compound that was left out, providing a probability for each sample of the left-out compound. Probabilities corresponding to samples of the same concentration value were summarized using the mean value. The penalty parameter "lambda" in the logistic regression was optimized via 10-fold cross-validation to minimize the mean cross-validated error.

A threshold was chosen for the predicted probabilities, with conditions above the threshold classified as test-positive and conditions below it classified as test-negative. The threshold was set to the predicted probability that maximized accuracy. The measures of sensitivity, specificity, accuracy, and AUC were calculated, as explained in the Result section.

2.3.4 Statistical analysis

For all experiments, the statistical errors are represented as mean ±SD or ±SEM. To calculate the p-value of significance, two-tailed Student's t-test or ANOVA were used, and p-values ≤ 0.05 were considered statistically significant.

2.3.5 Data availability

The microarray data have been deposited in the Gene Expression Omnibus (GEO) (NCBI): GSE187001

3 Result

3.1 Establishment of the monolayer protocol

The UKK test system was established by modulating the Wnt/β-catenin signaling pathway using two small molecules, CHIR and IWP2. These molecules are employed in a sequential manner, with CHIR activating the pathway and IWP2 inhibiting it. Human induced pluripotent stem cells (hiPSCs) were utilized to generate the three germ layers: endoderm, mesoderm, and ectoderm. The differentiation process of hiPSCs followed previously published protocols, combining the approaches described previously in published protocols [71, 72] and as has been described in **Figure 2**. Gene array analyses were conducted to determine the optimal time point for evaluating the impact of test substances on germ layer formation. In order to simplify and shorten the UKK cellular system compared to the previous EB-based method and to capture the effect of test compounds on germ layer formation during embryonic development, the drug exposure and RNA collection for microarray studies were limited to a 24-hour period after CHIR treatment, as illustrated in **Figure 2**.

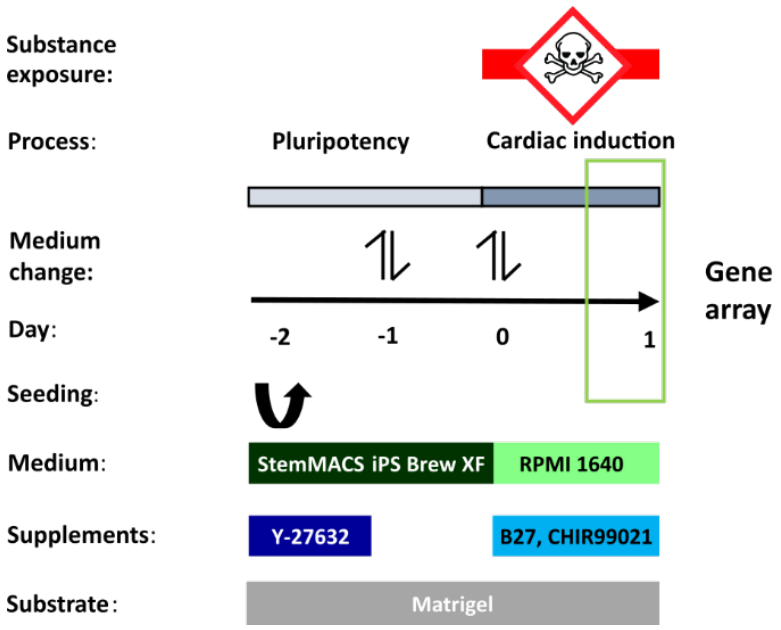

Figure 2: The UKK-24h-test. The plan illustrates the protocol spanning from day-2 to day1. During the pluripotency phase, the applied StemMACS iPS Brew XF medium maintained the hiPSCs' pluripotent state. The supplement Y-27632, provided on the day of seeding (day-2), promoted the survival of hiPSCs, which were seeded individually on matrigel. From day0 to 1, the transition to RPMI 1640 spiked with B27 and CHIR99021 initiated the cardiac differentiation of the cells. At the same time, the cells were exposed to potential (non) developmental toxic substances for a total of 24 hours. On day1, the cells were collected for gene array analysis. Media changes were performed as instructed.

3.2 Assessment of test compounds: selection, concentrations, and characteristics

A set of test compounds was carefully chosen to investigate the discriminative potential of the transcriptomics-based UKK2 in vitro test in distinguishing between teratogens and non-teratogens (**Table 9**). By utilizing the experimental setup in **Figure 2**, we aimed to evaluate the predictive performance of our test system. To achieve this, with our SYSDT project members, we deliberately included a diverse range of teratogenic and non-teratogenic compounds, considering three criteria for their inclusion in the study. The first criterion for compound selection involved published data regarding the teratogenic or non-teratogenic nature of the compound in humans and/or animals. The second criterion encompassed the availability of pharmacokinetic information derived from clinical studies and other sources, which enabled the determination of therapeutic compound concentrations C_{max} and concentrations 20 times higher than C_{max} for subsequent in vitro testing. A third criterion was adequate solubility, ensuring that C_{max} levels could be achieved in the culture medium using a maximum of 0.5 % dimethyl sulfoxide (DMSO) as the solvent.

A thorough search was conducted in collaboration with our partners to identify non-teratogenic compounds appropriate for the UKK2 test system. The search aimed to identify compounds without evidence of teratogenicity and were considered safe for the human fetus. Compounds falling under FDA and TGA pregnancy classes A and B were particularly interesting. In contrast, to identify teratogenic substances, we focused on existing data with in vivo evidence, especially in humans, specifically on compounds categorized as FDA and TGA class D and X. To ensure the biological relevance of the UKK2 test system and its applicability to human conditions, it was essential to determine appropriate in vitro concentrations for all 39 compounds by translating their therapeutic and in vivo plasma/blood concentrations. For all 39 substances, the in vivo concentrations could be translated into biologically relevant 1x C_{max} in vitro concentrations, and for the majority of substances, a 20x C_{max} could also be applied.

Based on these criteria, 16 non-teratogens and 23 teratogens were selected (**Table 9**). Solubility was sufficient to test all test compounds at 1- and 20-fold C_{max} except for leflunomide, phenytoin, teriflunomide and vismodegib, which were tested only at a 1-fold C_{max} as well as carbamazepine that was tested at 1- and 10-fold C_{max} due to solubility limitations. Valproic acid was tested at 1- and 1.67-fold C_{max} due to the known cytotoxic effects of higher concentrations.

Table 9: Substances and applied concentrations in the UKK2 test system

Compound	Abbre-viation	Pregnancy category[a]	Drug class	Tested concentration [µM]	
				1-fold C_{max}[b]	20-fold C_{max}[b]
Non-teratogens					
Ampicillin	AMP	A, B	Antibiotic	107	2140
Ascorbic acid	ASC	A	VItamin	200	4000
Buspirone	BSP	B	Anxiolytic, serotonin 5-HT1A receptor agonist	0.0244	0.488
Chlorpheniramine	CPA	B	Antihistamine, histamine H1 receptor antagonist	0.0304	0.608
Dextromethorphan	DEX	A	Antitussive and psychoactive agent	0.15	3
Diphenhydramine	DPH	A, B	Antihistamine, histamine H1 receptor antagonist	0.3	6
Doxylamine	DOA	A	Antihistamine, histamine H1 receptor antagonist	0.38	7.6
Famotidine	FAM	B	Antihistamine, histamine H2 receptor antagonist	1.06	21.2
Folic acid	FOA	A	Vitamin	0.38	7.6
Levothyroxine	LEV	A	Synthetic thyroid hormone	0.077	1.54
Liothyronine	LIO	A	Synthetic thyroid hormone	0.00307	0.06145
Magnesium (chloride)	MAG	n/a	Dietary supplement	1200	24000
Methicillin	MET	B	Antibiotic	140	2800
Ranitidine	RAN	B	Antihistamine, histamine H2 receptor antagonist	0.8	16
Retinol	RET	n/a	Vitamin and retinoid	1	20
Sucralose	SUC	n/a	Artificial sweetener	2.5	50
Teratogens					
9-cis-Retinoic acid	9RA	D	Retinoid, RAR and RXR ligand	1	20
Acitretin	ACI	X	Retinoid, RAR activator	1.2	24
Actinomycin D	ACD	D	Antineoplastic agent, RNA synthesis inhibitor	0.1	2
Atorvastatin	ATO	X[c]	Antilipemic agent, HMG-CoA reductase inhibitor	0.54	10.8
Carbamazepine	CMZ	D	Anticonvulsant, voltage-gated sodium channel blocker	19	10-fold C_{max} 190[f]
Doxorubicin	DXR	D	Antineoplastic agent, affects DNA and related proteins; produces ROS	1.84	36.8
Entinostat	ENT	n/a	Potential antineoplastic agent, HDAC inhibitor	0.2	4
Favipiravir	FPV	n/a	Antiviral drug, selective inhibitor of RNA polymerase of influenza virus	382	7600
Isotretinoin	ISO	X	Retinoid, RAR ligand	1.7	34
Leflunomide	LFL	X	Anti-inflammatory agent, DHODH inhibitor	370	--[f]
Lithium (chloride)	LTH	D	Mood stabilizer	1000	20000
Methotrexate	MTX	D / X	Antineoplastic, dihydrofolate reductase inhibitor	1	20
Methylmercury	MEM	n/a	Bioaccumulative environmental toxicant, hypothesized ROS production	0.020	0.4
Panobinostat	PAN	n/a, (D)[d]	Antineoplastic agent, HDAC inhibitor	0.06	1.2
Paroxetine	PAX	D	Antidepressant, SSR inhibitor	1.2	24
Phenytoin	PHE	D	Anticonvulsant, voltage-gated sodium channel blocker	20	---[f]
Teriflunomide	TER	X	Anti-inflammatory agent, DHODH inhibitor	370	---[f]
Thalidomide	THD	X	Antiangiogenic	3.9	78
Trichostatin A	TSA	n/a	Antifungal antibiotic, HDAC inhibitor	0.01	0.2
Valproic acid	VPA	D, X[e]	Anticonvulsant, voltage-gated sodium channel blocker, antifolate agent, HDAC inhibitor	600	1.67-fold C_{max} 1000[g]
Vinblastine	VIN	D	Antimitotic agent, affects microtubule dynamics	0.0247	0.494
Vismodegib	VIS	X	Antineoplastic agent, hedgehog pathway inhibitor	20	--[f]
Vorinostat	VST	D	Antineoplastic agent, HDAC inhibitor	3	60

[a] U.S. Food and Drug Administration (FDA) and Australian Therapeutic Goods Administration (TGA) pregnancy categories:

- A: Compounds are safe in the use during pregnancy, proven by well-controlled studies in humans or plenty data from pregnant women;
- B: Compounds are considered to be safe, but they lack sufficient human data;
- C and D: Compounds showed little or some evidence for teratogenicity in humans or animals;
- X: Compounds with known teratogenic activity in humans or with a suspected high teratogenic potential based on animal experiments;
- n/a = not available;

Information was obtained from www.drugs.com (accessed in November 2020) if not stated otherwise.

[b] Maximal plasma or blood concentrations which were usually observed in humans after the administration of therapeutic compound doses. Fetal enrichment was considered if relevant.

[c] (Pfizer Ireland Pharmaceuticals 2009).

[d] Approved, but not assigned (Recommendation: D).

[e] (FDA 2013).

[f] Carbamazepine and VPA were tested at 10-fold and 1.67-fold C_{max}, respectively, instead of 20-fold C_{max}; leflunomide, phenytoin, teriflunomide and vismodegib were tested at 1-fold C_{max} only because of limited solubility.

3.3 Gene expression profile-transcriptomic responses to substance exposure

We conducted gene expression studies using isolated RNA and whole genome microarrays to investigate the impact of teratogenic and non-teratogenic compounds on the transcriptome of cells and assess their differentiability based on gene expression profiles. Additionally, we qualitatively estimated the cytotoxic effects of these compounds by observing cell culture pictures and quantifying RNA yield as a measure of cell viability. If the amount of RNA measured was comparable to the amount of RNA from untreated cells, the test substance was characterized as non-cytotoxic. Compounds that demonstrated a clear reduction of viable cells or low RNA yields or no RNA yield, compared to untreated control cells, were called cytotoxic. No cytotoxicity was observed for non-teratogenic compounds, and only teratogens showed cytotoxic effects (**Table 10**). Most compounds showed no cytotoxicity at both the 1x C_{max} and 20x concentrations, except for TSA, which was cytotoxic at 20x.

Out of the tested compounds, only five showed positive results for cytotoxicity. For all other compounds, the RNA quantification results indicated that, after 24 hours of incubation, there was no significant cytotoxicity of the substances investigated in **Table 9**, since enough RNA was obtained to proceed with Affymetrix analysis.

3.3.1 Insights from principal component analysis

To obtain a preliminary understanding of the effects of substances on gene expression, we conducted a principal component analysis (PCA) using the gene expression data (**Figure 3**). Two data sets were analyzed: the first set included the expression of all 54,675 probe sets, while the second set focused on the 1000 probe sets with the highest variance across all samples. Although there were some differences in the positioning of individual substances between the two plots, the overall distribution and relative distances of substances remained similar. The PCA revealed that non-teratogenic substances formed a closely clustered group, partially intermixed with a subset of teratogenic substances, while the teratogenic substances were more widely spread along both PC1 and PC2. In the top 1000 PCA, most non-teratogenic substances formed a central cluster near the zero point on both axes, which also included several teratogenic substances at the 1x C_{max} concentration. However, in the PCA using all probe sets, retinol, sucralose, and diphenhydramine appeared slightly distant from the non-teratogenic cluster.

The analysis of the top 1000 probe sets demonstrated that principal components 1 and 2 explained with a greater proportion (37 %) of the variances between substances compared to the PCA involving all 54,675 probe sets (27 %) (**Figure 3A** and **3B**, respectively). Moreover, the clustering of non-teratogenic compounds appeared to be more compact in the top-1000 analysis than in the analysis

with all probe sets, indicating that the selection of the 1000 probe sets with the highest variance could be a preferable option for constructing a classifier. This suggests that these specific probe sets may provide valuable discriminatory information for distinguishing between teratogenic and non-teratogenic compounds.

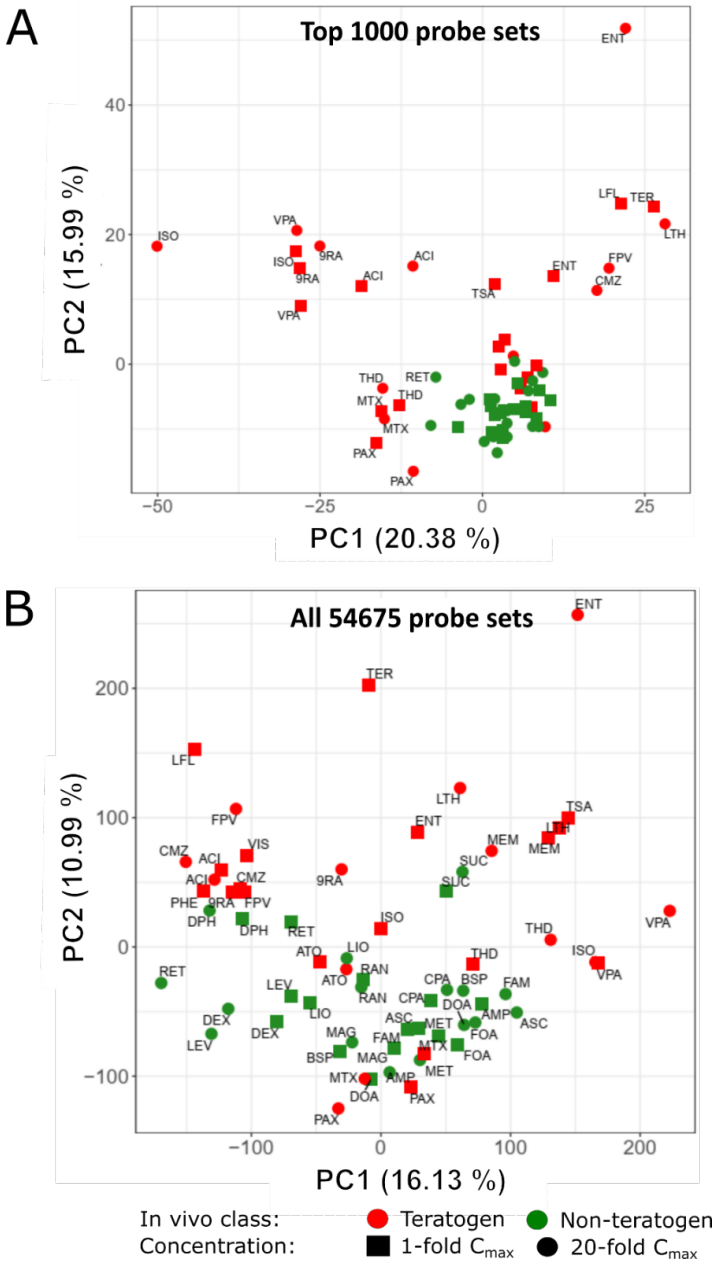

Figure 3: Principal Component Analysis (PCA) of Teratogenic and Non-teratogenic Compounds. Presented here are two PCA plots showcasing the distribution of teratogenic and non-teratogenic compounds. Plot (A) displays the analysis of the top 1000 probe sets with the highest variance across the mean of condition-wise samples, while plot (B) includes all 54,675 probe sets. The green and red tags represent in vivo non-teratogens and teratogens, respectively. Squares and circles indicate 1-fold C_{max} and 20-fold C_{max} concentrations, respectively. The x-axis represents the principal component (PC) 1, while PC2 is represented on the y-axis. The percentages in parentheses indicate the proportion of explained variance for each respective PC. Compound abbreviations can be found in **Table 9**."

3.3.2 Significantly deregulated genes exposed to non-teratogenic compounds after 24 h

To identify significant changes within the gene arrays' 54,675 probe sets, we analyzed the test compounds induced gene expression changes in all differentiated samples on day1. This involved processing the data using algorithm-based statistical multiarray methods and visualizing the results in volcano plots (**Figure 4 - Figure 7**). In these plots, each black dot represented a single probe set, with its test compound induced fold-change compared to the untreated control condition displayed on the x-axis in logarithmic form. The corresponding "limma" p-value, also in logarithmic form, was shown on the y-axis. Probe sets meeting two criteria were considered both statistically significant and biologically relevant: an FDR-adjusted p-value < 0.05 and a deregulation of more than two-fold up or down. These probe sets were highlighted in red to denote their significance.

In the non-teratogen condition, a considerable number of probe sets showed deregulation. The majority of these probesets ranged between a log2(FC) of 0 and 0.5, with some even reaching log2(FC) of 1. However, an all-or-nothing situation was not observed because some non-teratogenic compounds also induced significant expression changes. Ascorbic acid at 20x C_{max}, magnesium chloride at 1x C_{max} and 20x C_{max}, and sucralose at 1x C_{max} and 20x C_{max} exhibited higher upregulated or downregulated probe sets. Specifically, magnesium chloride 1x and 20x C_{max}, sucralose 1x and 20x C_{max} , showed the following up-/downregulated probe sets 270up/126down, 90up/137down, 461up/333down and 153up/38down, 136up/30down respectively. An overview of the number of upregulated and downregulated probe sets at 1x and 20x C_{max} is provided in **Table 10**. Overall, non-teratogenic substances did not induce significant gene expression changes after a 24-hour exposure, except for a few alterations observed in specific samples.

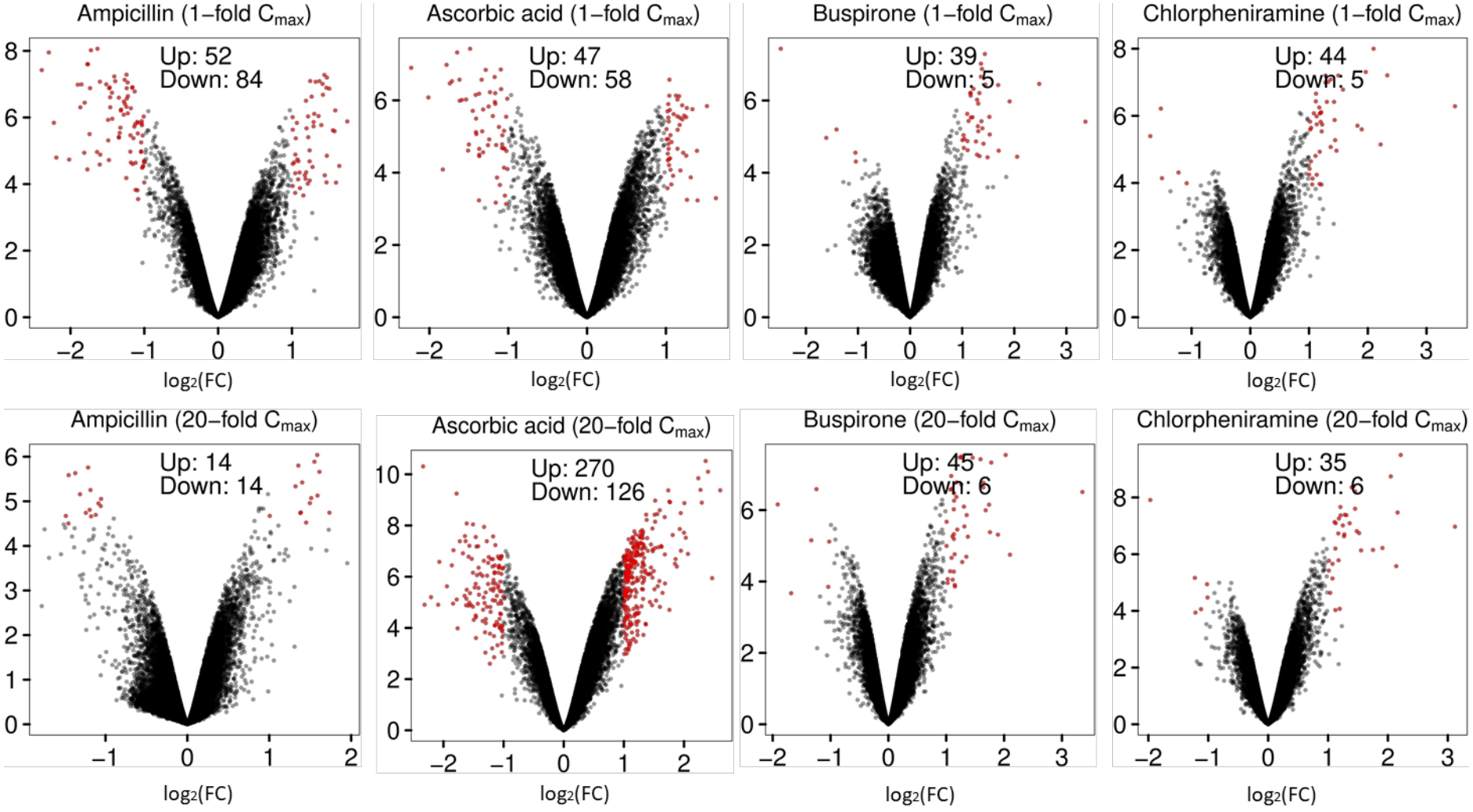

Figure 4: Genome-wide gene expression changes caused by ampicillin, ascorbic acid, buspirone and chlorpheniramine at the 1x and 20x C_{max}. The figure illustrates the fold-change on the x-axis in its logarithmic form (log2(FC)) and the corresponding, not FDR-adjusted "limma"-p-value on the y-axis in its negative, logarithmic form (-log10(p-value)) of each probe set-mean-value from n=3 independent biological experiments. Highlighted in red are all probe sets, which had an FDR-adjusted p-value of <0.05 and were at least two- fold up or ½-fold down regulated.

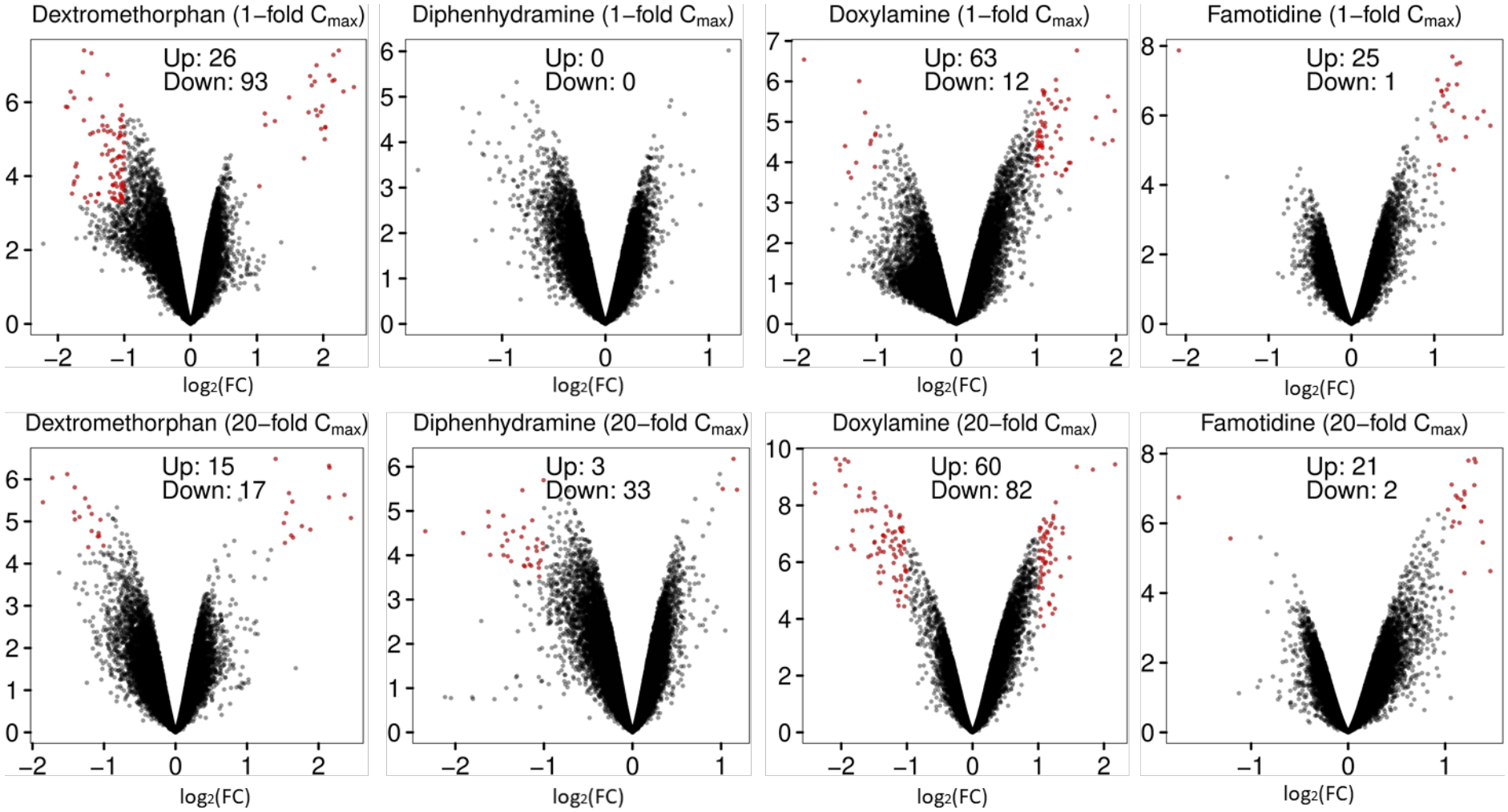

Figure 5: Genome-wide gene expression changes caused by by dextromethorphan, diphenhydramine, doxylamine and famotidine at the 1x and 20x C_{max}. The figure illustrates the fold-change on the x-axis in its logarithmic form (log2(FC)) and the corresponding, not FDR-adjusted "limma"-p-value on the y-axis in its negative, logarithmic form (-log10(p-value)) of each probe set-mean-value from n=3 independent biological experiments. Highlighted in red are all probe sets, which had an FDR-adjusted p-value of <0.05 and were at least two- fold up or ½-fold down regulated.

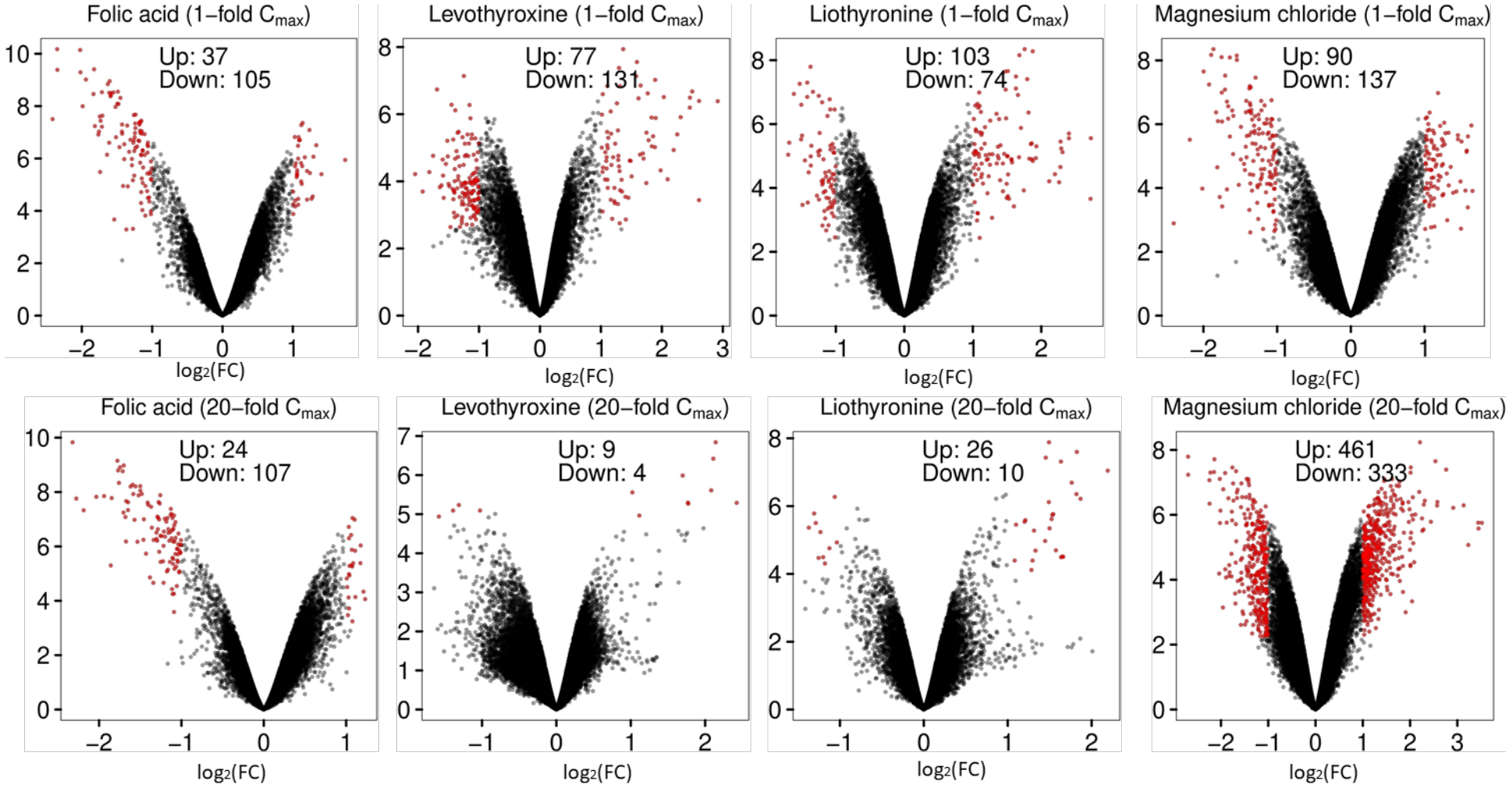

Figure 6: Genome-wide gene expression changes caused by by folic acid, levothyroxine, liothyronine and magnesium chloride at the 1x and 20x C_{max}. The figure illustrates the fold-change on the x-axis in its logarithmic form (log2(FC)) and the corresponding, not FDR-adjusted "limma"-p-value on the y-axis in its negative, logarithmic form (-log10(p-value)) of each probe set-mean-value from n=3 independent biological experiments. Highlighted in red are all probe sets, which had an FDR-adjusted p-value of <0.05 and were at least two- fold up or ½-fold down regulated.

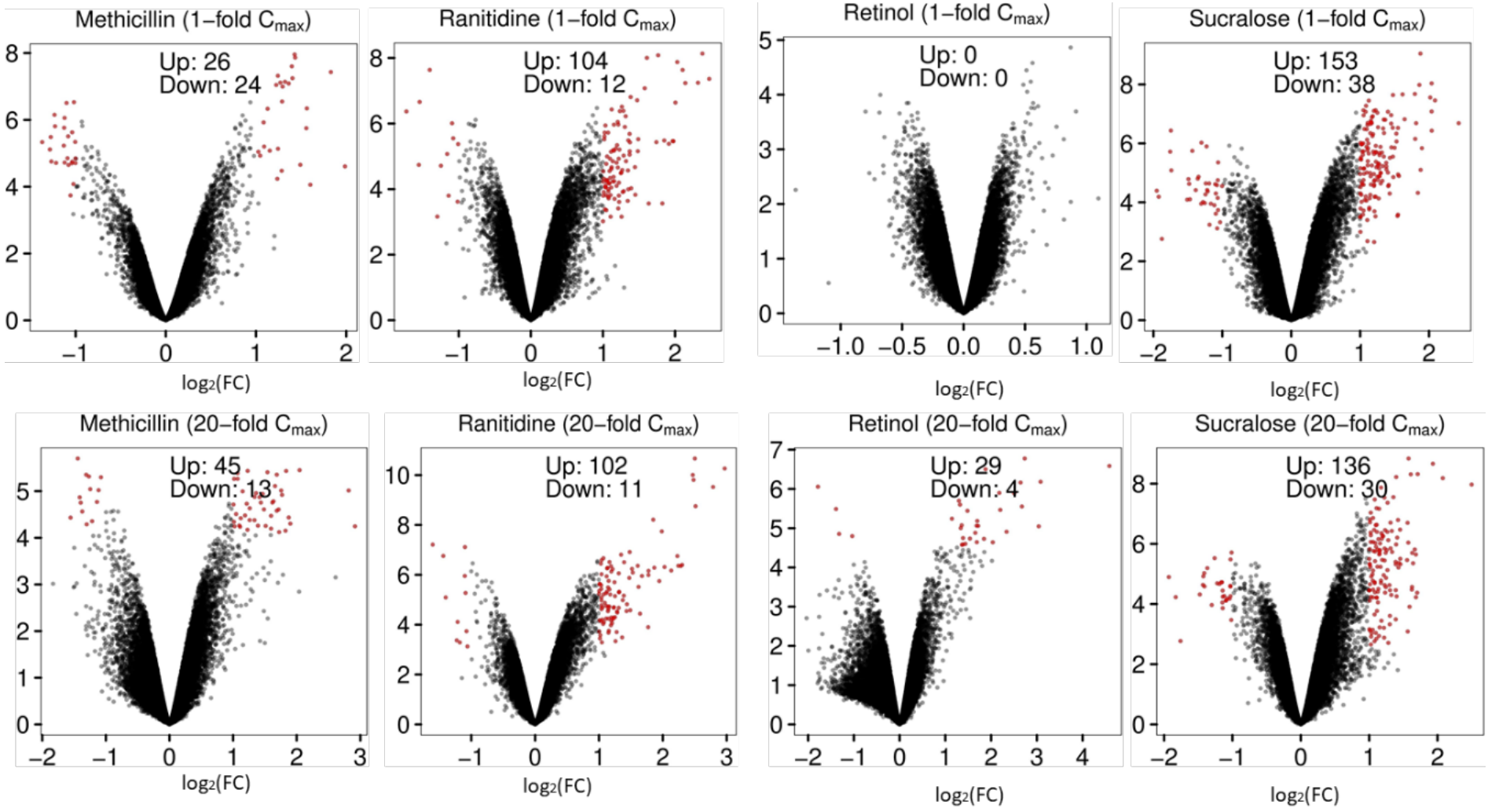

Figure 7: Genome-wide gene expression changes caused by by methicillin, ranitidine, retinol and sucralose at the 1x and 20x C_{max}. The figure illustrates the fold-change on the x-axis in its logarithmic form (log2(FC)) and the corresponding, not FDR-adjusted "limma"-p-value on the y-axis in its negative, logarithmic form (-log10(p-value)) of each probe set-mean-value from n=3 independent biological experiments. Highlighted in red are all probe sets, which had an FDR-adjusted p-value of < 0.05 and were at least two- fold up or ½-fold down regulated.

3.3.3 Significantly deregulated genes exposed to teratogenic compounds after 24 h

We followed the same analysis approach used for the non-teratogenic compounds to identify significant gene expression alterations in teratogen-exposed conditions. However, for teratogenic conditions where a strong cytotoxic effect was observed, a genome-wide gene expression analysis could not be conducted since no RNA was able to be collected. Therefore, measurements were not possible for actinomycin D, doxorubicin, panobinostat, vinblastine, and vorinostat.

Twelve teratogenic substances were measured at both the 1x and the 20x C_{max}. Among them, seven test subsances induce a strong transcriptomic response at both concentrations: at the 1x C_{max}, treatment with 9-cis retinoic acid, acitretin, entinostat, isotretinoin, lithium chloride, methotrexate and valproic acid led to a deregulation of 434up/297down, 570up/138down, 579up /156down and 1460up/567down, 395up/65down, 393up/359down, and 882up/407 down significant probe sets, respectively, and at the 20x C_{max} to 459up/209down, 437up/221down, 2916up /1336down, and 1154up/536down, 1176up/389down 359up/471down, and 1827up/731down, significantly deregulated probe sets, respectively (**Figure 8, Figure 9 & Figure 10**). Carbamazepine and favipiravir did not induce significant gene expression changes at the 1x C_{max}; they deregulated 551/431down probe sets at 10x C_{max} and 686up/405down probe sets at 20x C_{max}, respectively (**Figure 8 & Figure 9**). The compounds leflunomide, teriflunomide, and trichostatin A that were tested only at the 1x C_{max} due to limited solubility and induced 994up/2334down, 881up/620down and 548up/36down significantly deregulated probe sets respectively. The teratogenic substances methylmercury, paroxetine, and thalidomide induced similar significant probe sets at the 1x and the 20x C_{max} conditions. More specifically, at 1x C_{max} they induced 328up/49down, 157up/281down and 181up/48down, significant probe sets respectively, and at 20x C_{max} 108up/16down, 147up /473down and 190up/105down significant probe sets respectively. Vismodegib at the 1x C_{max} affected only 14up/18down probe sets, and phenytoin did not significantly affect any probe set at the 1x. **Table 10** provides a summary of all probe sets that showed significant deregulation in gene expression.

Overall, compared to non-teratogens, most of the teratogens exhibited a considerable number of significantly deregulated probe sets. However, it is important to mention that a few teratogens, including phenytoin and vismodegibm, did not show significant induction of probe set alterations.

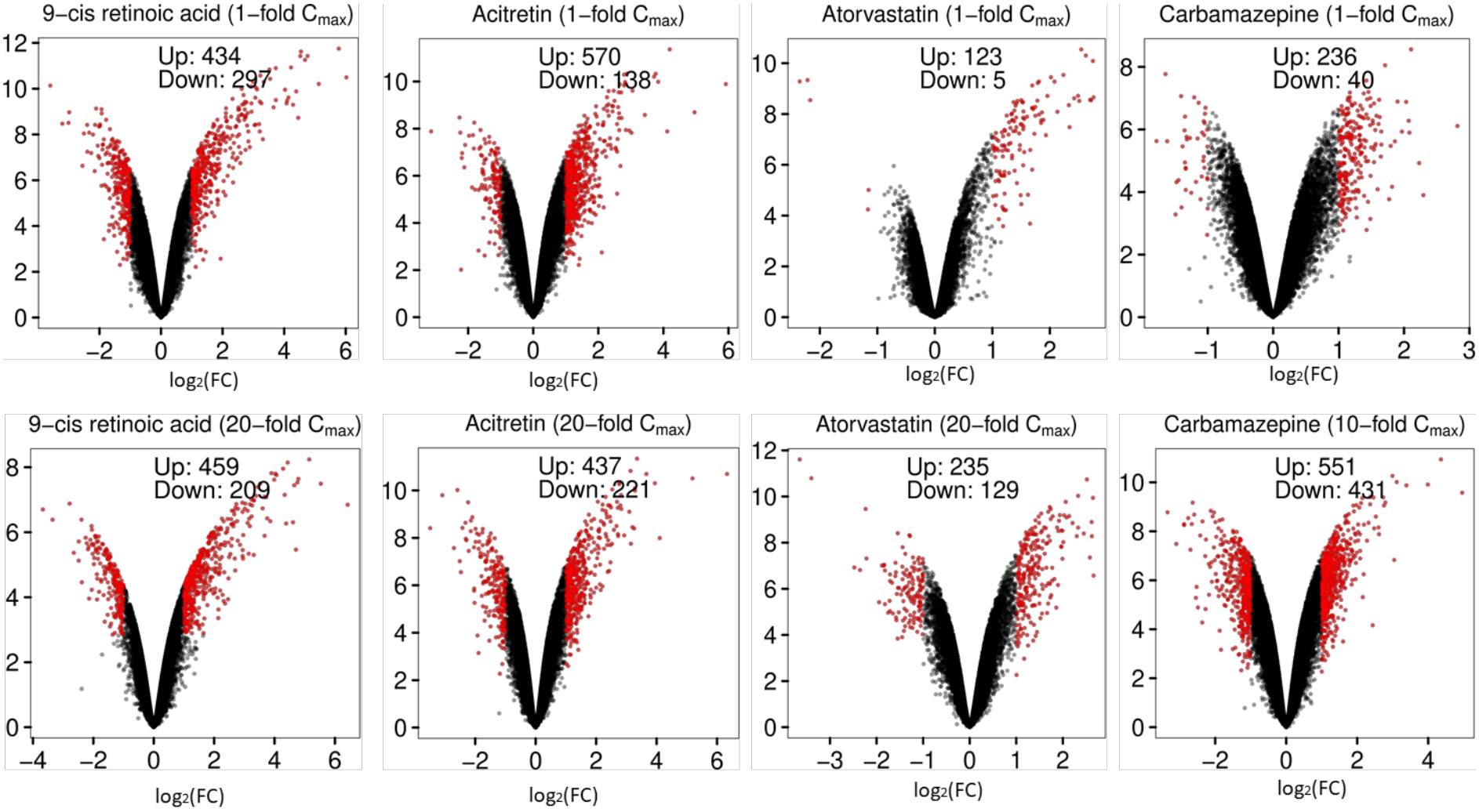

Figure 8: Genome-wide gene expression changes caused by by 9-cis retinoic acid, acitretin, atorvastatin and carbamazepine at the 1x and 20x C_{max}. The figure illustrates the fold-change on the x-axis in its logarithmic form (log2(FC)) and the corresponding, not FDR-adjusted "limma"-p-value on the y-axis in its negative, logarithmic form (-log10(p-value)) of each probe set-mean-value from n=3 independent biological experiments. Highlighted in red are all probe sets, which had an FDR-adjusted p-value of <0.05 and were at least two- fold up or ½-fold down regulated.

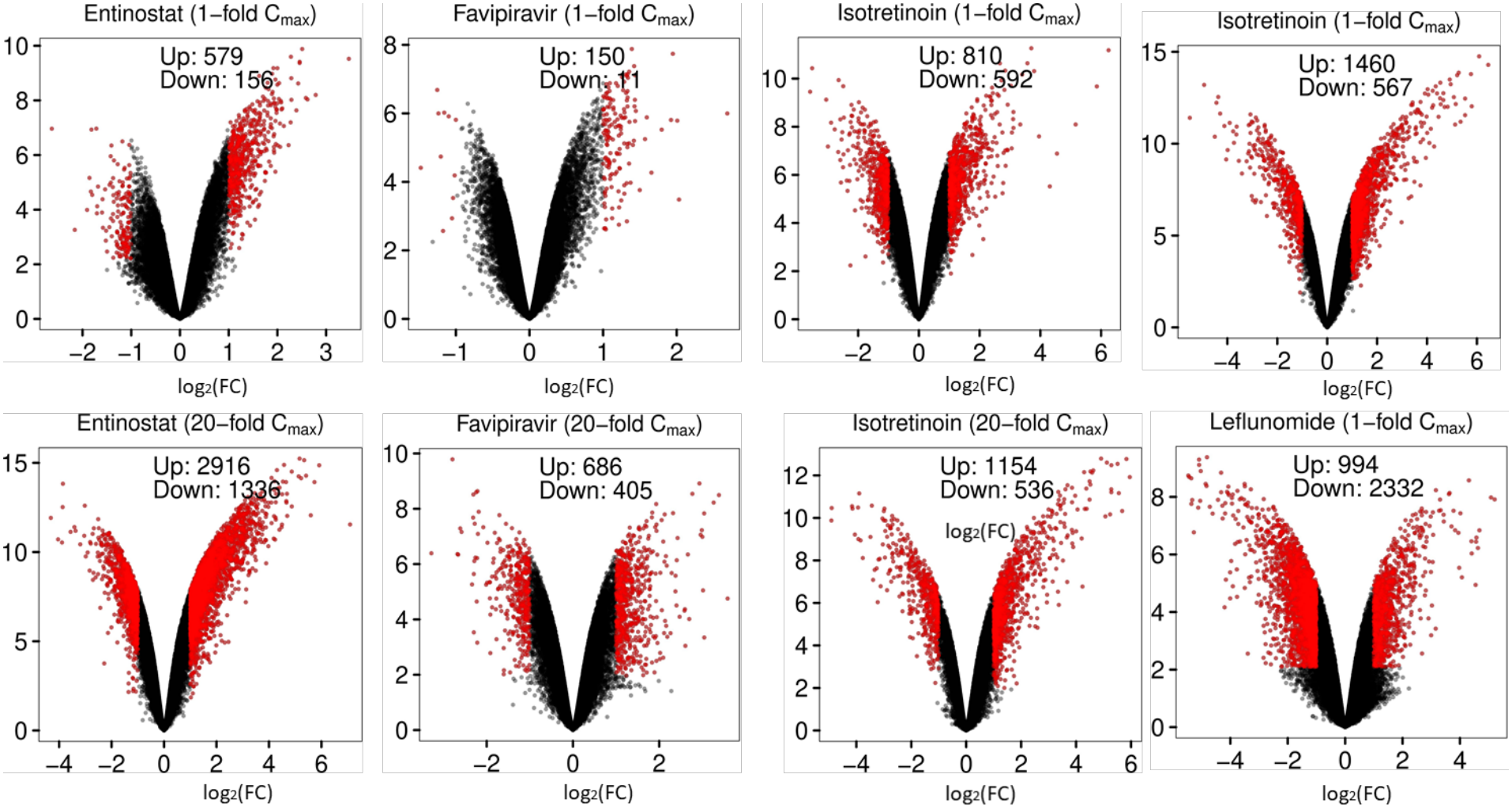

Figure 9: Genome-wide gene expression changes caused by by entinostat, favipiravir, isotretinoin and leflunomide at the 1x and 20x C_{max}. The figure illustrates the fold-change on the x-axis in its logarithmic form (log2(FC)) and the corresponding, not FDR-adjusted "limma"-p-value on the y-axis in its negative, logarithmic form (-log10(p-value)) of each probe set-mean-value from n=3 independent biological experiments. Highlighted in red are all probe sets, which had an FDR-adjusted p-value of <0.05 and were at least two-fold up or ½-fold down regulated.

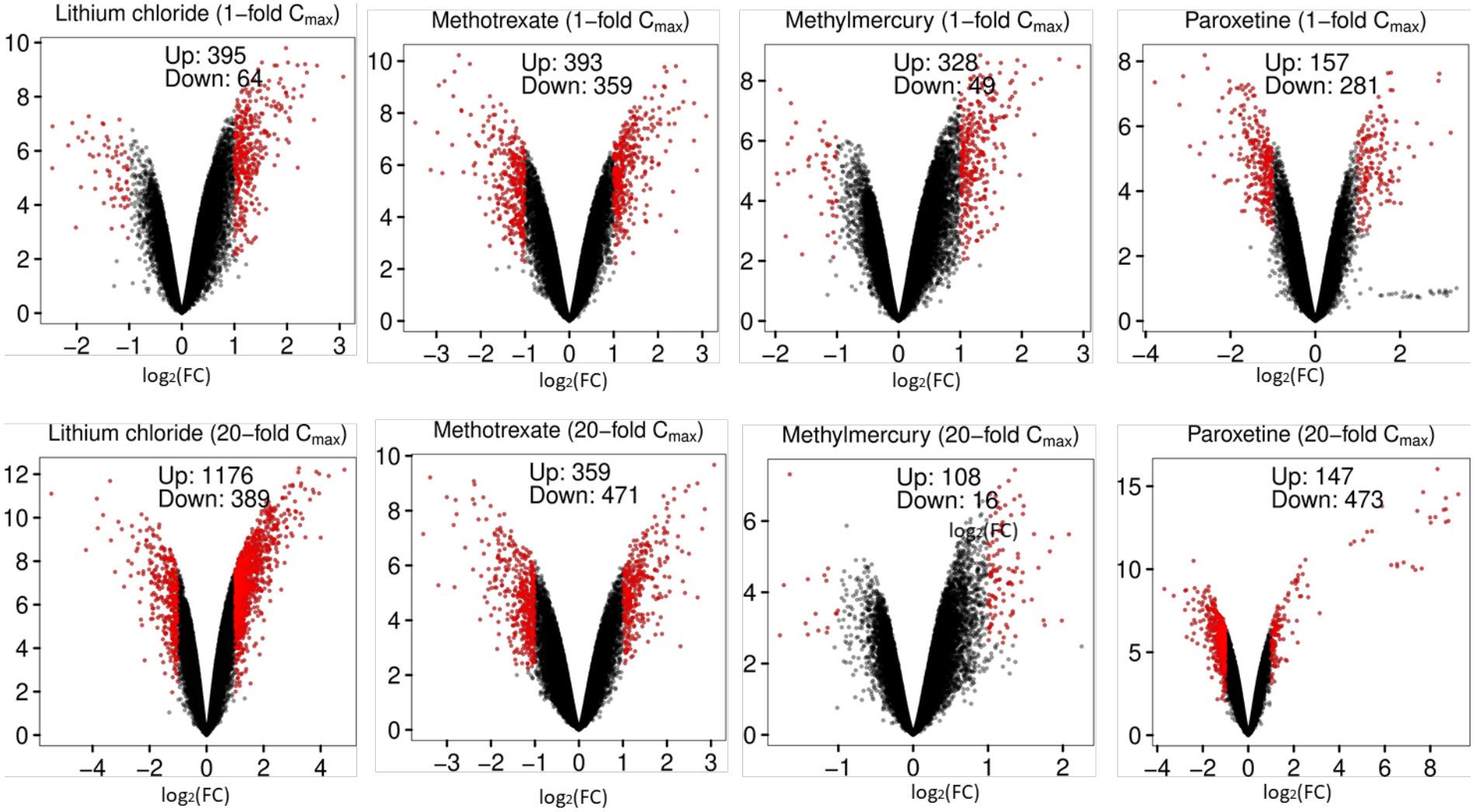

Figure 10: Genome-wide gene expression changes caused by lithium chloride, methotrexate, methylmercury and paroxetine at the 1x and 20x C_{max}. The figure illustrates the fold-change on the x-axis in its logarithmic form (log2(FC)) and the corresponding, not FDR-adjusted "limma"-p-value on the y-axis in its negative, logarithmic form (-log10(p-value)) of each probe set-mean-value from n=3 independent biological experiments. Highlighted in red are all probe sets, which had an FDR-adjusted p-value of < 0.05 and were at least two- fold up or ½-fold down regulated.

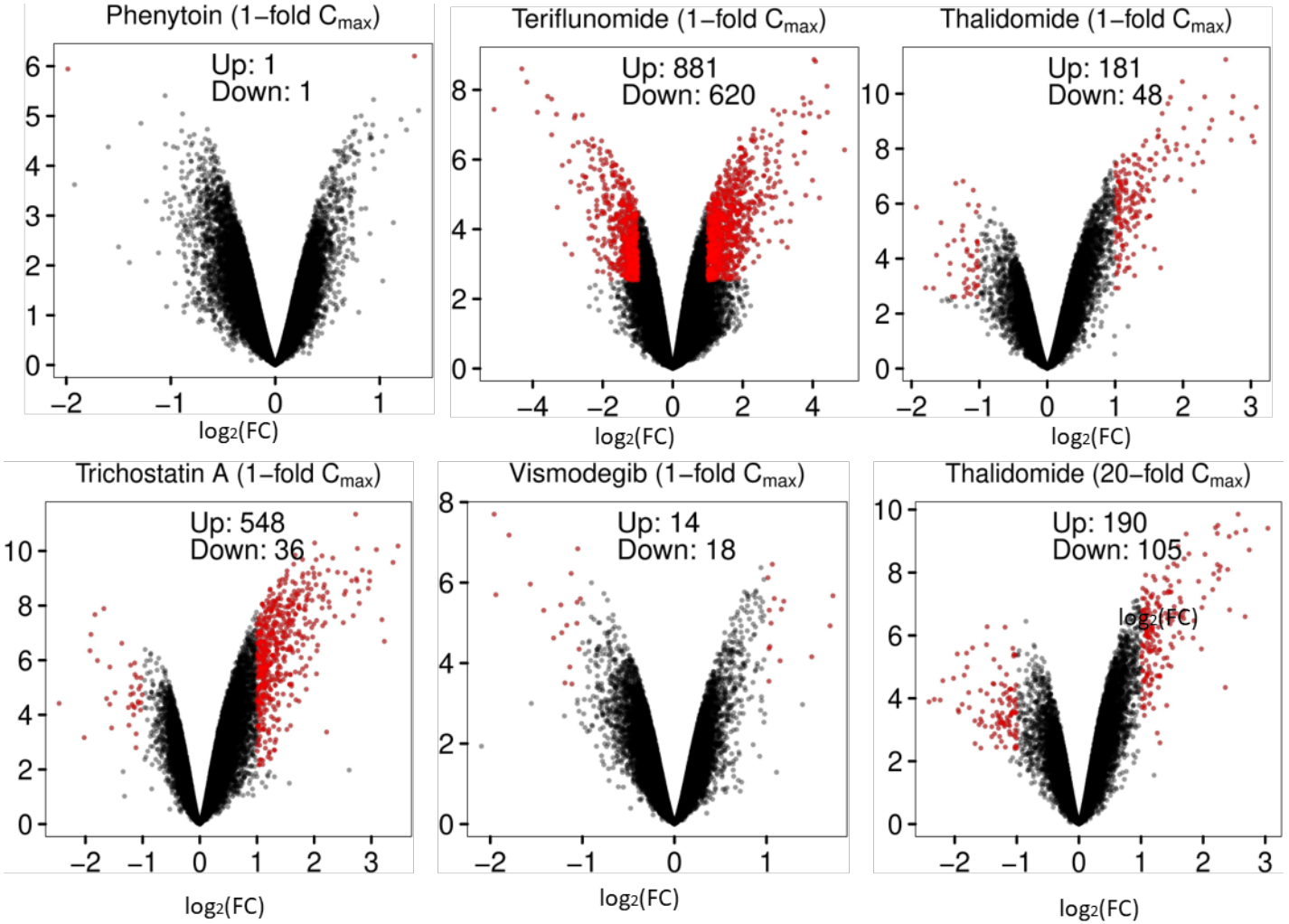

Figure 11: Genome-wide gene expression changes caused by by phenytoin, teriflunomide, thalidomidet, trichostatin a and Vismodegib. The figure illustrates the fold-change on the x-axis in its logarithmic form (log2(FC)) and the corresponding, not FDR-adjusted "limma"-p-value on the y-axis in its negative, logarithmic form (-log10(p-value)) of each probe set-mean-value from n=3 independent biological experiments. Highlighted in red are all probe sets, which had an FDR-adjusted p-value of < 0.05 and were at least two-fold up or ½-fold down regulated.

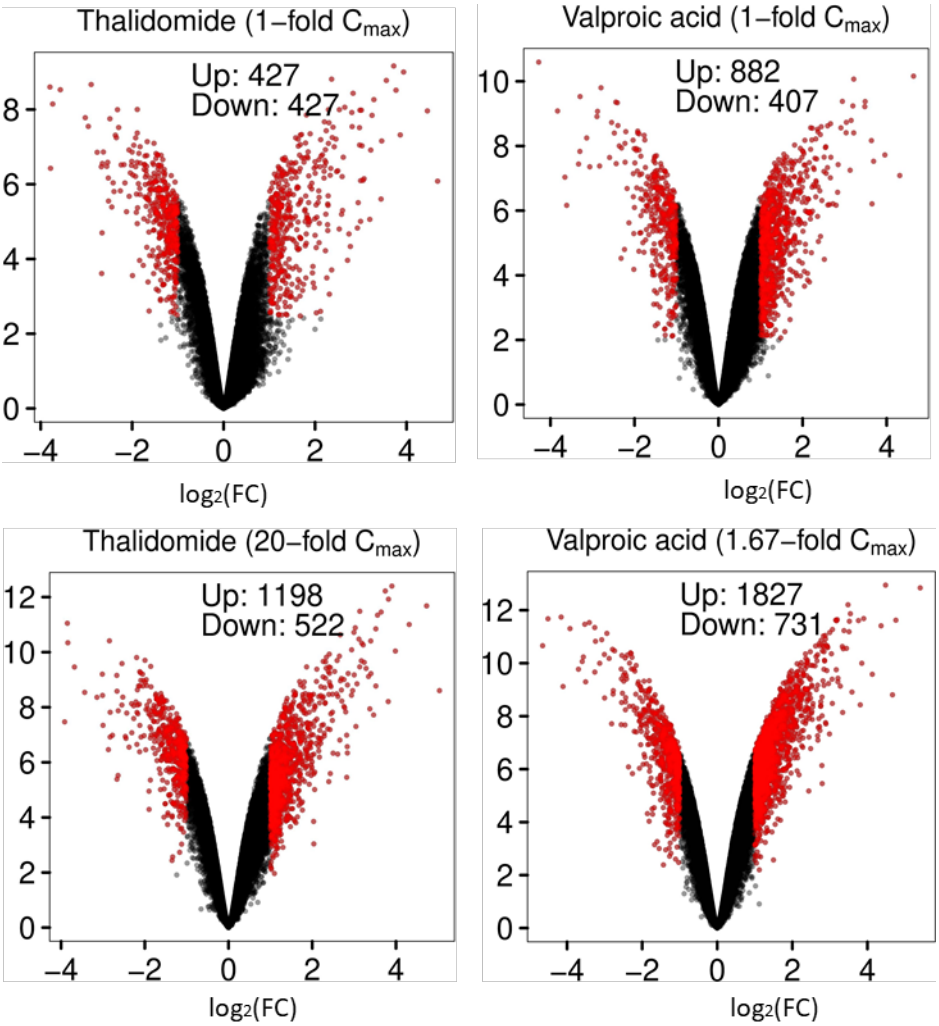

Figure 12: Genome-wide gene expression changes caused by by methicillin, ranitidine, retinol and sucralose at the 1x and 20x C_{max}. The figure illustrates the fold-change on the x-axis in its logarithmic form (log2(FC)) and the corresponding, not FDR-adjusted "limma"-p-value on the y-axis in its negative, logarithmic form (-log10(p-value)) of each probe set-mean-value from n=3 independent biological experiments. Highlighted in red are all probe sets, which had an FDR-adjusted p-value of < 0.05 and were at least two- fold up or ½-fold down regulated.

Table 10: Cytotoxicity and number of significantly deregulated probe sets in compound-exposed cells

			Number of up-/ downregulated probe sets[c]			
	Cytotoxicity[b]		1-fold C_{max}[a]		20-fold C_{max}[a]	
Compounds	1-fold C_{max}[a]	20-fold C_{max}[a]	Up	Down	Up	Down
Non-teratogens						
Ampicillin	No	No	52	84	14	14
Ascorbic acid	No	No	47	58	270	126
Buspirone	No	No	39	5	45	6
Chlorpheniramine	No	No	44	5	35	6
Dextromethorphan	No	No	26	93	15	17
Diphenhydramine	No	No	0	0	3	33
Doxylamine	No	No	63	12	60	82
Famotidine	No	No	25	1	21	2
Folic acid	No	No	37	105	24	107
Levothyroxine	No	No	77	131	9	4
Liothyronine	No	No	103	74	26	10
Magnesium chloride	No	No	90	137	461	333
Methicillin	No	No	26	24	45	13
Ranitidine	No	No	104	12	102	11
Retinol	No	No	0	0	29	4
Sucralose	No	No	153	38	136	30
Teratogens						
9-cis-retinoic acid	No	No	434	297	459	209
Acitretin	No	No	570	138	437	221
Actinomycin D	Yes	Yes	toxic	toxic	toxic	toxic
Atorvastatin	No	No	123	5	235	129
Carbamazepine	No	No[d]	236	40	551[d]	431[d]
Doxorubicin	Yes	Yes	toxic	toxic	toxic	toxic
Entinostat	No	No	579	156	2916	1336
Favipiravir	No	No	150	11	686	405
Isotretinoin	No	No	1460	567	1154	536
Leflunomide	No	---[e]	994	2332	---[d]	---[d]
Lithium chloride	No	No	395	64	1176	389
Methotrexate	No	No	393	359	359	471
Methylmercury	No	No	328	49	108	16
Panobinostat	Yes	Yes	toxic	toxic	toxic	toxic
Paroxetine	No	No	157	281	147	473
Phenytoin	No	---[d]	1	1	---[d]	---[d]
Teriflunomide	No	---[d]	881	620	---[d]	---[d]
Thalidomide	No	No	181	48	190	105
Trichostatin A	No	Yes	548	36	toxic	toxic
Valproic acid	No	No[e]	882	407	1827[d]	731[d]
Vinblastine	Yes	Yes	toxic	toxic	toxic	toxic
Vismodegib	No	---[d]	14	18	---[d]	---[d]
Vorinostat	Yes	Yes	toxic	toxic	toxic	toxic

[a] Maximal plasma or blood concentrations which were usually observed in humans after the administration of therapeutic compound doses. Fetal enrichment was considered if relevant.

[b] Yes, if the compound was highly cytotoxic; No, if the compound showed no cytotoxicity

[c] Gene array-probe sets that were deregulated with an FDR-adjusted p-value < 0.05 and an absolute fold-change > 2 compared to untreated control cells

[d] Carbamazepine and VPA were tested at 10-fold and 1.67-fold C_{max}, respectively, instead of 20-fold C_{max}; leflunomide, phenytoin, teriflunomide and vismodegib were tested at 1-fold C_{max} only because of limited solubility.

3.4 Cytotox 1000 classifier and SPS classifer (This part is from our publication Cherianidou et al 2021 [86])

Two approaches were employed to classify the test compounds based on gene expression and cytotoxicity. The first method, referred to as the ”SPS-procedure,” categorized a compound as test-positive or test-negative based on the number of significantly deregulated probe sets (SPS) compared to a specific threshold. Accuracy was highest using a threshold of 228 significantly deregulated probe sets (SPS), which was then applied in subsequent analyses (**Figure 13A**). Using the SPS-procedure, all non-teratogens were correctly classified as test-negative, except for ascorbic acid and magnesium chlorde, while the teratogens were correctly classified as test-positive, except for atorvastatin, favipiravir, methylmercury, phenytoin and vismodegib, which were falsely classified as test-negative. Cytotoxic conditions were considered positive and integrated into the classification by assigning them the highest observed number of SPS, which was 4252 SPS for entinostat at 20-fold C_{max} (**Table 10**).

The second approach involved penalized logistic regression using the top 1000 probe sets with the highest variance, referred to as the ”top-1000-procedure.” With this method, all teratogens, except atorvastatin, were correctly classified as test-positive, while the non-teratogens were correctly classified as test-negative, except for sucralose, Diphenhydramine and retinol, which were falsely classified as test-positive (**Figure 13B**). Detailed information on predicted probabilities and classification results can be found in **Tables S1** and **S2** in the **Supporting Information**.

To determine which procedure, SPS or top-1000, was superior in distinguishing teratogenic from non-teratogenic compounds, as well as whether 1-fold or 20-fold C_{max} and cytotoxicity information should be considered, further analysis was conducted. The top-1000-procedure yielded higher values for AUC, accuracy, and sensitivity compared to the SPS-procedure (**Table 11**). Classification based on gene expression data at 1-fold C_{max} demonstrated slightly higher AUC, accuracy, and sensitivity compared to 20-fold C_{max} for both procedures. Considering cytotoxicity alone resulted in relatively low metrics values. However, combining cytotoxicity information with gene expression consistently increased AUC, accuracy, and sensitivity for both the SPS- and top-1000-procedure compared to gene expression analysis alone. The highest values for AUC, accuracy, and sensitivity (0.96, 0.92, and 0.96, respectively) were achieved with the top-1000-procedure using gene expression data combined with cytotoxicity at the 1-fold C_{max} concentration. However, the specificity was only 0.88. On the other hand, the SPS-procedure consistently achieved the highest specificity of 1 at the 1-fold C_{max}. When considering cytotoxicity alone, a specificity of 1 was obtained, but with very low sensitivity, accuracy, and AUC.

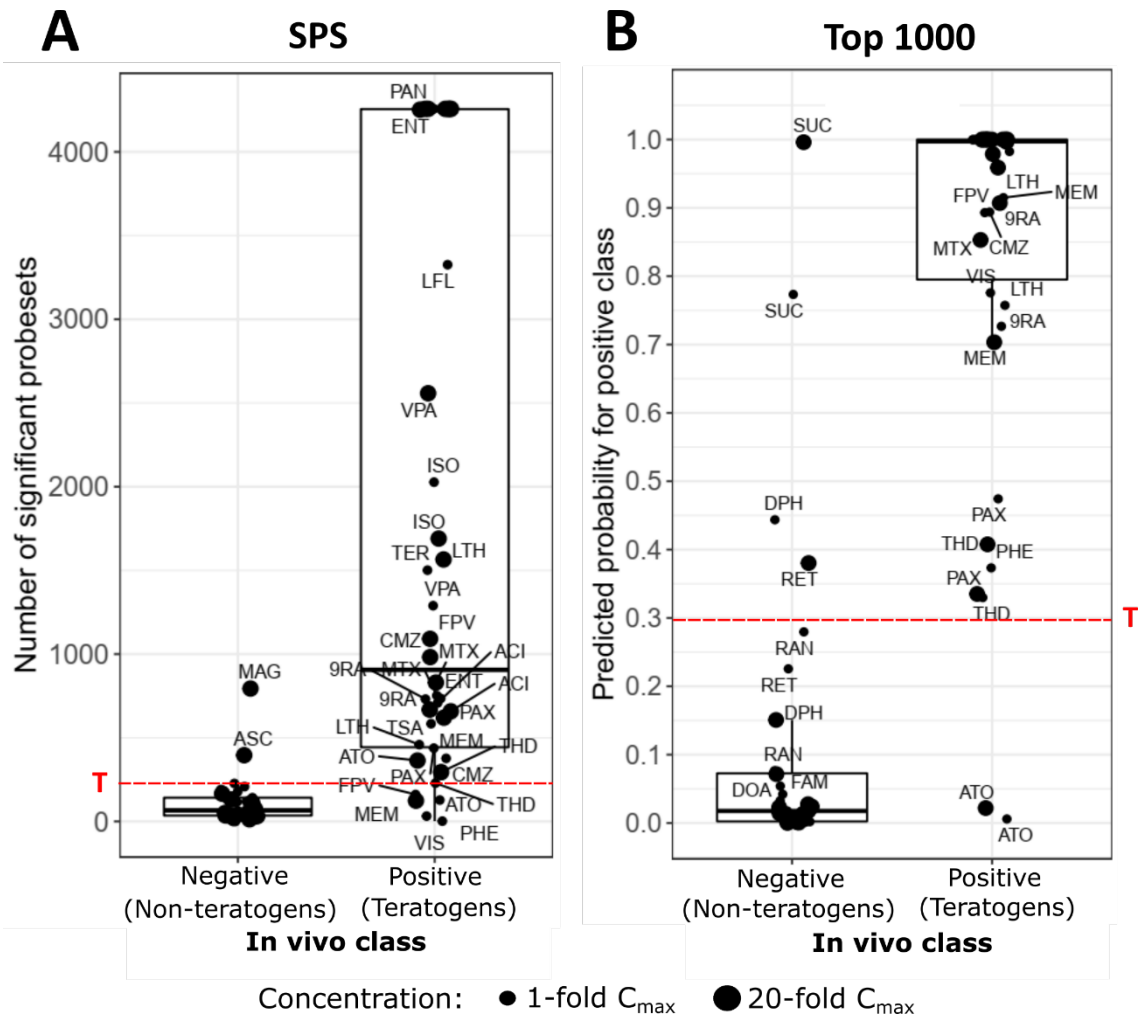

Figure 13: Classification of the teratogenic and non-teratogenic compounds by a classifier based on the number of significantly deregulated probe sets (A) and a penalized logistic regression based classifier based on the 1,000 genes with the highest variability (B).

The classifier "SPS" compares the number of significant probe sets (SPS) to the in vivo class. The number of SPS is given in the y-axis and the x-axis marks the in vivo class for negative (non-teratogen) and positive (teratogen) conditions. The threshold T at 228 SPS separates negative and positive in vitro test results for the calculation of accuracy, sensitivity and specificity. Key rules of the SPS classifier:

- The number of SPS was the sum of up- and downregulated probe sets with an FDR-adjusted p-value<0.05 and an absolute fold-change>2 compared to control conditions.
- The number of SPS in cytotoxic conditions corresponded to entinostat at 20-fold C_{max} (i.e. 4,252 SPS) which showed the highest number of SPS across all samples. The classifier "Top 1000" predicted the probability for positive class (PPPC) of every condition based on the 1000 probe sets with the highest variance among the genome-wide gene expression data. The PPPC is given on the y-axis and the x-axis marks the true (in vivo) class for negative (non-teratogen) and positive (teratogen) conditions. The threshold T at 0.3 PPPC separates negative and positive in vitro test results for the calculation of accuracy, sensitivity and specificity. Key rules of the Top 1000 classifier:
- The calculation of PPPC was based on a leave-one-out-cross-validation-algorithm and the 1000 probe sets with the highest variance.
- Cytotoxic conditions were considered to be 100 % positive (predicted probability of 1.0).

Table 11: Performance metrics of the classifiers

		Classifier SPS			Classifier Top 1000		
Metric	C_{max}	Cytotoxicity only	Gene expression only	Cytotoxicity and gene expression	Cytotoxicity only	Gene expression only	Cytotoxicity and gene expression
AUC	1-fold	0.61	0.87	0.90	0.61	0.94	0.96
	20-fold[a]	0.63	0.86	0.89	0.63	0.93	0.95
Accuracy	1-fold	0.54	0.77	0.90	0.54	0.79	0.92
	20-fold[a]	0.56	0.72	0.87	0.56	0.77	0.92
Sensitivity	1-fold	0.22	0.61	0.83	0.22	0.74	0.96
	20-fold[a]	0.26	0.61	0.87	0.26	0.70	0.96
Specificity	1-fold	1.00	1.00	1.00	1.00	0.88	0.88
	20-fold[a]	1.00	0.88	0.88	1.00	0.88	0.88

- Cytotoxicity only: Only cytotoxicity data were considered for the calculation of the metrics, i.e., cytotoxic conditions were considered as positive and non-cytotoxic conditions as negative test results.
- Gene expression only: Only gene expression data were considered for the calculation of the metrics
- Cytotoxicity and gene expression: All data for cytotoxicity as well as for gene expression were considered for the calculation of the metrics
- AUC (Area-under-curve): For each possible cut-off used as threshold, predictions were made for each of the conditions, based on which sensitivity and specificity were calculated. The ROC-curve (receiver operator characteristic) was obtained by plotting all pairs of (1-specificity) and sensitivity against each other. The AUC was determined as the area under this ROC-curve.
- Accuracy: Ratio of correct predictions ((true negatives and positives) / (true and false negatives and positives)
- Sensitivity: Ratio of detected teratogens (true positives/(false negatives + true positives)
- Specificity: Ratio of detected non-teratogens (true negatives / (true negatives + false positives)

[a] Including 10-fold C_{max} carbamazepine, 1.67-fold C_{max} VPA and 1-fold C_{max} samples of leflunomide, phenytoin, terifluno-mide and vismodegib

3.5 Biological interpretation of the transcriptomics (This part is from our publication Cherianidou et al 2021 [86])

To investigate the influence of teratogens and non-teratogens on gene expression, we examined the deregulated probe sets affected by these compounds. At the plasma peak concentration (1-fold C_{max}), a higher number of probe sets were significantly deregulated by the teratogens (n = 7869) compared to the non-teratogens (n = 975) (**Figure 14A**). Interestingly, there was a considerable overlap between the probe sets deregulated by the non-teratogens and those affected by the teratogens, with 797 probe sets being common to both groups (**Figure 14A**). Similar observations were made when analyzing the up- and downregulated probe sets separately (**Figure S1A & S2A**). The teratogens exhibited a much larger number of deregulated probe sets (n = 4869) compared to the non-teratogens (n = 559) in the upregulated category, as well as in the downregulated category (n = 4135 teratogens, n = 445 non-teratogens).

Similar trends were observed at 20 times the plasma peak concentration. The teratogens caused a higher number of significantly deregulated probe sets (n = 1396) compared to the non-teratogens (n = 1443). Interestingly, a substantial fraction of the probe sets affected by the non-teratogens (1048 of the 1396 probe sets) overlapped with those influenced by the teratogens (**Figure S3A**). When examining the up- and downregulated probe sets separately (**Figures S4A & S5A**), it was found that the teratogens exhibited a larger number of deregulated probe sets (n = 6384) compared to the non-teratogens (n = 990) in the upregulated category, as well as in the downregulated category (n = 3523 teratogens, n = 500 non-teratogens).

To investigate the biological functions, we differentiated three gene sets, based on their response to teratogens and non-teratogens. These sets were named the ”overlap gene set” for genes affected by both teratogens and non-teratogens, the ”teratogen gene set” for genes exclusively altered by teratogens, and the ”non-teratogen gene set” for genes exclusively influenced by non-teratogens. Initially, we examined the probe sets that showed significant deregulation by the highest number of test compounds (**Figure 14B, Supporting Information ”Top genes”**). In the overlap gene set, HOXB3, ACKR3, HOXB1, and PROX1 were the most frequently affected genes, being significantly deregulated by 16 compounds. The teratogen gene set was characterized by the most frequently deregulated genes, namely PROX1, HHEX, and SPR4-IT1, influenced by 11 compounds. Interestingly, PROX1 appeared as a top gene in both the teratogen and overlap gene sets, likely due to the probe set-based analysis where different probe sets were annotated to the same gene, PROX1. In contrast, the non-teratogen gene set had PRKCSH as the most frequently altered gene, influenced by only five compounds.

The genes in the overlap and teratogen gene sets suggest roles in development and differentiation. For instance, HOXB3, ACKR3, HOXB1, and PROX1, the top genes in the overlap gene set, are

transcription factors involved in the development of various tissues [87],[52],[88],[89].

Moreover, PROX1 and HHEX, the most frequently altered genes in the teratogen gene set, are known to participate in developmental processes [88], [89]. Additionally, the long non-coding RNA SPR4-IT1, associated with cancer, influences genes involved in differentiation and proliferation [90].

In contrast, the non-teratogen gene set appears to be associated with a variety of processes. For example, PRKCSH represents the beta-subunit of glucosidase II in the endoplasmic reticulum [91], SSU72 is a phosphatase [91], and PARL encodes a mitochondrial protease [92], suggesting no specific biological motif.

To gain insight into the biological themes underlying the expression changes, we conducted an over-representation analysis of Gene Ontology (GO) groups for the three gene sets (**Figure 14C, Supporting Information "GO analysis"**). The overlap gene set and teratogen gene set showed significant overrepresentation of 63 and 123 GO groups, respectively (**Figure 14C, Supporting Information "GO analysis"**). In contrast, the probe sets exclusively deregulated by non-teratogens did not yield any significantly overrepresented GO groups.

Both the teratogen and overlap gene sets exhibited overrepresentation of developmental processes in several tissues (**Figure 14D**). These included cardiac muscle, primitive streak, adenohypophysis, olfactory bulb, optic cup, and neural crest in the overlap gene set, as well as fat cell, outflow tract, osteoblast, and corticospinal tract in the teratogen gene set. Additionally, both gene sets showed enrichment for general motifs such as regulation of transcription. Analysis of enriched KEGG pathways revealed similar or identical pathways in the overlap and teratogen gene sets. Examples include signaling pathways regulating pluripotency, MAPK signaling pathways, and several cancer-associated pathways (**Figure 14E, Supporting Information "KEGG pathways"**). In contrast, the gene set of non-teratogens did not exhibit any significant overrepresentation of KEGG pathways.

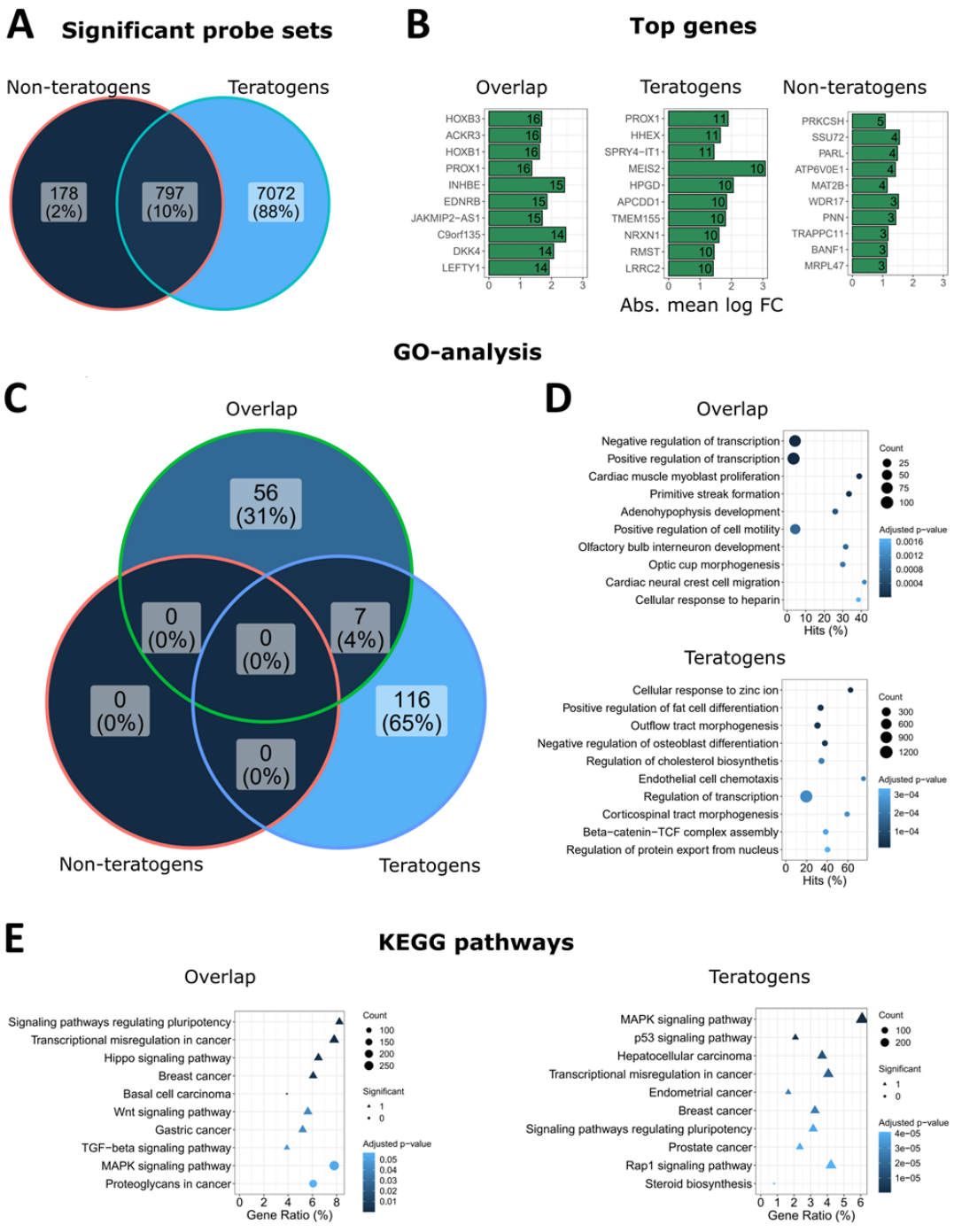

Figure 14: Biological interpretation of genes differentially expressed after exposure of hiPSCs to teratogens and non-teratogens at 1-fold C_{max}. (A) Numbers of SPS (log2 fold change > 1; adjusted p-value < 0.05) induced by non-teratogens and teratogens at the plasma peak concentration (1-fold C_{max}). (B) Top genes in the gene sets of the overlap, teratogens, and non-teratogens from (A). The numbers in the bars indicate the number of compounds that deregulated the specific genes. All differential genes are given in the Supporting Information "Top genes". (C) Numbers of significantly (adj. p-value < 0.05) over-represented GO groups in the overlap, teratogen, and non-teratogen gene sets. (D) Ten GO groups with the lowest adj. p-values in the overlap and teratogen gene sets. No significant GO groups were obtained for the non-teratogen gene set. The names of the GO groups were shortened. Full names and complete GO group lists can be found in the Supporting Information "GO analysis". "Count": number of significant genes from (A) linked to the GO group. "Hits": percentage of significant genes compared to all genes assigned to the GO group. (E) KEGG pathway enrichment analyses of the overlap and teratogen gene sets. The ten KEGG pathways with the lowest adj. p-values are given. No significant KEGG pathways were obtained for the non-teratogen gene set. Full names and complete KEGG-pathway lists are given in the Supporting Information "KEGG pathways". "Count": number of significant genes from (A) linked to the KEGG pathway. "Gene Ratio": percentage of significant genes associated to the pathway compared to the number of all significant genes associated to any pathway.

3.6 Differentiating hiPSCs (SBAD2) into cardiomyocytes: effects of teratogens and non-teratogens

Interestingly, among all the teratogens and non-teratogens, the teratogens ISO (isotretinoin), 9-cis retinoic acid and acitretin acting through the retinoid receptors (RR), completely inhibit the cardiomyogenesis process (no beating cluster could be identified) since no detection of any spontaneous beating areas as well as there was an absence of any cardiac sarcomere.

To investigate the early stages of cardiomyogenesis, we utilized the UKK2 cardiotoxicity test (UKK2-CTT), a cell monolayer-based directed differentiation protocol which is also an extension of the UKK2 protocol that has been discussed in the previous chapters of the Result section. As already mentioned, this protocol involves the sequential activation and inhibition of Wnt/β-catenin signalling, as depicted in **Figure 15A**. By inducing differentiation with the Wnt/β-catenin agonist CHIR, we observed a transition from pluripotency to the three germ layers, as indicated by transcriptome analysis at the end of day2 (**Figure 15B**).

In the first part of this thesis, we demonstrated that using hiPSCs (SBAD2 origin), we could differentiate between 23 teratogens (including ISO) and 16 non-teratogens based on their transcriptomes at the end of day1. These teratogens and non-teratogens were tested at two concentrations: the plasma peak concentration (C_{max}) and the 20-fold C_{max} concentration.

According to the cardiomyogenic UKK2-CTT, CHIR was removed after 24 hours of incubation on day2, and then IWP2, a Wnt/β-catenin small molecule inhibitor, was added to the medium for the following 48 hours on day2. This facilitated the transition from mesodermal cells to cardiac progenitors at day4 of differentiation. On day4, aggregated forms of cells started to appear, forming a network of branches. Only random spots exhibited contractile activity on day8, while on day14, the entire cell monolayer network (**Figure 16A**) displayed synchronous beating. As described previously, this differentiation protocol yielded a cardiomyocyte purity of over 90 % at day14 (as reference Avis Paper).

Interestingly, among all the tested teratogens and non-teratogens (see **Table 12**), teratogens such as ISO, 9-cis retinoic acid, and acitretin, which act through the retinoid receptors (RR), completely inhibited the cardiomyogenesis process. No areas of spontaneous beating or cardiac sarcomere were detected in these cases.

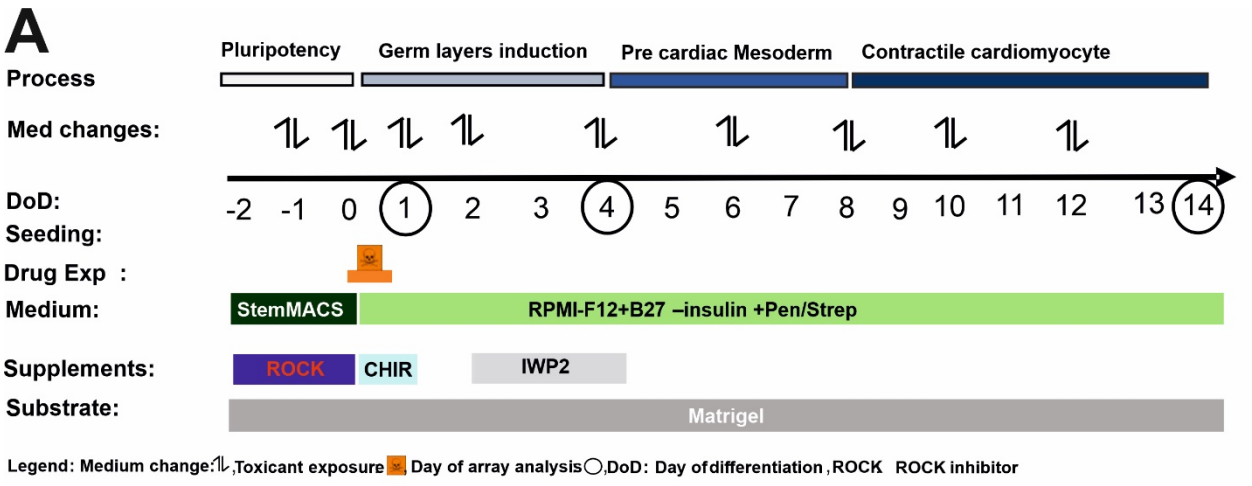

B Up and Down regulated SPS

Condition	up	down
IMR90 1hr CHIR	7	222
IMR90 24hrs CHIR	610	1723
IMR90 48hrs CHIR	1937	1817

C Heatmap of enriched terms across hiPS-IMR90

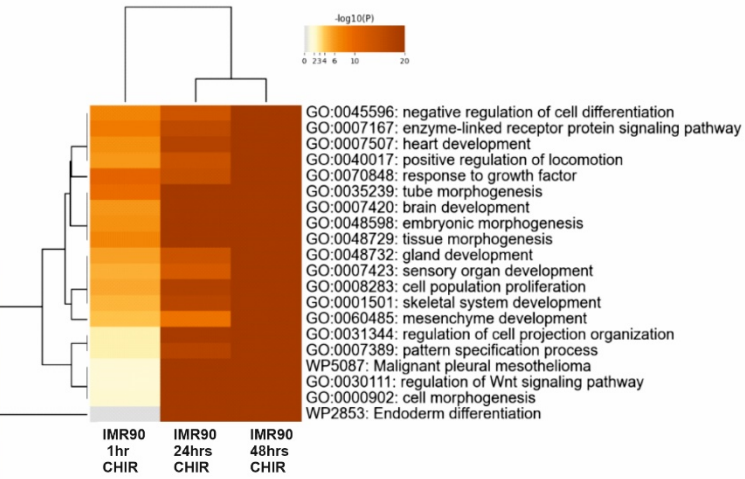

D Mesendoderm genes

Lineage	Gene	Avg(log2) values		
		1hr CHIR	24hr CHIR	48hr CHIR
mesendoderm development	*EOMES*	4.8	11.1	9.6
	MIXL1	4.4	10.7	11.8
	T	6.4	11.7	12.5
	WNT3	3.9	5.75	7.86
	LEF1	4.36	7.4	8.14
	DKK1	4.37	11.45	13.65

Figure 15: Transcriptome analysis of differentiated hiPSCs (IMR90) toward germ layer cells. (A) Overview of the UKK2-CTT for the in vitro cardiac differentiation of the experimental design from day-2 to day14. (B) To determine the the early germ layer formation, hiPSCs were exposure to 1 h, 24 h (day1) and 48 h CHIR (day2) compared with those of untreated controls. The hiPSCs were cultured as a monolayer on matrigel-coated plates for 2 days under pluripotent conditions and on day0 exposed to GSK3 inhibitor, CHIR99021 (10 µM) for 24 h. After microarray analysis of the RNA, the number of the up- and down regulated SPSs (log2 fold change $>$ 1; adjusted p-value $<$ 0.05) were determined. (C) Visualization of enriched gene ontology terms across IMR90 1h, 24 h and 48 h after CHIR. Heatmap showing the top 20 enrichment clusters, colored by p-values. (D) Mesendoderm gene table Representative mesendoderm genes increased gradually for the different timepoints, after exposure to CHIR in IMR90-hiPSCs.

3.7 Directed differentiation of hiPSCs (IMR90 origin) towards cardiomyocytes after exposure to selected compounds

In order to determine the optimal time for early germ layer formation induced by small molecule CHIR and subsequent differentiation into cardiomyocytes, we also compared transcriptomes at three time points: 1 hour, 24 hours (day1), and 48 hours (day2) (**Figure 15A**). The hiPSCs were cultured in the presence of CHIR for 1 hour, followed by an additional day of culture (day1), and then cultured for an additional 24 hours without CHIR (day2).

As shown in the table (**Figure 15B**), the number of differentially expressed genes (DEGs) increased with longer incubation time. At the 24-hour mark (day1) in the presence of CHIR, 610 probesets were significantly upregulated, while 1723 probesets were downregulated. Gene ontology (GO) analysis of the DEGs (**Figure 15C**) revealed significant enrichment in various developmental pathways, including embryonic morphogenesis, heart development (mesodermal origin), brain development (ectodermal origin), and partial gland development (endodermal origin) during these time points. This finding was supported by the substantial deregulation of mesoderm genes such as T (Brachyury), EOMES, and MIXL1, which are known to control pluripotency exit and germ layer segregation [93]. Additionally, WNT3, LEF1, and DKK1, which are markers for initiating cardiomyogenesis, exhibited significant upregulation (**Figure 15D, table**).

These findings provide evidence of robust activation of various differentiation processes that mirror embryonic development. Furthermore, they suggest that the initiation of germ layer formation occurred on day1 of differentiation. To identify further the pathways involved in cardiomyogenesis in hiPSCs, we performed transcriptomic analysis after differentiating the hiPSCs for day1, day4, and day14 in the presence and absence of the three selected teratogens (ISO, VPA, THD) and one non-teratogen (BSP) (The compounds valproic acid, thalidomide, isotretinoin and buspirone will be reffered by their respective abbreviations. This distinction is to differentiate them for the UKK-CTT exposure part). Among these compounds, ISO was identified as a clear inhibitor of cardiomyogenesis in hiPSCs (**Figure 16A**). RNA samples were collected on day1 (germ layer initiation), day4 (early cardiac progenitor cells), and day14 (cardiomyocytes) (**Figure 16A**, control and ISO morphology). As shown in **Figure 16A**, the control cardiomyocytes on day14 exhibited beating clusters of cardiomyocytes, indicating their functional maturity. In contrast, hiPSCs treated with ISO and differentiated for 14 days showed a static morphology without any visible beating clusters of cardiomyocytes.

To gain a comprehensive understanding of the genome-wide gene expression changes induced by the different test compounds, we conducted principal component analysis (PCA) based on the significantly altered transcripts (n=3, independent experiments; FDR p-value < 0.05; fold change $\geq$

2.0). PCA was performed using two different sets of probe sets: all 54,675 analyzed probe sets (**Figure 16B**) and the top 500 significantly deregulated probe sets with the highest variance (**Figure 16C**). The first two components, PC1 and PC2, represent the percentage of variance in the transcriptomes at different stages of differentiation, and they separate the samples accordingly.

The results showed that the triplicate transcriptomes for each time point had minimal differences, indicating the high quality of the microarray data. However, it is noteworthy that the ISO-14-days triplicate transcriptomes were distinct from the control, VPA, THD, and BSP 14 days triplicate transcriptomes in the PC1 direction (**Figure 16B**). Furthermore, when considering the top 500 probe sets with the highest variance, there was a clear separation of the ISO 14 days transcriptome in both PCA directions (**Figure 16C**).

To compare the differences between the three teratogens (ISO, VPA, THD) and the non-teratogen BSP at different periods of differentiation, we performed a new PCA analysis with the top 1000 SPs with high variance (**Figure 17A, B, C**) for each differentiation time point. As indicated the day1, day4 and day14 transcriptomes of BSP cluster together with the appropriate transcriptomes of the control (without DMSO) and DMSO-control (end concentration 0.1 %). Interestingly, a clear separation of the transcriptomes of the three teratogens (ISO, VPA and THD) was observed at all three differentiation time points (**Figure 17A, B, C**). To further examine the genome-wide expression changes, volcano plots were generated to compare the selected test compounds at day1, day4, and day14 with their respective controls (DMSO-control, day1, day4, and day14) (**Figure 18**) (at least 2-fold deregulated; FDR p-value < 0.05). In general, a large number of probe sets were found to be deregulated for the teratogens, particularly for ISO, while none were observed for the non-teratogen BSP. Interestingly, both THD and VPA showed a significant number of deregulated genes at day1 and day4, as also documented by the PCA plots. However, the number of developmental genes deregulated by ISO at day4 and day14 was much higher compared to VPA and THD, which correlates with the complete inhibition of cardiomyogenesis by ISO.

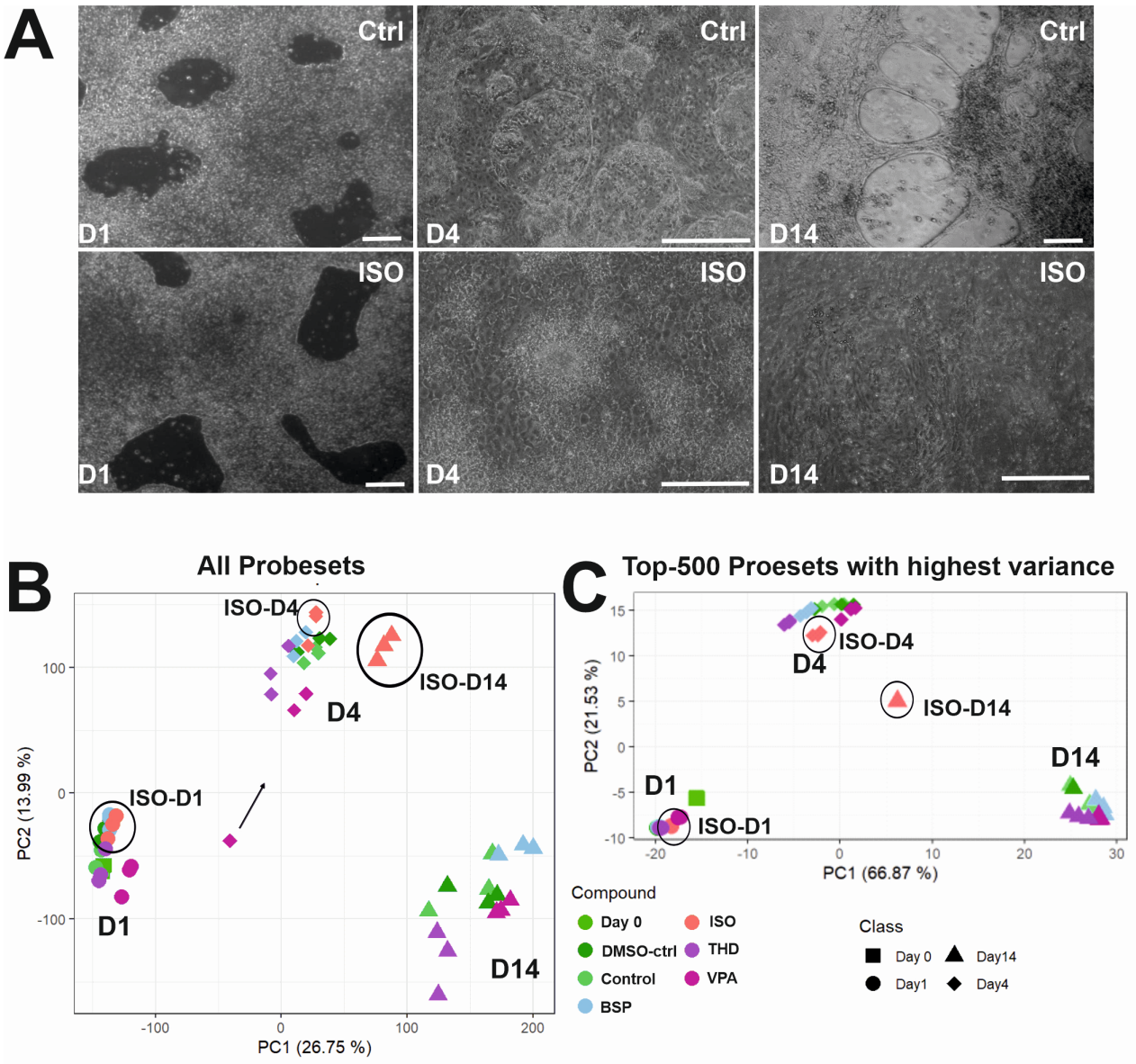

Figure 16: Transcriptome analysis of differentiated hiPSCs (IMR90) toward CMs. The hiPSCs were cultured as a mono-layer on matrigel-coated plates for 2 days under pluripotent conditions and on day0 exposed to GSK3 inhibitor, CHIR99021 (10 µM) for 24 h. After after 48 h exposed to Wnt inhibitor, IWP2 (5 µM). Spontaneously beating cardiac clusters were observed from day9 onwards. Simultaneously, cells were exposed to test substances for a single exposure of 24 h (day1). The cells were harvested for gene array analysis on day1, day4 and day14 (**Figure 1A**). Medium changes were done as indicated every alternate date. A Representative phase-contrast images of control and ISO treated hiPSC at day1-, 4 -and 14day. Scale bar, 100 µm. (B) PCA blot of 54,675 probe sets for three timepoints during the differentiation. (C) PCA blot of the 500 SPS with the highest variance across the mean of the condition-wise samples. The respective day is indicated by the shape and the respective measured compound is indicated by the color of the dot, are shown next to the plots. The distribution of the data points on the x-axis is given by the PC 1 and on the y-axis by PC2. The percentages in parentheses denote the proportion of explained variance for the respective PC.

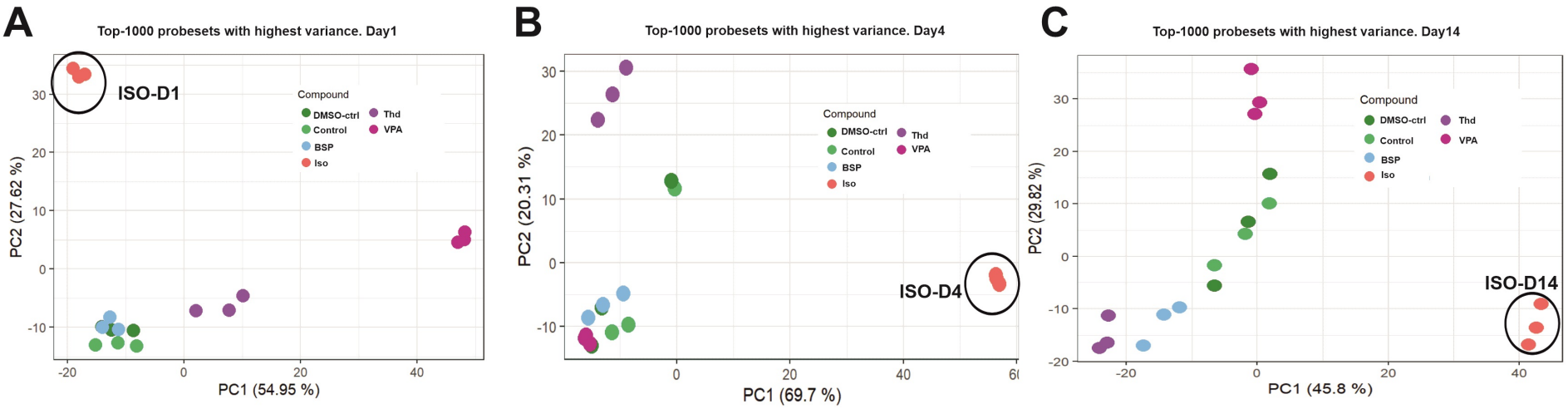

Figure 17: Comparison of the top1000 SPS with highest variance for ISO-, THD- and VPA-treated vs control day1, day4, and day14 differentiated hiPSCs (IMR90). (A), (B), (C) PCA-plots for each day, respectively. The different compounds are indicated by different colors. The distribution of the data points on the x-axis is given by the PC 1 and on the y-axis by PC2. The percentages in parentheses denote the proportion of explained variance for the respective PC.

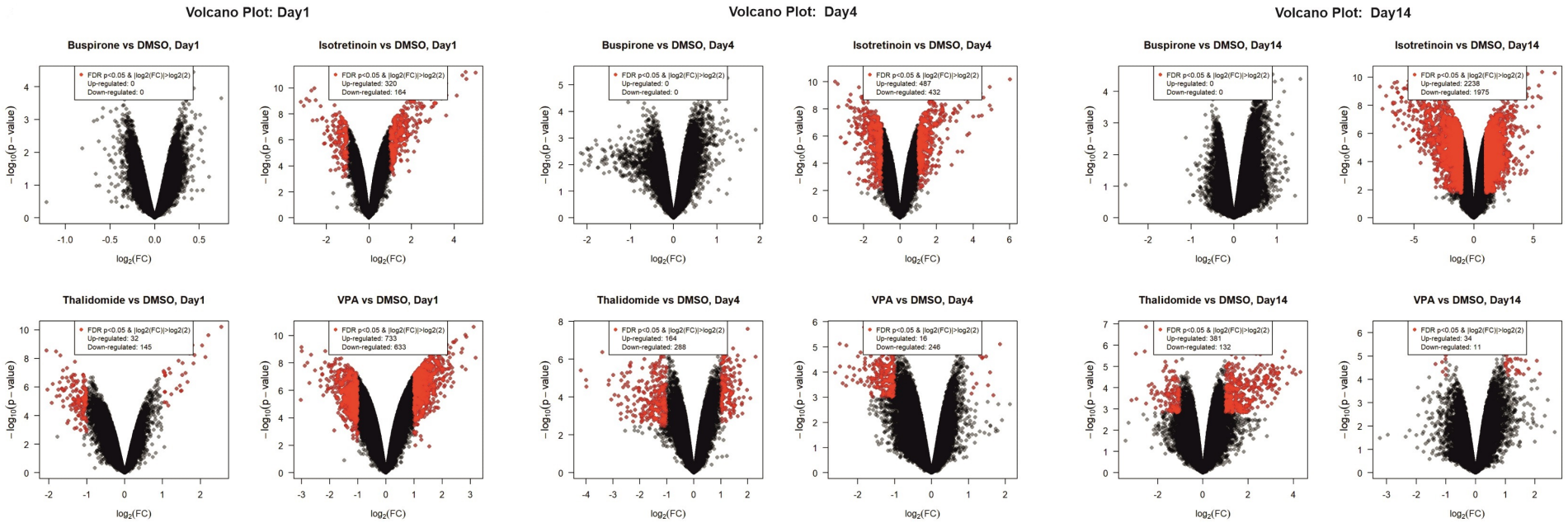

Figure 18: Genome-wide gene expression changes caused by by isotretinoin, thalidomide, valproic acid and buspirone at day1, day4 and day14 at C_{max} concentration. The figures illustrate the fold-change on the x-axis in its logarithmic form (log2(FC)) and the corresponding, not FDR-adjusted "limma"-p-value on the y-axis in its negative, logarithmic form (-log10(p-value)) of each probe set-mean-value from n=3 independent biological experiments. Highlighted in red are all probe sets, which had an FDR-adjusted p-value of <0.05 and were at least two- fold up or ½-fold down regulated

3.7.1 Identification of differentiation processes at day1 of hiPSCs (IMR90) differentiation affected by Isotretinoin, VPA, Thalidomide and Buspirone

To study the biological significance of the differential expressed genes, we compared the SPs (FDR p-value < 0.05; fold change $\geq$ 2), of ISO between ISO and other compounds (VPA, THD, and BSP) during the transition through mesoderm at day1. On day1, the ISO-specific exposure led to 273 (94 downregulated and 173 upregulated) differentially expressed SPS (FDR p-value < 0.05; fold change $\geq$ 2) (**Figure 19A & 19B**). To characterize the biological functions of genes deregulated by the three teratogens at day1, the up-and downregulated SPS were separately analyzed by the Metascape functional enrichment tool [85]. No deregulated SPS were identified by BSP as a non-teratogen.

The GO analysis of the ISO-specific downregulated genes recognized enriched GOs such as -tissue morphogenesis-, -regulation of nervous system development-,- endocardial cushion development - and the -canonical Wnt pathway signalling- (**Figure 19C**). In Supplementary **Figure S6A** are shown the corresponding genes belonging to these GOs. The KEGG analysis reveals pathways such as the Ras and PI3k-Akt Signaling pathways (**Figure S6B**). Analysis of the ISO-specific upregulated SPS recognized prominent general early developmental GOs (such as -embryonic organ development-, -brain development-, -activation of anterior HOX genes in the hindbrain, -neural crest differentiation-, (**Figure 19D**). The table with the GO genes (**Figure S6C**) reveals the genes that are related to the above mentioned significant processes and KEGG pathways (**Figure S6D**) such as -signaling pathways regulating pluripotency-, -TGF-beta signaling- (all having a crucial role during general developmental processes). The **Figure S6A** summarizes the most prominent enriched GO terms and their corresponding downregulated genes, while **Figure S6C** presents the upregulated genes. Notably, key genes essential for heart development, such as BMP2, DKK1, EOMES, and GATA4, were identified in the GO terms ”canonical Wnt signaling pathway” and ”heart development,” indicating their downregulation in ISO-treated samples. **Figure S7A & S7B** display the top 50 ISO-specific down- and upregulated genes, along with their associated GO terms, suggesting inhibition of cardiomyogenesis and initiation of neurogenesis. Interestingly, the Wnt signalling pathway, which is normally activated by CHIR in DMSO-control samples, is downregulated in ISO-treated hiPSCs. Additionally, we validated the microarray data at day1 using qPCR for five arbitrarily selected genes, confirming their deregulation pattern (marked with a square and star in **Figure S7C**) and highlighting the significant deregulation in ISO-treated conditions compared to the other three compounds.

Thus, analysis on day1 revealed that ISO-specific exposure led to distinct gene expression patterns associated with tissue morphogenesis, nervous system development, embryonic organ development, and canonical Wnt signalling, indicating potential effects on cardiomyogenesis inhibition and neurogenesis initiation.

3.7.2 Identification of differentiation processes at day4 of hiPSCs (IMR90) differentiation affected by Isotretinoin, VPA, Thalidomide and Buspirone

A similar analysis was conducted to examine the ISO-specific deregulated genes on day4, which represents the transition from cardiac mesoderm differentiation to cardiac progenitors. Exposure to the ISO-specific set resulted in the differential expression of 574 probe sets (272 downregulated and 292 upregulated) with significant changes (FDR p-value < 0.05; fold change $\geq$ 2) (**Figure 19E, F**). The downregulated genes were primarily associated with mesoderm-derived organs such as heart development and ectoderm-derived organs such as brain development (**Figure 19G**). The table containing the gene ontology (GO) genes (**Figure S8A**) displayed the downregulated genes enriched in heart-related terms and KEGG pathways including TGF-beta signaling, dilated cardiomyopathy, and hypertrophic myopathy (**Figure S8B**).

On the other hand, the upregulated genes were enriched in GOs primarily involved in anterior-posterior patterning specification, brain development, and other early morphogenesis processes (**Figure 19H**). The table with the GO genes (**Figure S8C**) and KEGG pathways revealed associations with Hedgehog, Hipo, Wnt, and pluripotency-regulating signaling pathways (**Figure S8D**). The top 50 ISO-specific upregulated genes (**Figure S9A**) belonged to GOs crucial for pattern specification processes, while the downregulated genes (**Figure S9B**) were involved in signaling pathways related to heart development. The expression of seven arbitrary genes using qPCR validated the microarray data on day4, confirming the deregulation pattern of these genes (**Figure S9C**).

In summary, the analysis of the ISO-specific set on day1 and day4 identified genes associated with heart development and signaling pathways such as Wnt/β-catenin, TGF-beta, and BMP, which are known to regulate mesodermal differentiation. These genes could serve as potential biomarker candidates for a successful transition to a mesodermal state and play a key role in fate specification during heart development. Additionally, the significantly downregulated VPA-specific genes on day1 and the THD-specific deregulated genes on day4 were analyzed using Metascape. The Supplementary **Figure S10** (**Figure S10A-K**) provides GOs related to heart development. Based on the presence of beating clusters of cardiomyocytes on day14, it can be inferred that VPA and THD do not have significant effects on mesoderm-dependent cardiomyogenesis but may partially inhibit the development of fully functional cardiomyocytes (see **Figure 21A-E**).

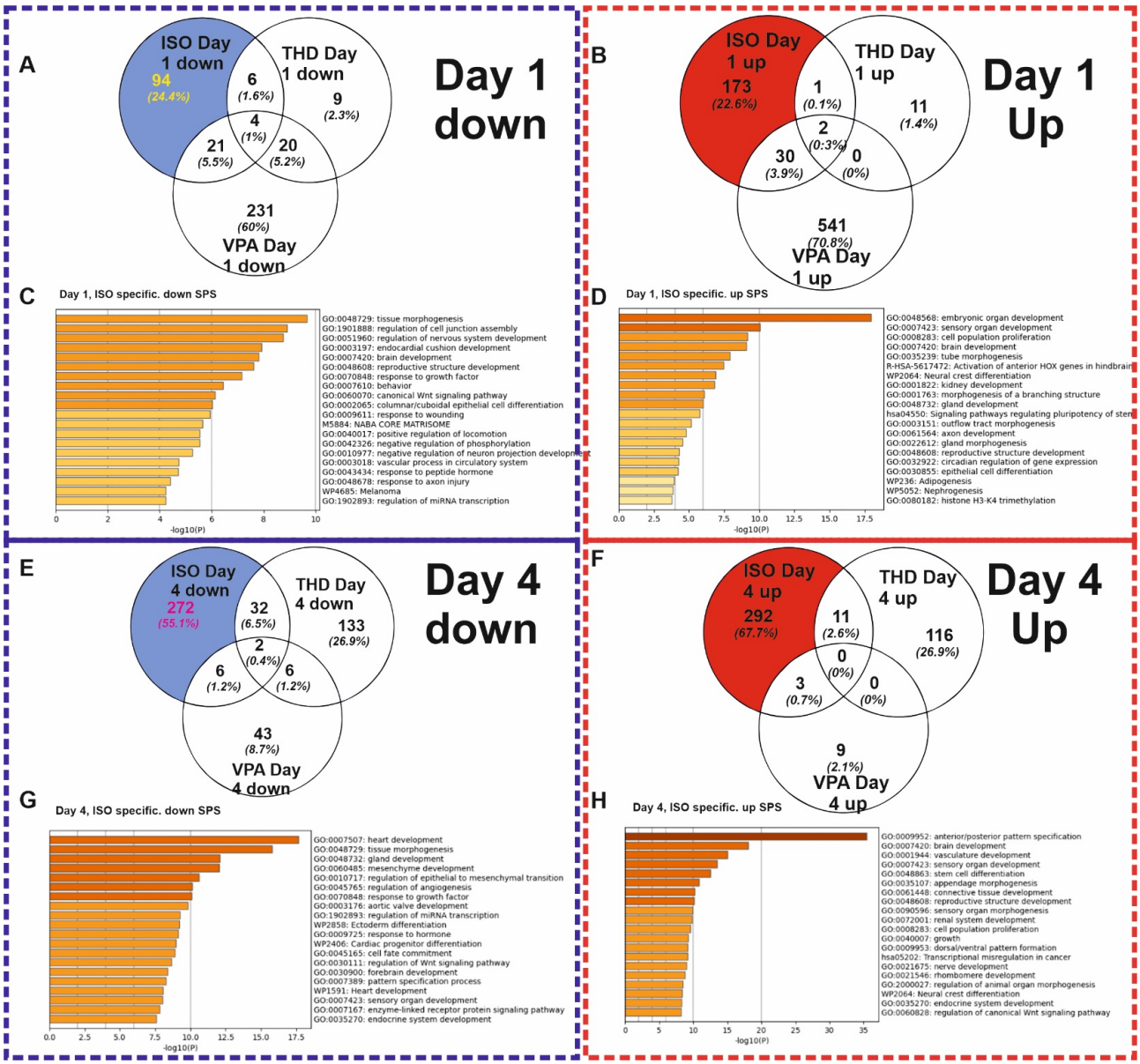

Figure 19: Biological interpretation of the ISO-specific differentially expressed genes after exposure of hiPSCs (IMR90) to ISO, THD and VPA at day1. (A), (B) The Venn diagrams shows the number of down-regulated and up-regulated SPS (log2 fold change > 1; adjusted p-value < 0.05), respectively induced by the selected compounds. (C), (D) Metascape analysis for specific ISO-induced downregulated and upregulated SPS, respectively. Analysis shows the statistically enriched BPs and pathways as coloured by the p values. (E), (F) The Venn diagrams shows the number of down-regulated and up-regulated SPS (log2 fold change > 1; adjusted p-value < 0.05), respectively induced by the selected compounds. (G), (H) Metascape analysis for specific ISO-induced downregulated and upregulated SPS, respectively. Analysis shows the statistically enriched BPs and pathways as coloured by the p values.

3.8 Identification of a shared pattern after retinoids exposure between two different hiPSC lines

We conducted a comparison of transcriptomes between three retinoids (acitrecin, 9cis-retinoic acid, and ISO) in SBDA2 hiPSCs [28] and ISO in IMR90 hiPSCs on day1 of differentiation (**Figure 20**). Interestingly, all three retinoid compounds completely inhibited cardiomyogenesis, as observed on day14 when differentiating both SBDA2 hiPSCs and IMR90 hiPSCs in the presence of ISO.

Figure 20A & B displays the overlapping genes that were either upregulated or downregulated on day1 compared to the control conditions. We identified 31 downregulated genes (**Figure 20A**) and 100 upregulated genes (**Figure 20B**) that were common among all three retinoids on day1 during the differentiation of SBDA2 hiPSCs compared to control cells. We reanalyzed the transcriptome data of day1 SBDA2 hiPSCs for this purpose. Further analysis of the common retinoid compounds in SBDA2 hiPSCs on day1 and IMR90 hiPSCs on day1 with ISO resulted in 69 common genes. Among these genes, 12 were downregulated (**Figure 20C**) and 57 were upregulated (**Figure 20D**) in response to all three retinoids on day1 of differentiation.

From these genes, we selected 31 that were highly deregulated (at least 2-fold up- or downregulated) and biologically significant. The expression levels of these genes across all teratogens and non-teratogens are represented in the heatmap (**Figure 20E**). The heatmap clearly distinguishes between retinoids, teratogens, and non-teratogens, indicating that these genes have strong potential as cardiac mesodermal markers essential for cardiac development. Further analysis of these genes using Metascape revealed significant enrichment in developmental processes, including embryonic organ development, heart development, angiogenesis, and regulation of the WNT signalling pathway (**Figure 20F**). Full description of the 31 genes can be found in the supplementary table 3 (**Table S3**).

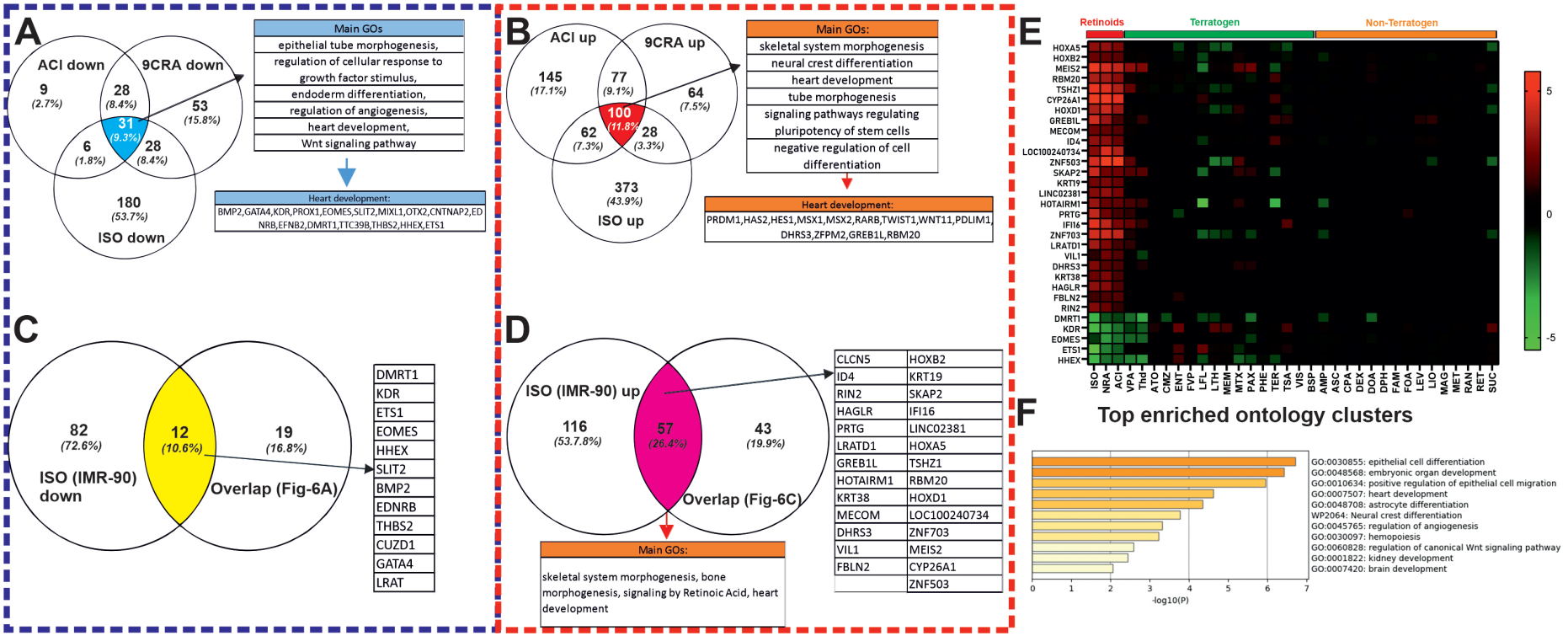

Figure 20: Common gene signature between the differential expressed genes at day1 in ISO-treated SPDA2 hiPSCs and ISO-treated IMR90 hiPSCs. (A), (B) Venn diagrams show the number of common retinoids specific (ISO; 9-cis retinoic acid: 9CRA and Acitretin: ACI) downregulated and upregulated genes, respectively, in SBDA2 hiPSC at day1. The commonly down- and upregulated genes (31 and 100 respectively) were analysed by the Metascape tool to identify the statistically enriched GOs and pathways. (C), (D) the Venn diagrams show the number of the common genes between the ISO-specific upregulated and downregulated genes at day1 in IMR90 hiPSCs, respectively, and in the Retinoids specific genes in SBDA2 as shown in (A) and (B) commonly down- and upregulated genes: 12 and 57 respectively). (E) The heatmap shows the 31 down- and upregulated genes out of the 69 differential expressed common genes (12 and 57) with a log2FC value higher than 1. On the x-axis are the abbreviations of the teratogens and non-teratogens (Table 1 in [27]) and on the y-axis the 31 commonly deregulated genes. (F) Metascape analysis of the 31 selected genes showing prominent enriched BPs and pathways coloured by p-values.

3.9 Impact of teratogens and non-teratogens on beating activity of the cardiomyocytes

We further carried out a general assessment of cardiomyocyte differentiation until day14 based on the beating activity of the SBDA2 and IMR90 derived CMs as compared to the control CMs. Among all the teratogens tested using the UKK2-CTT, only the retinoids completely inhibited the formation of beating cardiomyocytes by day14, whereas treatment with the non-teratogens had no effects on the beating frequency of the cardiomyocytes at day14. To further investigate the impact of well-documented teratogens such as VPA and THD on the cardiomyogenesis process we generated a live imaging transgenic IMR90 hiPSCs cell line using the CRISPR-Cas9 and a homology-directed recombination approach as we described previously [79, 80]. The ACTN2-cop green fluorescent protein (ACTN2-cop-eGFP+-hiPSC line (IMR90 origin) enables the live imaging of sarcomeres after differentiation to ACTN2-cop-eGFP+-CMs, since the α-cardiac specific actinin (ACTN2) is enriched in the sarcomeres, the smallest contractile unit of cardiomyocytes.

As illustrated in **Figure 21** the control day14 ACTN2-cop-eGFP+-CMs show an intact muscle striation structure and a beating activity of 65 beats per min (**Video S1**). As expected, no cardiomyocytes were observed at day14 in the presence of ISO (**Figure 21B**). The heat map representation of the top 50 deregulated genes (**Figure S9**) reflects the influence of ISO on the transcriptome on day14 and the absence of any cardiac markers. The non-teratogen BSP did neither affect the striation structure of the CMs nor the beating activity (**Figure 21C & Video S2**). However, VPA and THD compromised the cardiac muscle striation of ACTN2-cop-eGFP+-hiPSC (**Figure 21D & Figure 21E**, respectively) and reduced the beating activity as compared to control, BSP and other non-teratogens. Using the software VA1.9 [2, 31], we also analysed the beating frequency and the fluctuations of the contraction and relaxation velocity of the differentiated cardiomyocytes on day14, as has already been described [2, 31]. As shown in **Figure 21F**, VPA and THD-exposed exhibited a decreased beating frequency compared to the control and the non-teratogen BSP. There was no significant change in the contraction velocity, but the relaxation phase was significantly increased in VPA-exposed CMs and almost three times higher in THD-exposed CMs (**Figure 21E, G**).

To specifically identify a teratogen that inhibits cardiac development based on the retinoids gene signature, we defined the "Cardiac Developmental Index" (CDI31g). This index ranges from 0 to 1, with a maximum value of 1 indicating that all 31 developmental-related genes are deregulated by the compound (number of deregulated genes divided by 31 deregulated genes). If no genes are differentially expressed, the CDI31g value for the compound is zero. In the case of retinoid compounds, all three of them deregulated the expression of 31 developmental-related genes in the SBDS2 cell line, with 5 genes downregulated and 26 genes upregulated. When compared to the non-teratogens, the teratogens exhibited higher CDI31g scores. Specifically, VPA and THD, as teratogens, showed 12 and 10 deregulated genes, resulting in CDI31g scores of 0.38 and 0.32, respectively (**Table 12**). The dis-

tribution of these genes in the IMR90 cell line (**Figure S9B**) confirmed their significant deregulation compared to the other two teratogens (VPA and THD) and the non-teratogen BSP. Live cell imaging further revealed the deterioration of sarcomeric α-actinin and irregular structure of actinin filaments in VPA (**Figure 21D**) and THD (**Figure 21E**) treated conditions, in contrast to untreated cardiomyocytes. The non-teratogen BSP did not affect the beating activity or muscle striation, resulting in a CDI score of 0.

In summary, the CDI31g score based on the retinoids gene signature allowed us to distinguish teratogens from non-teratogens in terms of their specific inhibition of cardiac development. VPA and THD demonstrated higher CDI31g scores, accompanied by significant gene deregulation and observable structural changes in cardiomyocytes.

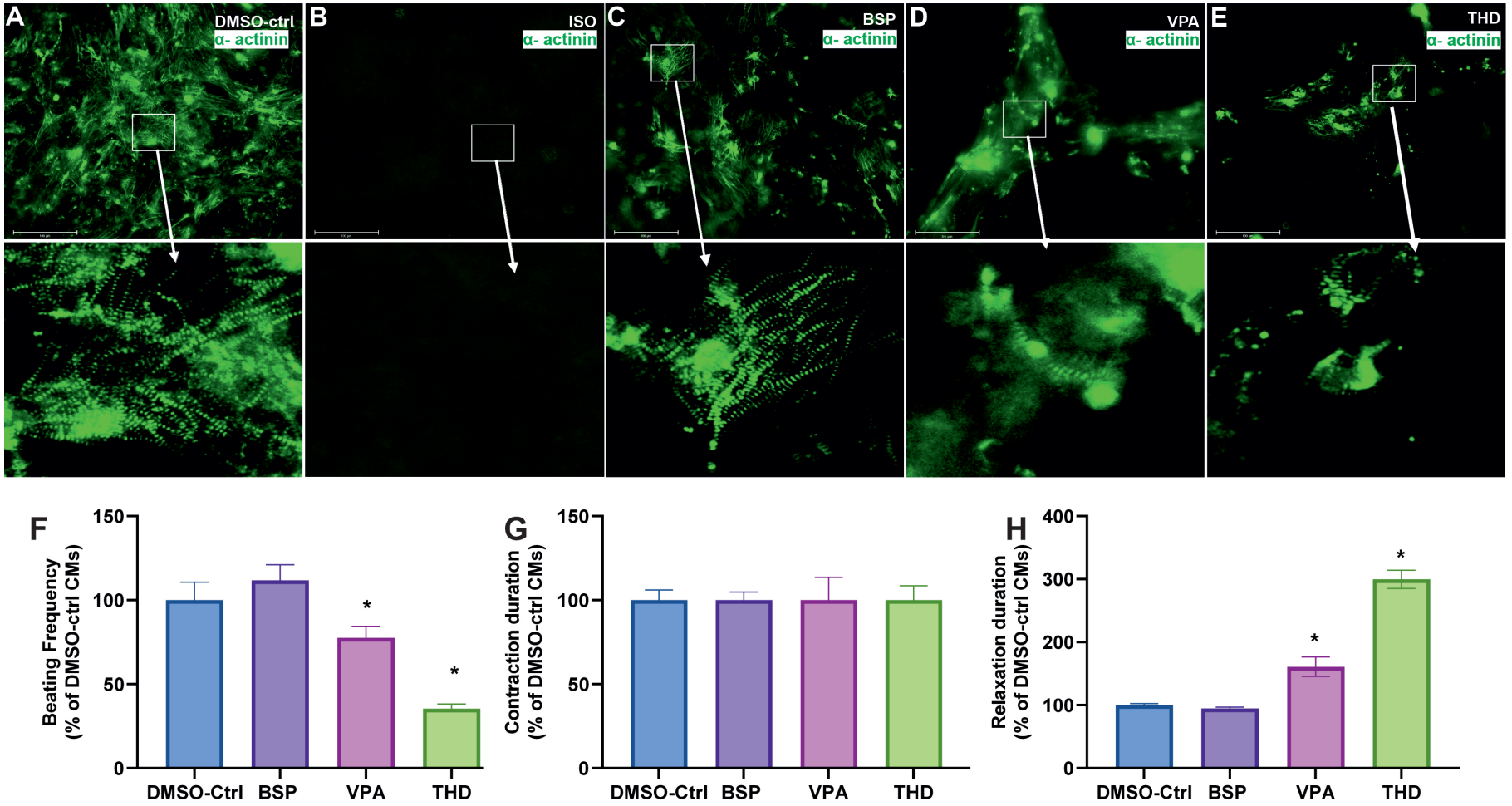

Figure 21: Effects of ISO, THD and VPA on contractility of ACTN2 copGFP+-CMs on day14. (A), (B), (C), (E) Representative immunofluorescence live imaging of sarcomeric ACTN2-copGFP+-CMs at day14 obtained after differentiation of IMR90 ACTN2 copGFP+-hiPScCs on day14 in the absence and presence of ISO, VPA, BSP and THD, respectively (scale bar: 100 μm), arrows indicate the sarcomere striation morphology. (F), (G), (H) The diagrams show the beating frequency, the contraction and the relaxation duration at day14, respectively, for control, BSB, VPA and THD. The values are expressed as a percentage of the control CMs values, which were set to 100%. (mean ± SEM, n = 3, * $p < 0.05$).

Table 12: Beating profile and CDI score for non teratogens and teratogens

Compound	Abbreviation	Tested concentration [µM]	Beating[a]	CDIscore
		1-fold C_{max}		
Non-teratogens				
Ampicillin	AMP	107	Yes	0.1*[a]
Ascorbic acid	ASC	200	Yes	0
Buspirone	BSP	0,0244	Yes	0
Chlorpheniramine	CPA	0,0304	Yes	0
Dextromethorphan	DEX	0,15	Yes	0
Diphenhydramine	DPH	0,3	Yes	0
Doxylamine	DOA	0,38	Yes	0,03
Famotidine	FAM	1,06	Yes	0
Folic acid	FOA	0,38	Yes	0,03
Levothyroxine	LEV	0,077	Yes	0,03
Liothyronine	LIO	0,00307	Yes	0.06*[b]
Magnesium (chloride)	MAG	1200	Yes	0
Methicillin	MET	140	Yes	0
Ranitidine	RAN	0,8	Yes	0
Retinol	RET	1	Yes	0
Sucralose	SUC	2,5	Yes	0,2
Teratogens				
9-cis-Retinoic acid	9RA	1	No	1
Acitretin	ACI	1,2	No	1
Isotretinoin	ISO	1,7	No	1
Atorvastatin	ATO	0,54	Yes	0
Carbamazepine	CMZ	19	Yes	0,03
Entinostat	ENT	0,2	Yes	0.2*[c]
Favipiravir	FPV	382	Yes	0
Leflunomide	LFL	370	Yes	0.3*[d]
Lithium (chloride)	LTH	1000	Yes	0.2*[e]
Methotrexate	MTX	1	Yes	0,2
Methylmercury	MEM	0,02	Yes	0.1*[f]
Paroxetine	PAX	1,2	Yes	0.2*[g]
Teriflunomide	TER	370	Yes	0.3*[h]
Thalidomide	THD	3,9	Yes	0,3
Trichostatin A	TSA	0,01	Yes	0.1*[i]
Valproic acid	VPA	600	Yes	0,4
Vismodegib	VIS	20	Yes	0

Compounds, abbreviations, C_{max} concentrations, beating profile and CDI score.

[a] Yes, if on day14 was observed beating CMs; No, if on day14 were not observed any beating CMs.

The CDI score is defined as Cardiotoxicity Developmental Index. This index has a maximal value of 1, which is reached when all 31 genes from are deregulated by a compound; likewise, it has a minimal value of 0 if no gene

is deregulated. The CDI score is calculated only on the hiPSC-SBDA2 cells. The beating and Cytotoxicity refers to hiPSC-IMR90 as well as hiPSC-SBDA2.

*indicate a different deregulation pattern as the retinoinds and the 31 ''gold standard'' genes

^{*a}(Total 3 out 31, 2 downregulated instead of up regulated like in retinoids)

^{*b}(Total 7 out 31, 1 downregulated instead of up regulated like in retinoids)

^{*c}(Total 6 out 31, 2 downregulated instead of up regulated like in retinoids, 3 upregulated instead of being down-regulated like in retinoinds)

^{*d}(Total 10 out 31, 4 downregulated instead of up regulated like in retinoids, 1 is upregulated instead of being downregulated like in retinoinds)

^{*e}(Total 7 out 31, 5 downregulated instead of up regulated like in retinoids, 1 is upregulated instead of being downregulated like in retinoinds)

^{*f}(Total 4 out 31, 3 downregulated instead of up regulated like in retinoids, 1 is upregulated instead of being downregulated like in retinoinds)

^{*g}(Total 6 out 31, 1 downregulated instead of up regulated like in retinoids)

^{*h}(Total 8 out 31, 3 downregulated instead of up regulated like in retinoids)

^{*i}(Total 4 out 31, 1 downregulated instead of up regulated like in retinoids, 1 is upregulated instead of being downregulated like in retinoinds)

4 Discussion

Congenital malformations, affect million children globally and can result from exposure to teratogens during pregnancy [94]. Many drugs can potentially act as teratogens, posing risks to fetal development. The Organization for Economic Cooperation and Development (OECD) has established guidelines for assessing the toxicity of chemicals to address the developmental risks associated with drug exposure. Traditionally, these guidelines have relied on animal testing, but ethical concerns, high costs, and the limited predictability of species-specific responses have prompted the development of advanced in vitro toxicity testing systems. However, the new systems, based on human cell platforms, aim to eliminate the reliance on animal models and provide a more relevant approach for evaluating the potential toxicity of substances.

To date, ECVAM has validated several in vitro tests for developmental toxicity and cardiotoxicity, but none specifically for developmental embryotoxicity and cardiotoxicity in a single test. For developmental embryotoxicity, ECVAM has validated the following in vitro tests: the Embryonic Stem Cell Test (EST), the Whole Embryo Culture (WEC) test, and the Micromass (MM) test [95].

Despite some limitations and reduced predictivity observed in subsequent investigations with additional chemicals [96, 97] the Embryonic Stem Cell Test (EST) continues to be utilized in the industry for pre-screening and prioritization purposes. Additionally, it remains a valuable tool for conducting research on the molecular mechanisms underlying chemical interference with embryonic cell differentiation [98]. While its predictive capacity may vary depending on the specific chemicals being tested, the EST is a valuable resource in understanding and assessing the effects of substances on embryonic development.

The ”mEST” assay has certain limitations, particularly in predicting human-specific responses to unresponsive teratogens. Notably, compounds such as thalidomide and isotretinoin are non-teratogenic in mice but teratogenic in humans [99, 100]. Additionally, this assay has been unable to capture the teratogenicity of compounds like methyl mercury and dimethadione [101]. Recent studies comparing the biochemical response to teratogenic thalidomide in mice and humans have revealed that thalidomide targets the SALL4 protein specifically in human cells but not in rodent cells [102]. On the other hand, It is important to highlight that mEST assay has also shown its efficacy in predicting the potential developmental cardiotoxicity of specific antiepileptic drugs such as valproic acid, phenytoin, phenobarbital, and trimethadione [103].

Induced pluripotent stem cells (iPSCs) have emerged as a reliable and ethically unproblematic source of human cells for in vitro toxicity models [104, 105]. Their ability to differentiate into various tissue types [106], provides researchers a valuable tool for simulating developmental processes. Notably, iPSCs possess the characteristic of modifiable differentiation routes, allowing for the manipulation of cell differentiation through exposure to specific compounds. This flexibility enables the investigation of compound effects on differentiating iPSCs and can improve toxicity testing systems' predictivity by discriminating diverse developmental toxicants. Furthermore, combining iPSCs with transcriptomics as a readout parameter shows promise in this regard.

This Ph.D. thesis focuses on the optimization and analysis of the UKK2 test system, which aims to assess the risk of developmental toxic compounds. Therefore, the iPSCs were directed toward germ layer formations and further into functional cardiomyocytes and inbetween were exposed to 39 different substances at therapeutic concentrations relevant to human in vivo conditions. Additionally, four compounds from this selection were specifically chosen to assess their potential cardiotoxic effects.

To expand the applicability of the UKK2 test, the entire differentiation protocol was utilized, encompassing cardiac differentiation. This incorporation of another developmental process enhanced the test system. An additional cardiac endpoint, α-cardiac actinin 2, was analyzed to classify selected representative test compounds based on the structure of α-cardiac actinin 2.

In the following chapters of the discussion, we are going to discuss the results we obtained and provide insighst into the performance and the potential applications of the UKK2 test system.

4.1 Effects of teratogenic and non-teratogenic substances on early differentiation at day1

Analyzing the first part of the discussion, the functionality of the UKK2 test system was utilized to assess the chosen set of test compounds on gene expression patters and the cellular viability. We confirmed the cytotoxicity with microscopic analysis and evaluated the gene expression changes using Affymetrix analysis. To identify significant differences in gene expression, a multivariate analysis was conducted, considering an FDR-adjusted p-value of less than 0.05 and a two-fold upregulation or a 1/2-fold downregulation as thresholds.

The first gene expression data were capture on the principal component analysis (PCA) plots (**Figure 3**) and revealed distinct genetic variations between teratogenic and non-teratogenic substances. Regardless of whether all 54, 675 probe sets or only the top 1000 probe sets were considered, both PCA plots exhibited similar distribution patterns among conditions. A prominent cluster primarily

consisting of non-teratogenic substances was observed, while teratogenic substances formed a distinct cluster, indicating potential similarities in the deregulation of genes induced by teratogens.

4.1.1 Effects of non-teratogenic substances and their biological interpretation.

16 out of the 39 substances selected for this study were confirmed to be non-teratogenic in humans at therapeutic concentrations and had obtained approval from regulatory authorities such as the FDA or TGA, classifying them as safe for use during pregnancy. To determine the therapeutic concentrations, an extensive literature review was conducted with our project partners. These non-teratogenic compounds were then exposed to differentiating hiPSCs at 1x and 20x C_{max} concentrations. No significant cytotoxicity was observed for any of the non-teratogenic compounds at either concentration. Although some substance-induced effects on gene expression were detected, they were only significant in a few cases (**Table 10**). For instance, magnesium chloride induced 227 and 794 gene expression changes at 1x and 20x concentrations respectively, while sucralose induced 191 and 166 changes at the same concentrations. Ascorbic acid at 20x concentration resulted in 396 gene expression changes. It is worth noting that high concentrations of ascorbic acid and magnesium chloride have been associated with adverse effects [107] suggesting that the elevated concentrations used in vitro may also impact differentiating cells in vivo.

In comparison to the genetic effects caused by teratogenic substances discussed in the following chapter, which induced several hundreds or thousands of significant changes, the effects of the non-teratogenic compounds were relatively minor. These effects were considered to be more attributable to the chosen multivariate analysis and threshold criteria rather than a genuine impact of the compounds themselves. Overall, the non-teratogenic substances did not significantly affect the differentiation process, except for ascorbic acid and magnesium chloride, which aligns with existing publications

This part is from our publication Cherianidou et. al 2021 [86]

As expected, the number of genes showing expression changes was significantly lower for non-teratogens compared to teratogens. Surprisingly, a substantial proportion (approximately 82%) of the genes affected by non-teratogens overlapped with those regulated by teratogens. Furthermore, similar functional categories (GO groups) and biological pathways (KEGG pathways) associated with developmental processes were affected. These findings indicate that non-teratogens can also disrupt the differentiation of hiPSCs if applied at sufficiently high concentrations. Thus, it is crucial to determine exposure levels that are relevant in vivo during the evaluation process. Analyzing the genes differentially expressed in the in vitro cardiomyogenic protocol (UKK2) [71, 72] not only revealed an over-representation of genes related to cardiac muscle development, but also the differentiation of various other tissues, including primitive streak, adenohypophysis, olfactory bulb, optic cup, neu-

ral crest, fat cells, and osteoblasts. Additionally, numerous signaling pathways such as Wnt, MAPK kinase, P53, Rap1, Hippo, and TGF-beta signaling were enriched. Although further investigation is needed to understand the underlying biological mechanisms, the broad range of pathways and functional categories involved can be advantageous for comprehensive identification of human teratogens in testing protocols.

4.1.2 Effects of teratogenic substances

Among the selected 39 substances, 23 have been identified through human and animal research as having teratogenic effects on humans when used at therapeutic concentrations, and they habe classified also by the FDA or TGA under pregnancy categories D and X. These teratogenic compounds were tested in the UKK2 test system at 1x and 20x C_{max} concentrations (**Table 10**). In contrast to non-teratogenic compounds, five teratogenic compounds exhibited cytotoxicity either at both 1x and 20x C_{max} concentrations or only at the 20x C_{max}. Notably, the antineoplastic agents actinomycin D, doxorubicin, vinblastine, and the HDAC inhibitors panobinostat and vorinostat were particularly cytotoxic, causing cell death even at the 1x C_{max} concentration. This sensitivity and response of differentiating stem cells to these test compounds and their impact on disruption of transcription may be attributed to the rapid growth and the dynamic nature of transcriptional events occurring during stem cell differentiation.

Regarding specific teratogens, the retinoids 9-cis retinoic acid, acitretin, and isotretinoin induced significant changes in gene expression, with isotretinoin causing the highest number of alterations (1460up/567down). This indicates the presence of retinoid receptors and associated pathways in our differentiating cells. The DHODH inhibitor leflunomide (994up/2332down) and its active metabolite teriflunomide also affected gene expression, albeit to a slightly lesser extent. The hedgehog pathway inhibitor vismodegib did not induce significant changes in gene expression, suggesting insensitivity of SBAD2 cells to this class of inhibitors.

At the 1x concentration, vismodegib, a hedgehog pathway inhibitor, did not produce significant changes in the gene expression. However, at 20x concentrations, vismodegib exhibited poor solubility and was ineffective, similar to the teratogenic anticonvulsant phenytoin. Phenytoin, which blocks voltage-gated sodium channels, also did not induce significant gene expression changes at therapeutic concentrations. The concentrations of phenytoin used were at the upper limits of solubility, with the highest applied concentrations corresponding to 1x C_{max}. SBAD2 cells demonstrated lower sensitivity to this particular class of substances compared to others, as evidenced by the lack of cytotoxic effects.

On the other hand, atorvastatin, favipiravir, lithium chloride, and carbamazepine induced a higher number of gene expression changes at the 20x concentration compared to the 1x concentration.

Trichostatin A exhibited toxicity at the 20x concentration, while at the 1x concentration, it already induced a significant number of gene expression changes. Similarly, entinostat and valproic acid showed significant alterations in gene expression at the 1x concentration, with an increased number of changes observed at the 20x concentration. Methotrexate, methylmercury, and thalidomide were detected as teratogens already at the 1x concentration, with minimal changes observed at the 20x concentration.

Overall, the genome-wide transcriptome analyses revealed that teratogenic compounds induced substantial gene expression changes and exhibited cytotoxicity in differentiating SBAD2-hiPSCs, distinguishing them from non-teratogenic substances. These findings highlight the potential of these compounds to act as teratogens and underline the importance of concentration-dependent effects. Notably, phenytoin and vismodegib showed limited effects in our system, indicating a lower sensitivity of SBAD2 cells to these substances compared to others.

4.2 The two classifiers (this part is from our publication Cherianidou et al 2021 [86])

The UKK2 test system's in vitro results were utilized to develop two classifiers, namely "Cytotox1000" and "Cytotox SPS," to compare the in vitro findings with the in vivo situation and evaluate system performance.

Employing a penalized logistic regression procedure (referred to as the top-1000 procedure) at 1-fold C_{max}, along with cytotoxicity information, classification achieved an AUC of 0.96, an accuracy of 0.92, a sensitivity of 0.96, and a specificity of 0.88. These performance metrics were unexpectedly favorable, especially considering that the system was based on human induced pluripotent stem cells (hiPSCs) with a focus on cardiac differentiation. Although most of the tested teratogens were not specifically known for their effects on cardiac development, they are associated with disruptions in other aspects of embryo-fetal development, such as limb deformations by thalidomide [108] spina bifida by valproic acid [109] or developmental neurotoxicity due to methylmercury exposure [110]. The positive results obtained in the UKK2 test may be attributed to the hiPSCs activating numerous gene regulatory networks during differentiation that overlap with those involved in various embryo-fetal developmental processes. Thus, even if a specific developmental process like limb development is not replicated in the test, exposure to teratogens at in vivo relevant concentrations can still lead to gene expression changes in the hiPSCs.

The aim of this study was to address three key questions regarding the implementation of a transcriptomics-based developmental in vitro test. Firstly, it was observed that utilizing a penalized logistic regression procedure (referred to as the top-1000 procedure) with leave-one-out cross-validation based on the

1000 probe sets exhibiting the highest variance enables classification with higher AUC and accuracy compared to solely using the number of differential genes (SPS-procedure). However, the top-1000 procedure showed higher sensitivity while the SPS-procedure demonstrated higher specificity, albeit without cross-validation using the leave-one-out approach like the top-1000 procedure. To address the second question of whether a test should be considered positive when cytotoxicity occurs, the results clearly indicate that incorporating information on cytotoxicity improves the classification procedure, yielding higher metrics. Cytotoxicity alone resulted in an AUC of 0.61 and 0.63 for 1-fold and 20-fold C_{max}, respectively, which surpasses random results but is inferior to the procedure incorporating gene expression. Although a specific cytotoxicity test based on mitochondrial activity was not performed in this study due to the initial experimental design, the findings highlight the importance of including a sensitive cytotoxicity test, such as the CellTiter-Blue Cell Viability Assay [111] [112] in future studies to enhance the metrics. The third question investigated in this study examined whether classification accuracy is improved at 20-fold C_{max} compared to 1-fold C_{max}. Surprisingly, no significant differences in the metrics were observed between the two concentrations. In fact, the values were slightly higher for 1-fold C_{max} than for 20-fold C_{max}. This finding is unexpected, as previous studies on hepato and nephrotoxicity have reported better classification at concentrations at least 20-fold higher than the C_{max} [111] [113]. The difference observed between developmental toxicity and liver/kidney toxicity could be attributed to the fact that a significant portion of liver or kidney toxic compounds often require metabolic activation[114] [86]. Since the metabolic activities of cultured cells are typically lower than those in vivo, higher concentrations of test compounds may be necessary in vitro to induce similar toxic effects. On the other hand, metabolism may have less impact on the developmental toxicants analyzed in this study, which could explain the positive outcome obtained with 1-fold C_{max}. Further investigations in future studies should consider concentration-dependent testing, including lower concentrations than the maximum observed concentration (C_{max}), to gain additional insights. Additionally, the misclassifications of certain compounds should be carefully examined as they can highlight limitations of the test system, which can be addressed in future experiments. For example, compounds such as MAG and ASC at 20-fold C_{max} in the SPS procedure, and RET at 20-fold C_{max} in the top-1000 procedure, were identified as false positives. However, it should be noted that RET is known to be teratogenic at high doses[115] and overdoses of ASC and MAG have been associated with adverse effect [107], suggesting that the high concentrations used in vitro may also impact differentiating cells in vivo. On the other hand, the misclassification of SUC, DPH, and ATO by the top-1000 procedure indicates the need for further improvements in the test.

To summarize, we have successfully developed the UKK2 test, a transcriptomics- and hiPSC-based assay that demonstrates a strong correlation with in vivo developmental toxicity. Despite its current limitations, this assay, which involves a short 24-hour incubation period with test compounds, holds potential as a valuable component of a comprehensive testing battery employed during the early stages of drug discovery. End of the citation from [86]

In a recent publication with partners, we conducted a comparative analysis between the UKK2 test and UKN1 test, a neuronal differentiation-based approach [116]. Using the same experimental setup but employing distinct protocols for the UKN1 test, we observed a remarkable 90 % overlap in the tested compounds. Moreover, when we combined the arithmetic means of the classifiers, we observed a slight improvement. Additionally, we identified a significant overlap in critical developmental pathways and Gene Ontology (GO) groups, including PI3K-Akt, P53, TGF-beta, MAPK, EGFR, and Hippo pathways. This combined utilization of the UKK2 and UKN1 tests represents a significant advancement in the detection of developmental toxicity. Furthermore, it was observed that both UKN1 and UKK2 exhibited a significant overlap in the overrepresented Gene Ontology (GO) groups. Specifically, 83 % of all probe sets at 20-fold C_{max} showed an overlap, although the overlap of significant probe sets was relatively smaller at 27 %. Additionally, several critical signaling pathways involved in developmental processes, including PI3K-Akt, P53, TGF-beta, MAPK, EGFR, and Hippo pathways, were found to be influenced by teratogens in both tests, indicating a shared impact on these pathways.

Thus, combining the results from both tests further improved the classification metrics, and the shared representation of gene ontology groups and critical signaling pathways indicated common mechanisms influenced by teratogens in both tests.

4.3 Transcriptomic analysis reveals early germ layer formation and cardiomyogenic pathways in human pluripotent stem cells

To investigate the early germ layer formation induced by CHIR and its activation of the canonical Wnt/β-catenin signaling pathway leading to mesoderm and cardiomyocyte development, we conducted a comparative analysis of transcriptomes at different time points: 1 hour, 24 hours (day1), and 48 hours (day2). Our findings revealed a proportional increase in the number of differentially expressed genes as the incubation time progressed (**Figure 15**). Notably, these genes were enriched in developmental processes related to embryonic morphogenesis, heart development (mesodermal origin), brain development (ectodermal origin), and partial gland development (endodermal origin). This enrichment suggests that our model, particularly at the 24-hour time point, shares important characteristics with in vivo development. Therefore, the genes identified at this time point could potentially serve as a foundation for developing a gene set that could be employed as a biomarker for predicting developmental toxicity.

Our findings were further supported by the significant upregulation of key mesoderm genes, such as T (Brachyury), EOMES, and MIXL1, as well as markers associated with the initiation of cardiomyogenesis, including WNT3, LEF1, and DKK1. These observed gene expression patterns and enrichment

analysis results provide evidence for the robust activation of differentiation processes that mimic embryonic development. Moreover, our study suggests that the initiation of germ layer formation takes place on the first day of differentiation. Importantly, our results are consistent with previous studies utilizing human embryonic stem cell (hESC)-derived embryoid bodies and employing microarray analysis, which has demonstrated the presence of lineage-specific markers for ectoderm, mesoderm, and extra-embryonic endoderm [69, 76, 117].

Next, we wanted to examine the developmental pathways that are being deregulated during cardiogenesis. Therefore, we performed transcriptomic analysis this thime at three different time points (day1, day4 and day14) using the UKK2 differentiation protocol for 14 days. The exposure scheme remained the same as in the first part (24h) and the selected compounds were 3 teratogens (VPA, THD, ISO) and one non teratogen (BSP). Notably, ISO exhibited a clear inhibitory effect on cardiomyogenesis. Our attention at this section was directed towards the two early developmental stages of gastrulation and cardiac specification, which are recapitulated through the differentiation protocol. This approach enabled us to expose the cells to teratogens during these specific stages and identify deregulated genes as potential biomarkers for teratogenicity prediction.

4.4 Integration of cardiomyogenesis and developmental embryotoxicity assessment in human Pluripotent stem cells

In the second part of the thesis, we sought to mimic the process of cardiomyogenesis by utilizing the Wnt signaling pathway, as previously described [71, 72]. This approach would allow us to identify key gene signatures associated with cardiomyogenesis, which could then be utilized to identify compounds or environmental factors that specifically inhibit this developmental process.

In the UKK2-CTT, we subjected all the compounds to differentiation (only for 24 h at day1) and continue the differentiation until day14 according to our protocol scheme. Notably, among the tested compounds, retinoids such as Isotretinoin, acitrecin, and 9cis-retinoic acid demonstrated complete inhibition of the cardiomyogenesis process. Intrigued by this finding, we expanded our investigation by incorporating the teratogens ISO, VPA, and THD, along with the non-teratogen BSP, to identify specific gene signatures and pathways associated with cardiomyogenesis. This was achieved through transcriptome analysis conducted at different stages of differentiation, coupled with functional assessments of alterations during cardiomyocyte contractions.

Furthermore we sought to interpret the CDI31g score of all teratogens from UKK2 in relation to the existing literature, emphasizing for cardiac developmental toxicity (more detailed about CDI31score in 4.4.3 and in Table 12). Although THD and VPA are primarily recognized for their associations with

limb malformations [118] and neurological teratogenic effects leading to congenital malformations [109], recent studies have shed light on their potential involvement in heart malformations. Specifically, research utilizing zebrafish [119] and murine fetal heart [120] has demonstrated a connection between VPA and heart malformations. Similarly, investigations have linked THD to developing heart malformations [121, 122]. These emerging findings suggest a possible cardiotoxic effect of THD and VPA, expanding our understanding beyond their previously established teratogenic effects. While atorvastatin is not commonly associated with cardiotoxicity, no substantial reports have linked it to cardiac toxicity. In the case of carbamazepine, cardiotoxic effects have only been observed at acute concentrations in humans, as indicated by available literature [123]. Cardiotoxic effects in acute concentrations were observed in methotrexate as well [124]. Entinostat, on the other hand, has demonstrated cardiotoxicity in hiPSC cardiomyocytes [125]. Limited literature suggests that teratogens such as lithium chloride, MeHg, and paroxetine may also exhibit some degree of cardiotoxicity [126, 127, 128, 129]. However, no relevant literature regarding their cardiotoxic effects could be found for teratogens such as favipiravir, vismodegib, leflunomide, and teriflunomide.

Thus, these findings highlight the inhibitory effects of certain compounds, including retinoids, on cardiomyogenesis, while also suggesting potential cardiotoxic effects of teratogens such as THD and VPA, expanding our understanding beyond their established teratogenic effects.

4.4.1 Investigation of molecular mechanisms and signaling pathways in developmental abnormalities caused by Isotretinoin

To achieve our goal from the previous chapter, we conducted the transcriptomic analysis to compare the effects of ISO, THD, VPA, and BSP on cardiomyogenesis during different time points. The analysis revealed a clear separation of samples from different time points on the principal component analysis (PCA) plot. Additionally, the volcano plot confirmed the substantial deregulation of significant probe sets (SPS) for all three teratogens, with ISO exhibiting the highest number of deregulated genes on day14. These findings indicated that ISO triggered a distinct transcriptomic differentiation trajectory compared to the other compounds, starting from day1.

Our subsequent investigation aimed to uncover the molecular mechanisms underlying the disruption or shift in differentiation caused by ISO. This exploration sought to provide insights into the factors contributing to developmental abnormalities, particularly during cardiogenesis.

One of the first functional organs during emrbryonic development is the heart. During gastrulation, the vertebrate heart is derived from lateral mesoderm [49, 119]. Normal mesoderm formation occurs when epiblast cells ingress through the primitive streak (PS), a process regulated by BMP, Nodal, Wnt, and FGF signaling pathways [130]. Previous studies have shown that Nodal-mediated suppression of neural development depends on active Wnt signalling [131]. Wnt/β-catenin signaling

has a biphasic role in controlling cardiomyocyte differentiation, promoting cardiogenesis at the early stages of development, and contributing to the proper size of the heart-forming field at later stages [49].

Proper regulation of retinoic acid (RA) signaling is vital for various aspects of heart development, such as cardiac mesoderm formation, cardiac progenitor specification, heart tube formation, ventricular and atrial differentiation among other [132]. However, an imbalance in the activation of the retinoic signaling pathway can have teratogenic effects on heart development in vertebrates [133]. The production of RA is tightly regulated by enzymes, and their expression levels vary significantly during embryonic development. The expression and activity of these enzymes (RDHs and RALDHs) are spatially and temporally regulated during embryonic development [134]. Different concentrations of RA can exert distinct effects on cardiac lineage commitment and differentiation. High concentrations of RA promote the differentiation of mesodermal cells into cardiac progenitors, while lower concentrations are required for the subsequent differentiation of cardiac progenitors into functional cardiomyocytes [132]. Additionally, the concentration of RA, along with cardiomyogenic factors such as BMP2, can direct the differentiation of hiPSCs into specific cardiac cell types, such as sinoatrial node or epicardial cardiomyocytes [133]. Studies have demonstrated that the addition of high concentrations of RA (0.5 to 1 mM) to mesoderm-differentiated hiPSCs can induce the formation of different types of cardiomyocytes [132]. Relatively high concentrations of RA also promote the development of neural progenitors in hESC EBs [69], achieved through the simultaneous inhibition of the Nodal/Activin and BMP signaling pathways [135]. Additionally, previous studies have shown that RA represses mesodermal cell fates [136] and inhibits the RA signaling pathway, resulting in a transient overexpression of transcription factors T Brachyury and Mixl, which are necessary for mesoderm formation [137, 138].

In conclusion, our study underscores the detrimental impact of ISO, on cardiomyogenesis, and emphasizes the significance of retinoic acid pathway, in the process of heart development and the specification of cardiac cells. The identification of the RA pathway as a key player in developmental toxicity testing highlights its importance and potential as a biomarker for detecting different forms of developmental toxicity. This finding emphasizes the value of targeting the RA pathway in assessing the adverse effects of substances on embryonic development.

4.4.2 Dysregulation of signaling pathways in retinoid-induced cardiogenic mesoderm specification

In the UKK2-CTT, the concurrent exposure of hiPSCs to CHIR (a WNT activator) and retinoids (ISO, 9cis-retinoic acid, and acitretin) led to an enrichment of neuronal development events and inhibited mesoderm induction. Treatment with retinoids resulted in an increased expression of HOX genes in the hindbrain during embryonic development and a decrease in the transcription factor eomeso-

dermin (EOMES), which is necessary for the specification of early stages of heart development and the direction of pre-cardiac mesoderm fate specification [139]. The dysregulation of Wnt signaling molecules, such as HHEX, ZNF503, and KDR, may also contribute to inhibiting cardiogenic mesoderm specification caused by retinoid exposure.

Excessive retinoic acid (RA) signaling has been shown to increase HOX activity during heart development in zebrafish embryos, resulting in the loss of atrial and ventricular cardiomyocytes [140]. Our study also revealed a significant upregulation of HOXA5, HOXB5, and HOXD1 RNA levels after ISO treatment on day1, suggesting the involvement of the HOXA family in RA-induced heart teratogenicity.

Of particular interest, the TGF-β superfamily members lefty1 and lefty2, which play crucial roles in cardiomyogenesis, were highly upregulated under retinoid-treated conditions starting from day1 (**Figure S12**). Both factors play an important role in left and right pattering, and their upregulation normally inhibits heart development via inhibition of NODAL signaling pathway [141, 142]. The binding of Lefty1 and Lefty2 to Nodal inhibits the Nodal signaling pathway by inactivating the active Nodal/Activin receptor complex [143]. These findings suggest that the loss of Nodal function prevents mesoderm formation, thereby impacting further cardiac specification during embryonic development.

4.4.3 Developmental gene signature and teratogenic potential in early cardiogenesis

In our study, we aimed to identify an early gene signature associated with heart development by utilizing two different hiPSC lines and three distinct retinoids. Our analysis successfully revealed a set of 31 genes that play a significant role in early heart development. To assess the predictive capability of the UKK2-CTT, we introduced the CDI31g index, which allows differentiation between teratogens and non-teratogens (**Table 12**). It was observed that teratogens exhibited CDI31g values close to 0, indicating a lack of cardiotoxicity. On the other hand, all three retinoids in our test system had a CDI31g value of 1, suggesting the presence of cardiotoxicity.

Among the identified genes, important representatives of the retinoic acid pathway, such as CYP26A1 and DHRS3, were included. Additionally, we found genes associated with tissue morphogenesis processes (HOXA5, HOXB2, ID4, KDR, EOMES, GREB1L, DMRT1, DHRS3, RBM20, MECOM, ZNF503) as well as genes specifically involved in heart development (KDR, SOX9, EOMES, DHRS3, GREB1L, RBM20). These findings highlight the relevance of these genes in heart development and provide valuable insights for further investigations in the field of cardiotoxicity and teratogenicity.

Interestingly, the CDI31g values for THD and VPA were 0.3 and 0.4, respectively, suggesting potential teratogenic effects, particularly for THD, in cardiac development. This observation aligns with previous studies that demonstrated cardiac defects induced by THD in developing chicken embryos [122] and mice [144]. Additionally, THD treatment in patients with multiple myeloma (MM) resulted in cardiotoxicity, manifested as severe bradycardia [145, 146]. Similar cardiotoxic effects were observed in patients with amyotrophic lateral sclerosis (ALS) who received THD treatment [147]. In our hiPSC experiments, we observed beating clusters of cardiomyocytes (CMs) after 24 hours of THD and VPA treatment, indicating that these compounds did not significantly affect cardiomyogenesis in these cells. However, the beating frequency of the resulting cardiomyocytes was significantly reduced by both THD and VPA, primarily due to the prolongation of the relaxation phase. This suggests that the functional properties of the developed cardiomyocytes were affected by the compounds. Furthermore, we observed that VPA and THD regulated a relatively high number of genes on day1 and day4, respectively. These gene regulations were associated with the differentiation-modulating activities of VPA and THD, as observed through the structural changes in α-cardiac actinin 2 on day14.

Comparing the structure of cardiac α-actinin 2 in the control condition with the treatment involving the non-teratogen BSP and the teratogens VPA and THD, notable damage to the cardiomyocytes was observed. Cardiomyocytes, specialized muscle cells, exhibit a highly organized arrangement of myofilaments called sarcomeres, which are essential for mechanical cardiac contraction. Sarcomeric proteins, including those in the thin filament, thick filament, and Z-disc, contribute to the formation of functional contractile units. Any disturbances or malfunctioning of these proteins can lead to cardiomyopathy or heart failure [148]. Live cell imaging clearly showed significant disorganization of cardiac α-actinin 2, a cardiac myofilament protein crucial for the structural organization of the sarcomere and the proper functioning of the heart muscle.

In conclusion, our findings highlight the significance of developmental genes in the cardiogenesis process during early embryonic development. The identified early heart developmental gene signature provides valuable insights into heart development and offers the potential for predicting the teratogenic potential of chemicals or drugs. The evaluation of the UKK2-CTT using the CDI31g index revealed indications of teratogenic effects, particularly for THD, in cardiac development. This aligns with previous studies demonstrating cardiac defects associated with THD exposure. Our hiPSC experiments further elucidated the functional impact of THD and VPA on cardiomyocytes, highlighting the importance of monitoring cardiac parameters beyond cardiomyogenesis. Additionally, the observed gene regulations at different timepoints and the structural changes in α-cardiac actinin 2 underscore the differentiation-modulating activities of VPA and THD. These findings contribute to our understanding of the complex interactions between teratogens and cardiogenesis, aiding in developing safer drugs and chemicals.

4.5 Assessment of drug exposure effects on early developmental patterning in hPSC-based models

Several studies based on human pluripotent stem cells (hPSCs) have focused on assessing the effects of drug exposure that replicate gastrulation-like stages, germ layer specification, and subsequent differentiation into mesendoderm and cardiac lineages, as outlined in the literature [149, 150, 151, 152]. Embryonic toxicity testing has utilized two distinct types of models involving human pluripotent stem cells: embryoid bodies (EBs) and gastruloid models. These models are employed to assess the effects of drug exposure on germ layer specification and to investigate developmental toxicity specifically related to the heart.

Embryoid bodies have been extensively employed as an early human stem cell-based model. They accurately represent cellular differentiation into all three germ layers, making them suitable for studying the toxic impacts of compounds during the blastocyst stage. On the other hand, gastruloids offer an additional advantage by potentially revealing spatial organization abnormalities, thereby providing valuable insights into developmental defects.

In our previously published UKK test [75] , both human induced pluripotent stem cells (hiPSCs), and human embryonic stem cells (hESCs) were utilized. The pluripotent cells underwent differentiation into germ layers (EBs) over a continuous 14-day period, with exposure to the 12 test compounds at their maximum non-cytotoxic concentration. Through the analysis of genome-wide expression data, two indices were defined to assess the developmental hazards associated with each test compound. In comparison to the aforementioned UKK test, the newly established UKK2 test presents several advantages and upgrades. Firstly, it exclusively employs human-induced pluripotent cells, addresses ethical concerns associated human ES cells. Furthermore, the test concentrations used in UKK2 are in line with in vivo relevant concentrations, increasing the physiological significance of the results. Additionally, the duration of the test has been significantly reduced to 24 hours, thereby minimizing the time of drug exposure. The UKK2 test was assessed with 39 test compounds, and the subsequent GO and KEGG pathway analyses successfully identified pathways that are also implicated in in vivo settings. These findings parallel the outcomes observed in the previous UKK test. Altogether, this comprehensive approach utilizing transcriptomics and iPS cells demonstrates the utility of detecting early developmental effects, highlighting their potential as valuable tools in developmental toxicity assessment.

In the field of mesendoderm direction and cardiac specification, several models have been previously published [153, 154, 155, 65, 156], employing either 2D or 3D conditions in cell culture. These models have provided valuable insights into the specific stages of cardiac commitment that are affected by drug exposure. To investigate this further, various drug exposure timeframes corresponding to different stages of pregnancy have been applied, and readouts have been evaluated at multiple

time points during differentiation. Notably, Liu et al. [157] conducted a study using a monolayer protocol and induced pluripotent stem cells (iPSCs), confirming the disruption of early mesoderm and subsequent inhibition of cardiac differentiation caused by ISO. In comparison, our UKK-CTT platform utilized three different retinoids and also confirmed the inhibition of cardiac mesoderm formation after only 24 hours of exposure to the compounds. However, it is important to note that drugs may sometimes act at different stages of cardiac differentiation. For instance, in the case of ribavirin [158], it did not affect the differentiation of pluripotent cells into mesoderm but did disrupt the differentiation process after mesoderm formation towards cardiac differentiation, as mentioned in the reference reference. This highlights the complexity of drug effects on cardiac development and underscores the need for comprehensive investigations to understand the precise mechanisms and stages affected by different compounds.

In summary, the investigation into drug exposure timing has revealed the presence of a critical phase in cardiac commitment, which is particularly susceptible to specific drugs. Understanding the timing of drug administration is crucial in unraveling the intricate mechanisms underlying cardiac development and identifying periods of heightened vulnerability. This knowledge has the potential to guide targeted interventions and enhance drug safety during critical stages of cardiac commitment.

4.6 Conclusion and future perspectives

In this thesis, we have discussed the development and application of the UKK2 and UKK-CTT method for assessing drug-induced developmental toxicity in human pluripotent stem cell based models. Our UKK-CTT offers several advantages, including the ability to study specific signaling pathways during german layer formation and the cardiomyogenesis at the earliest stages of mesodermal formation as well as its rapid implementation under monolayer conditions at an in vivo relevant concentration (C_{max}). This allowed the efficient screening of multiple substances based our two classifiers and on the CDI31g index, and enabled the discrimination of teratogens that specifically inhibit functional cardiomyogenesis. Furthermore, the integration of GFP tagged α-cardiac actinin 2 structure as an phenotypical endpoint enabled us to gain insights into the impact of teratogens on the cardiac muscle structure and functionality (**Figure 21**).

Severe cardiovascular dysfunction during the early stages of gestation, approximately 3–4 weeks, can be lethal for embryos [159]. Therefore, identifying cardiac developmental toxicity is challenging due to the limited retrospective clinical data that primarily capture defects observed after birth. These data only provide a narrow window into the potential impact of drugs during embryonic development. Here, our UKK-CTT design has captured crucial information regarding cardiac developmental toxicity that is often overlooked in retrospective studies.

While our UKK-CTT represents a significant advancement in human pluripotent based models for developmental toxicity screening, there are several limitations with this approach. The lack of physiological relevance between cardiomyocytes derived from a 2D differentiation protocol and a 3D structure and cellular interactions found in native heart. The missing intercellular interactions with other cell types, such as endothelial cells, fibroblast and immune cells, is also an important limitation that is not covered with the oversimplified approach of a 2D models. Additional limitations are, the limited cell maturity, tissue complexity and insufficient mechanical forces of cardiomyocytes in 2D models [160]. To overcome these limitations, already researches are exploring models that are based on 3D organoids organ-on-a-chip systems [161] , and co-culture models [162] that aim to better recapitulate the complexity of native cardiac tissue and improve the predictive value of toxicity testing. Although the application of hPSC-derived heart organoids in developmental toxicity assays is in its early stages, they can serve as complementary tests to the well-established 2D models, which are better suited for assessing teratogenicity at the cellular differentiation level rather than revealing structural defects.

In conclusion, the development and application of the UKK2 and UKK-CTT method in hPSC-based models have provided valuable insights into drug-induced developmental toxicity. These findings contribute to the understanding of the critical phases of embryonic development and form a basis for targeted interventions and improved drug safety in these vulnerable phases. The future integration of advanced 3D models and the ongoing improvements of hPSC-based platforms hold great promise for enhancing our ability to predict and mitigate developmental toxicity risks in human pregnancies.

5 References

1) Kim, J.H. and A.R. Scialli, Thalidomide: The Tragedy of Birth Defects and the Effective Treatment of Disease. Toxicological Sciences, 2011. 122(1): p. 1-6.

2) Pizzino, G., et al., Oxidative Stress: Harms and Benefits for Human Health. Oxidative Medicine and Cellular Longevity, 2017. 2017.

3) Predieri, B., et al., Endocrine Disrupting Chemicals' Effects in Children: What We Know and What We Need to Learn? International Journal of Molecular Sciences, 2022. 23(19).

4) Willhite, C.C. and P.E. Mirkes, 2014: p. - 44.

5) E, U., et al., - Teratology - past, present and future. - Interdiscip Toxicol. 2012 Dec;5(4):163-8. doi: 10.2478/v10102-012-0027-0., (- 1337-6853 (Print)): p. - 163-8.

6) Waldorf, K.M.A. and R.M. McAdams, Influence of infection during pregnancy on fetal development. Reproduction, 2013. 146(5): p. R151-R162.

7) Lloyd, K.A., A scientific review: mechanisms of valproate-mediated teratogenesis. Bioscience Horizons: The International Journal of Student Research, 2013. 6.

8) Mehmet Semih, D., 2020.

9) MT, M., - Thalidomide embryopathy: a model for the study of congenital incomitant. - Trans Am Ophthalmol Soc. 1991;89:623-74., (- 0065-9533 (Print)): p. - 623-74.

10) MM, v.G., et al., - Teratogenic mechanisms of medical drugs. - Hum Reprod Update. 2010 Jul-Aug;16(4):378-94. doi: 10.1093/humupd/dmp052. Epub, (- 1460-2369 (Electronic)): p. - 378-94.

11) BJ, W., et al., - Genetic basis of susceptibility to teratogen induced birth defects. - Am J Med Genet C Semin Med Genet. 2011 Aug 15;157C(3):215-26. doi:, (- 1552-4876 (Electronic)): p. - 215-26.

12) MA, M. and S. LL, - Enzymatic Metabolism of Vitamin A in Developing Vertebrate Embryos. - Nutrients. 2016 Dec 15;8(12):812. doi: 10.3390/nu8120812., (- 2072-6643 (Electronic)): p. T - epublish.

13) B, S. and M. A, - Retinol Dehydrogenases Regulate Vitamin A Metabolism for Visual Function. - Nutrients. 2016 Nov 22;8(11):746. doi: 10.3390/nu8110746., (- 2072-6643 (Electronic)): p. T - epublish.

14) Fuchs, E. and H. Green, 1981. - 25(- 3): p. - 625.

15) JT, B. and G. CB, - The Role of Retinoic Acid (RA) in Spermatogonial Differentiation. - Biol Reprod. 2016 Jan;94(1):10. doi: 10.1095/biolreprod.115.135145. Epub 2015 Nov, (- 1529-7268 (Electronic)): p. - 10.

16) X, Z., W. W, and Y. Y, - The expression of retinoic acid receptors in thymus of young children and the. - J Clin Immunol. 2008 Jan;28(1):85-91. doi: 10.1007/s10875-007-9122-y. Epub 2007, (- 0271-9142 (Print)): p. - 85-91.

17) EM, W., B.-E.D. S, and R. R, - The vicious cycle of vitamin a deficiency: A review. - Crit Rev Food Sci Nutr. 2017 Nov 22;57(17):3703-3714. doi:, (- 1549-7852 (Electronic)): p. - 3703-3714.

18) JN, H., et al., - Evaluation of vitamin A toxicity. - Am J Clin Nutr. 1990 Aug;52(2):183-202. doi: 10.1093/ajcn/52.2.183., (- 0002-9165 (Print)): p. - 183-202.

19) HM, D., et al., - Dietary vitamin A and teratogenic risk: European Teratology Society discussion. - Eur J Obstet Gynecol Reprod Biol. 1999 Mar;83(1):31-6. doi:, (- 0301-2115 (Print)): p. - 31-6.

20) F, L.-C., C. L, and B. M, - Current standard treatment of adult acute promyelocytic leukaemia. - Br J Haematol. 2016 Mar;172(6):841-54. doi: 10.1111/bjh.13890. Epub 2015 Dec 21., (- 1365-2141 (Electronic)): p. - 841-54.

21) YD, F., S. PN, and M. PJ, - The evidence for a beneficial role of vitamin A in multiple sclerosis. - CNS Drugs. 2014 Apr;28(4):291-9. doi: 10.1007/s40263-014-0148-4., (- 1179-1934 (Electronic)): p. - 291-9.

22) Semba, R.D., - On the 'Discovery'of Vitamin A. 2012. - 61(- 3): p. - 198.

23) JL, N., - Functions of Intracellular Retinoid Binding-Proteins. - Subcell Biochem. 2016;81:21-76. doi: 10.1007/978-94-024-0945-1_2., (- 0306-0225 (Print)): p. - 21-76.

24) LL, S., et al., - RDH10 is essential for synthesis of embryonic retinoic acid and is required for. - Genes Dev. 2007 May 1;21(9):1113-24. doi: 10.1101/gad.1533407., (- 0890-9369 (Print)): p. - 1113-24.

25) SE, B., et al., - The retinaldehyde reductase DHRS3 is essential for preventing the formation of. - FASEB J. 2013 Dec;27(12):4877-89. doi: 10.1096/fj.13-227967. Epub 2013 Sep 4., (- 1530-6860 (Electronic)): p. - 4877-89.

26) G, D., - Retinoic acid synthesis and signaling during early organogenesis. - Cell. 2008 Sep 19;134(6):921-31. doi: 10.1016/j.cell.2008.09.002., (- 1097-4172 (Electronic)): p. - 921-31.

27) JB, M., et al., - Dynamic patterns of retinoic acid synthesis and response in the developing. - Dev Biol. 1998 Jul 1;199(1):55-71. doi: 10.1006/dbio.1998.8911., (- 0012-1606 (Print)): p. - 55-71.

28) Niederreither, K. and P. Dollé, - Retinoic acid in development: towards an integrated view. 2008. - 9(- 7): p. - 553.

29) Duester, G., Retinoic acid synthesis and signaling during early organogenesis. Cell, 2008. 134(6): p. 921-931.

30) Hale, F., The relation of vitamin A to anophthalmos in pigs. American Journal of Ophthalmology, 1935. 18(12): p. 1087-1093.

31) Wilson, J.G. and J. Warkany, Malformation in the genito-urinary tract induced by maternal vitamin A deficiency in the rat. Obstetrical & Gynecological Survey, 1948. 3(6): p. 807.

32) Wilson, J.G. and J. Warkany, Aortic-arch and cardiac anomalies in the offspring of vitamin A deficient rats. American Journal of Anatomy, 1949. 85(1): p. 113-155.

33) Jg, W., R. Cb, and W. J., - An analysis of the syndrome of malformations induced by maternal vitamin A. - Am J Anat. 1953 Mar;92(2):189-217. doi: 10.1002/aja.1000920202., (- 0002-9106 (Print)): p. - 189-217.

34) Jg, W. and W. J., - Aortic-arch and cardiac anomalies in the offspring of vitamin A deficient rats. - Am J Anat. 1949 Jul;85(1):113-55. doi: 10.1002/aja.1000850106., (- 0002-9106 (Print)): p. - 113-55.

35) F, P., et al., - Mutations in STRA6 cause a broad spectrum of malformations including. - Am J Hum Genet. 2007 Mar;80(3):550-60. doi: 10.1086/512203. Epub 2007 Jan 29., (- 0002-9297 (Print)): p. - 550-60.

36) M, P., et al., - ALDH1A2 (RALDH2) genetic variation in human congenital heart disease. - BMC Med Genet. 2009 Nov 3;10:113. doi: 10.1186/1471-2350-10-113., (- 1471-2350 (Electronic)): p. - 113.

37) EJ, L., et al., - Retinoic acid embryopathy. - N Engl J Med. 1985 Oct 3;313(14):837-41. doi: 10.1056/NEJM198510033131401., (- 0028-4793 (Print)): p. - 837-41.

38) KJ, R., et al., - Teratogenicity of high vitamin A intake. - N Engl J Med. 1995 Nov 23;333(21):1369-73. doi: 10.1056/NEJM199511233332101., (- 0028-4793 (Print)): p. - 1369-73.

39) Kamm, J.J., Toxicology, carcinogenicity, and teratogenicity of some orally administered retinoids. Journal of the American Academy of Dermatology, 1982. 6(4): p. 652-659.

40) Kistler, A. and H. Hummler, Teratogenesis and reproductive safety evaluation of the retinoid etretin (Ro 10-1670). Archives of toxicology, 1985. 58: p. 50-56.

41) Lammer, E.J., et al., Retinoic acid embryopathy. New England Journal of Medicine, 1985. 313(14): p. 837-841.

42) Webster, W., et al., Isotretinoin embryopathy and the cranial neural crest: an in vivo and in vitro study. Journal of craniofacial genetics and developmental biology, 1986. 6(3): p. 211-222.

43) Cohen, M., et al., Thymic hypoplasia associated with isotretinoin embryopathy. American Journal of Diseases of Children, 1987. 141(3): p. 263-266.

44) Kistler, A., Inhibition of chondrogenesis by retinoids: limb bud cell cultures as a test system to measure the teratogenic potential of compounds. Concepts in Toxicology, 1985. 3: p. 86-100.

45) Niederreither, K., et al., Embryonic retinoic acid synthesis is essential for heart morphogenesis in the mouse. Development, 2001. 128(7): p. 1019-1031.

46) K, N., et al., - Embryonic retinoic acid synthesis is required for forelimb growth and. - Development. 2002 Aug;129(15):3563-74. doi: 10.1242/dev.129.15.3563., (- 0950-1991 (Print)): p. - 3563-74.

47) Hochgreb, T., et al., A caudorostral wave of RALDH2 conveys anteroposterior information to the cardiac field. 2003.

48) T, P., et al., - The role of CYP26 enzymes in defining appropriate retinoic acid exposure during. - Birth Defects Res A Clin Mol Teratol. 2010 Oct;88(10):883-94. doi:, (- 1542-0760 (Electronic)): p. - 883-94.

49) Keegan, B.R., et al., Retinoic acid signaling restricts the cardiac progenitor pool. Science, 2005. 307(5707): p. 247-249.

50) Vitobello, A., et al., Hox and Pbx factors control retinoic acid synthesis during hindbrain segmentation. Developmental cell, 2011. 20(4): p. 469-482.

51) Uehara, M., et al., CYP26A1 and CYP26C1 cooperatively regulate anterior–posterior patterning of the developing brain and the production of migratory cranial neural crest cells in the mouse. Developmental biology, 2007. 302(2): p. 399-411.

52) Bertrand, N., et al., Hox genes define distinct progenitor sub-domains within the second heart field. Developmental biology, 2011. 353(2): p. 266-274.

53) Stefanovic, S. and S. Zaffran, Mechanisms of retinoic acid signaling during cardiogenesis. Mechanisms of development, 2017. 143: p. 9-19.

54) I, F., M. C, and W. H, - Toxicity testing is evolving! - Toxicol Res (Camb). 2020 Apr 24;9(2):67-80. doi: 10.1093/toxres/tfaa011., (- 2045-452X (Print)): p. - 67-80.

55) Li, Z., 2011: p. - 563.

56) Richard J. Albertini, G.B., Noncancer endpoints associated with butadiene exposure: biomarkers, genotoxicity and reproductive toxicity Toxicology, 1996. 113(113): p. 56-58.

57) Zeiger, E., A. Auletta, and J. Cavagnaro, Validation and Regulatory Acceptance of Toxicological Test Methods: A Report of the Ad Hoc Interagency Coordinating Committee on the Validation of Alternative Methods. 1998: DIANE Publishing Company.

58) LD, W., - The ICH S5(R2) guideline for the testing of medicinal agents. - Methods Mol Biol. 2013;947:1-11. doi: 10.1007/978-1-62703-131-8_1., (- 1940-6029 (Electronic)): p. - 1-11.

59) SL, M., et al., - Current and future needs for developmental toxicity testing. - Birth Defects Res B Dev Reprod Toxicol. 2011 Oct;92(5):384-94. doi:, (- 1542-9741 (Electronic)): p. - 384-94.

60) Kagawa, H., et al., - Human blastoids model blastocyst development and implantation. 2022. - 601(- 7894): p. - 605.

61) Yanagida, A., et al., 2021. - 28(- 6): p. - 1022.e4.

62) C, M., et al., - Differentiation of human embryonic stem cells to cardiomyocytes: role of. - Circulation. 2003 Jun 3;107(21):2733-40. doi: 10.1161/01.CIR.0000068356.38592.68., (- 1524-4539 (Electronic)): p. - 2733-40.

63) E, F., et al., - Stem Cells for Next Level Toxicity Testing in the 21st Century. - Small. 2021 Apr;17(15):e2006252. doi: 10.1002/smll.202006252. Epub 2020 Dec 23., (- 1613-6829 (Electronic)): p. - e2006252.

64) Mantziou, V., et al., 2021. - 105: p. - 90.

65) Kameoka, S., et al., A high-throughput screen for teratogens using human pluripotent stem cells. toxicological sciences, 2014. 137(1): p. 76-90.

66) Martin, M., et al., - Advances in 3D Organoid Models for Stem Cell-Based Cardiac Regeneration. 2023. - 24(- 6).

67) Hoang, P., et al., Engineering spatial-organized cardiac organoids for developmental toxicity testing. Stem Cell Reports, 2021. 16(5): p. 1228-1244.

68) J, C., et al., - Assessing self-renewal and differentiation in human embryonic stem cell lines.

69) J, I.-E., et al., - Differentiation of human embryonic stem cells into embryoid bodies compromising. - Mol Med. 2000 Feb;6(2):88-95., (- 1076-1551 (Print)): p. - 88-95.

70) J, Y., et al., - Flk1-positive cells derived from embryonic stem cells serve as vascular. - Nature. 2000 Nov 2;408(6808):92-6. doi: 10.1038/35040568., (- 0028-0836 (Print)): p. - 92-6.

71) Lian, X., et al., Robust cardiomyocyte differentiation from human pluripotent stem cells via temporal modulation of canonical Wnt signaling. Proceedings of the National Academy of Sciences, 2012. 109(27): p. E1848-E1857.

72) H, N., et al., - Cyclooxygenases Inhibitors Efficiently Induce Cardiomyogenesis in Human. - Cells. 2020 Feb 27;9(3):554. doi: 10.3390/cells9030554., (- 2073-4409 (Electronic)): p. T - epublish.

73) van Dartel, D.A., et al., Monitoring developmental toxicity in the embryonic stem cell test using differential gene expression of differentiation-related genes. Toxicological sciences, 2010. 116(1): p. 130-139.

74) KJ, C., et al., - Evaluation of 309 environmental chemicals using a mouse embryonic stem cell. - PLoS One. 2011;6(6):e18540. doi: 10.1371/journal.pone.0018540. Epub 2011 Jun 7., (- 1932-6203 (Electronic)): p. - e18540.

75) V, S., et al., - Definition of transcriptome-based indices for quantitative characterization of. - Arch Toxicol. 2017 Feb;91(2):839-864. doi: 10.1007/s00204-016-1741-8. Epub 2016, (- 1432-0738 (Electronic)): p. - 839-864.

76) S, J., et al., - Cytosine arabinoside induces ectoderm and inhibits mesoderm expression in human. - Br J Pharmacol. 2011 Apr;162(8):1743-56. doi: 10.1111/j.1476-5381.2010.01197.x., (- 1476-5381 (Electronic)): p. - 1743-56.

77) Y, M., Y. O, and B. N, - Teratogen screening using transcriptome profiling of differentiating human. - J Cell Mol Med. 2011 Jun;15(6):1393-401. doi: 10.1111/j.1582-4934.2010.01105.x., (- 1582-4934 (Electronic)): p. - 1393-401.

78) K, M., et al., - Identification of thalidomide-specific transcriptomics and proteomics signatures. - PLoS One. 2012;7(8):e44228. doi: 10.1371/journal.pone.0044228. Epub 2012 Aug 28., (- 1932-6203 (Electronic)): p. - e44228.

79) A, A., et al., - Live-Cell Imaging of the Contractile Velocity and Transient Intracellular Ca(2+). - Cells. 2022 Apr 9;11(8):1280. doi: 10.3390/cells11081280., (- 2073-4409 (Electronic)): p. T - epublish.

80) A, A., et al., - Microgravity-induced stress mechanisms in human stem cell-derived cardiomyocytes. - iScience. 2022 Jun 11;25(7):104577. doi: 10.1016/j.isci.2022.104577. eCollection, (- 2589-0042 (Electronic)): p. - 104577.

81) RN, V.G., et al., - Amplified RNA synthesized from limited quantities of heterogeneous cDNA. - Proc Natl Acad Sci U S A. 1990 Mar;87(5):1663-7. doi: 10.1073/pnas.87.5.1663., (- 0027-8424 (Print)): p. - 1663-7.

82) ME, R., et al., - limma powers differential expression analyses for RNA-sequencing and microarray. - Nucleic Acids Res. 2015 Apr 20;43(7):e47. doi: 10.1093/nar/gkv007. Epub 2015 Jan, (- 1362-4962 (Electronic)): p. - e47.

83) Smyth, G.K., - limma: Linear Models for Microarray Data. 2005: p. - 420.

84) Benjamini, Y. and Y. Hochberg, - Controlling the False Discovery Rate: A Practical and Powerful Approach to Multiple Testing. 1995. - 57(- 1): p. - 300.

85) Zhou, Y., et al., Metascape provides a biologist-oriented resource for the analysis of systems-level datasets. Nature Communications, 2019. 10(1): p. 1523.

86) A, C., et al., - Classification of Developmental Toxicants in a Human iPSC Transcriptomics-Based. - Chem Res Toxicol. 2022 May 16;35(5):760-773. doi: 10.1021/acs.chemrestox.1c00392., (- 1520-5010 (Electronic)): p. - 760-773.

87) D, T., et al., - Regulation of Hoxb3 expression in the hindbrain and pharyngeal arches by rae28, a.

88) T, E., et al., - Transcription factor PROX1: its role in development and cancer. - Cancer Metastasis Rev. 2012 Dec;31(3-4):793-805. doi: 10.1007/s10555-012-9390-8., (- 1573-7233 (Electronic)): p. - 793-805.

89) H, P., et al., - The homeobox gene Hhex regulates the earliest stages of definitive hematopoiesis. - Blood. 2010 Aug 26;116(8):1254-62. doi: 10.1182/blood-2009-11-254383. Epub 2010, (- 1528-0020 (Electronic)): p. - 1254-62.

90) J, L., et al., - SPRY4-IT1: A novel oncogenic long non-coding RNA in human cancers. - Tumour Biol. 2017 Jun;39(6):1010428317711406. doi: 10.1177/1010428317711406., (- 1423-0380 (Electronic)): p. - 1010428317711406.

91) JP, D., et al., - Germline mutations in PRKCSH are associated with autosomal dominant polycystic. - Nat Genet. 2003 Mar;33(3):345-7. doi: 10.1038/ng1104. Epub 2003 Feb 10., (- 1061-4036 (Print)): p. - 345-7.

92) Spinazzi, M. and B. De Strooper, 2016. - 60: p. - 28.

93) J, T., et al., - Eomes and Brachyury control pluripotency exit and germ-layer segregation by. - Nat Cell Biol. 2019 Dec;21(12):1518-1531. doi: 10.1038/s41556-019-0423-1. Epub, (- 1476-4679 (Electronic)): p. - 1518-1531.

94) RA, K. and G. N, - Teratogenic Genesis in Fetal Malformations. - Cureus. 2021 Feb 5;13(2):e13149. doi: 10.7759/cureus.13149., (- 2168-8184 (Print)): p. - e13149.

95) Genschow, E., et al., 2002. - 30(- 2): p. - 176.

96) JA, P., et al., - Assessment of the Embryonic Stem Cell Test and application and use in the. - Birth Defects Res B Dev Reprod Toxicol. 2008 Apr;83(2):104-11. doi:, (- 1542-9741 (Electronic)): p. - 104-11.

97) P, M.-S., et al., - A review of the implementation of the embryonic stem cell test (EST). The report. - Altern Lab Anim. 2009 Jul;37(3):313-28. doi: 10.1177/026119290903700314., (- 0261-1929 (Print)): p. - 313-28.

98) Robinson, J.F. and A.H. Piersma, - Toxicogenomic Approaches in Developmental Toxicology Testing. 2013: p. - 473.

99) ER, L., et al., - Thalidomide metabolism and hydrolysis: mechanisms and implications. - Curr Drug Metab. 2006 Aug;7(6):677-85. doi: 10.2174/138920006778017777., (- 1389-2002 (Print)): p. - 677-85.

100) H, N., - Teratogenicity of isotretinoin revisited: species variation and the role of. - J Am Acad Dermatol. 2001 Nov;45(5):S183-7. doi: 10.1067/mjd.2001.113720., (- 0190-9622 (Print)): p. - S183-7.

101) C, R., et al., - Assaying embryotoxicity in the test tube: current limitations of the embryonic. - Crit Rev Toxicol. 2012 May;42(5):443-64. doi: 10.3109/10408444.2012.674483., (- 1547-6898 (Electronic)): p. - 443-64.

102) DG, B., et al., - Thalidomide Inhibits Human iPSC Mesendoderm Differentiation by Modulating. - Sci Rep. 2020 Feb 18;10(1):2864. doi: 10.1038/s41598-020-59542-x., (- 2045-2322 (Electronic)): p. - 2864.

103) BK, A. and P. MK, - Developmental cardiotoxicity effects of four commonly used antiepileptic drugs in. - Toxicol In Vitro. 2014 Aug;28(5):948-60. doi: 10.1016/j.tiv.2014.04.001. Epub, (- 1879-3177 (Electronic)): p. - 948-60.

104) Pang, L., 2020. - 23-24: p. - 55.

105) C, T., et al., - Human Induced Pluripotent Stem Cells as a Screening Platform for Drug-Induced. - Front Pharmacol. 2021 Mar 10;12:613837. doi: 10.3389/fphar.2021.613837., (- 1663-9812 (Print)): p. - 613837.

106) S, Y., et al., - Pluripotency of embryonic stem cells. - Cell Tissue Res. 2008 Jan;331(1):5-22. doi: 10.1007/s00441-007-0520-5. Epub 2007, (- 1432-0878 (Electronic)): p. - 5-22.

107) JM, T. and M. PT, - Hypomagnesemia and hypermagnesemia. - Rev Endocr Metab Disord. 2003 May;4(2):195-206. doi: 10.1023/a:1022950321817., (- 1389-9155 (Print)): p. - 195-206.

108) N, V., - Thalidomide-induced teratogenesis: history and mechanisms. - Birth Defects Res C Embryo Today. 2015 Jun;105(2):140-56. doi:, (- 1542-9768 (Electronic)): p. - 140-56.

109) A, O., - Valproic acid in pregnancy: how much are we endangering the embryo and fetus? - Reprod Toxicol. 2009 Jul;28(1):1-10. doi: 10.1016/j.reprotox.2009.02.014. Epub, (- 1873-1708 (Electronic)): p. - 1-10.

110) MR, K., et al., - Evidence on the human health effects of low-level methylmercury exposure. - Environ Health Perspect. 2012 Jun;120(6):799-806. doi: 10.1289/ehp.1104494. Epub, (- 1552-9924 (Electronic)): p. - 799-806.

111) W, A., et al., - Prediction of human drug-induced liver injury (DILI) in relation to oral doses. - Arch Toxicol. 2019 Jun;93(6):1609-1637. doi: 10.1007/s00204-019-02492-9. Epub, (- 1432-0738 (Electronic)): p. - 1609-1637.

112) X, G., et al., - Relevance of the incubation period in cytotoxicity testing with primary human. - Arch Toxicol. 2018 Dec;92(12):3505-3515. doi: 10.1007/s00204-018-2302-0. Epub, (- 1432-0738 (Electronic)): p. - 3505-3515.

113) JG, H., et al., - In vitro prediction of organ toxicity: the challenges of scaling and secondary. - Arch Toxicol. 2020 Feb;94(2):353-356. doi: 10.1007/s00204-020-02669-7. Epub 2020, (- 1432-0738 (Electronic)): p. - 353-356.

114) M, L., et al., - Adverse outcome pathways: opportunities, limitations and open questions. - Arch Toxicol. 2017 Nov;91(11):3477-3505. doi: 10.1007/s00204-017-2045-3. Epub, (- 1432-0738 (Electronic)): p. - 3477-3505.

115) A, C., et al., - Nuclear retinoid receptors and pregnancy: placental transfer, functions, and. - Cell Mol Life Sci. 2016 Oct;73(20):3823-37. doi: 10.1007/s00018-016-2332-9. Epub, (- 1420-9071 (Electronic)): p. - 3823-37.

116) F, S., et al., - High Accuracy Classification of Developmental Toxicants by In Vitro Tests of. - Cells. 2022 Oct 27;11(21):3404. doi: 10.3390/cells11213404., (- 2073-4409 (Electronic)): p. T - epublish.

117) O, K., et al., - Characterization of gastrulation-stage progenitor cells and their inhibitory. - Stem Cells. 2010 Jan;28(1):75-83. doi: 10.1002/stem.260., (- 1549-4918 (Electronic)): p. - 75-83.

118) N, V., - The teratogenic effects of thalidomide on limbs. - J Hand Surg Eur Vol. 2019 Jan;44(1):88-95. doi: 10.1177/1753193418805249. Epub, (- 2043-6289 (Electronic)): p. - 88-95.

119) Ueno, S., et al., 2007. - 104(- 23): p. - 9690.

120) NA, P., et al., - Characterizing the effects of in utero exposure to valproic acid on murine fetal. - Birth Defects Res. 2019 Nov 15;111(19):1551-1560. doi: 10.1002/bdr2.1610. Epub, (- 2472-1727 (Electronic)): p. - 1551-1560.

121) A, K., et al., - A HAND to TBX5 Explains the Link Between Thalidomide and Cardiac Diseases. - Sci Rep. 2017 May 3;7(1):1416. doi: 10.1038/s41598-017-01641-3., (- 2045-2322 (Electronic)): p. - 1416.

122) P, K., et al., - Thalidomide remodels developing heart in chick embryo: discovery of a thalidomide. - Naunyn Schmiedebergs Arch Pharmacol. 2018 Oct;391(10):1093-1105. doi:, (- 1432-1912 (Electronic)): p. - 1093-1105.

123) JD, A., et al., - Cardiovascular effects of carbamazepine toxicity. - Ann Emerg Med. 1995 May;25(5):631-5. doi: 10.1016/s0196-0644(95)70176-1., (- 0196-0644 (Print)): p. - 631-5.

124) S, S., H.-O. K, and F. B, - Methotrexate-induced acute cardiotoxicity requiring veno-arterial extracorporeal.

125) I, K., et al., - Functional and Transcriptional Characterization of Histone Deacetylase. - Stem Cells Transl Med. 2016 May;5(5):602-12. doi: 10.5966/sctm.2015-0279. Epub, (- 2157-6564 (Print)): p. - 602-12.

126) OI, A.H., et al., - The molecular mechanisms of lithium-induced cardiotoxicity in male rats and its. - Hum Exp Toxicol. 2020 May;39(5):696-711. doi: 10.1177/0960327119897759. Epub 2020, (- 1477-0903 (Electronic)): p. - 696-711.

127) N, R.-K., et al., - Methylmercury Toxicity During Heart Development: A Combined Analysis of. - Cardiovasc Toxicol. 2022 Dec;22(12):962-970. doi: 10.1007/s12012-022-09772-4., (- 1559-0259 (Electronic)): p. - 962-970.

128) PHY, C., et al., - Prenatal methylmercury exposure is associated with decrease heart rate. - Environ Res. 2021 Sep;200:111744. doi: 10.1016/j.envres.2021.111744. Epub 2021, (- 1096-0953 (Electronic)): p. - 111744.

129) AM, F., - Drugs in Pregnancy and Lactation 8th Edition: A Reference Guide to Fetal and, in - Obstet Med. 2009 Jun;2(2):89. doi: 10.1258/om.2009.090002. Epub 2009 May 22.

130) PP, T. and L. DA, - Gene function in mouse embryogenesis: get set for gastrulation. - Nat Rev Genet. 2007 May;8(5):368-81. doi: 10.1038/nrg2084. Epub 2007 Mar 27., (- 1471-0056 (Print)): p. - 368-81.

131) N, E., et al., - Retinoic acid synthesis promotes development of neural progenitors from mouse. - Stem Cells. 2010 Sep;28(9):1498-509. doi: 10.1002/stem.479., (- 1549-4918 (Electronic)): p. - 1498-509.

132) A, W., et al., - Retinoic acid signaling in heart development: Application in the differentiation. - Stem Cell Reports. 2021 Nov 9;16(11):2589-2606. doi:, (- 2213-6711 (Electronic)): p. - 2589-2606.

133) S, B. and M. SM, - Mesoderm patterning by a dynamic gradient of retinoic acid signalling. - Philos Trans R Soc Lond B Biol Sci. 2020 Oct 12;375(1809):20190556. doi:, (- 1471-2970 (Electronic)): p. - 20190556.

134) Rhinn, M. and P. Dollé, 2012. - 139(- 5): p. - 858.

135) DS, K., et al., - Robust enhancement of neural differentiation from human ES and iPS cells. - Stem Cell Rev Rep. 2010 Jun;6(2):270-81. doi: 10.1007/s12015-010-9138-1., (- 2629-3277 (Electronic)): p. - 270-81.

136) Y, O., et al., - Retinoic-acid-concentration-dependent acquisition of neural cell identity during. - Dev Biol. 2004 Nov 1;275(1):124-42. doi: 10.1016/j.ydbio.2004.07.038., (- 0012-1606 (Print)): p. - 124-42.

137) JJ, P. and E. MJ, - Mml, a mouse Mix-like gene expressed in the primitive streak. - Mech Dev. 1999 Sep;87(1-2):189-92. doi: 10.1016/s0925-4773(99)00135-5., (- 0925-4773 (Print)): p. - 189-92.

138) Inman, K.E. and K.M. Downs, 2006. - 6(- 8): p. - 793.

139) I, C., et al., - The T-box transcription factor Eomesodermin acts upstream of Mesp1 to specify. - Nat Cell Biol. 2011 Aug 7;13(9):1084-91. doi: 10.1038/ncb2304., (- 1476-4679 (Electronic)): p. - 1084-91.

140) JS, W. and Y. D, - Increased Hox activity mimics the teratogenic effects of excess retinoic acid. - Dev Dyn. 2009 May;238(5):1207-13. doi: 10.1002/dvdy.21951., (- 1058-8388 (Print)): p. - 1207-13.

141) DK, K., et al., - Lefty1 and lefty2 control the balance between self-renewal and pluripotent. - Stem Cells Dev. 2014 Mar 1;23(5):457-66. doi: 10.1089/scd.2013.0220. Epub 2013, (- 1557-8534 (Electronic)): p. - 457-66.

142) C, M., et al., - lefty-1 is required for left-right determination as a regulator of lefty-2 and. - Cell. 1998 Aug 7;94(3):287-97. doi: 10.1016/s0092-8674(00)81472-5., (- 0092-8674 (Print)): p. - 287-97.

143) AF, S. and S. MM, - Nodal signalling in vertebrate development. - Nature. 2000 Jan 27;403(6768):385-9. doi: 10.1038/35000126., (- 0028-0836 (Print)): p. - 385-9.

144) G, W., et al., - Sodium valproate-induced congenital cardiac abnormalities in mice are associated. - J Biomed Sci. 2010 Mar 10;17(1):16. doi: 10.1186/1423-0127-17-16., (- 1423-0127 (Electronic)): p. - 16.

145) IE, F., et al., - Bradycardia during therapy for multiple myeloma with thalidomide. - Am J Cardiol. 2004 Apr 15;93(8):1052-5. doi: 10.1016/j.amjcard.2003.12.061., (- 0002-9149 (Print)): p. - 1052-5.

146) R, M. and Y. ET, - Mechanisms of Cardiotoxicity of Cancer Chemotherapeutic Agents: Cardiomyopathy. - Can J Cardiol. 2016 Jul;32(7):863-870.e5. doi: 10.1016/j.cjca.2016.01.027. Epub, (- 1916-7075 (Electronic)): p. - 863-870.e5.

147) T, M., et al., - Thalidomide causes sinus bradycardia in ALS. - J Neurol. 2008 Apr;255(4):587-91. doi: 10.1007/s00415-008-0756-3. Epub 2008 Apr, (- 0340-5354 (Print)): p. - 587-91.

148) PM, H. and S. BD, - Targeting the sarcomere to correct muscle function. - Nat Rev Drug Discov. 2015 May;14(5):313-28. doi: 10.1038/nrd4554. Epub 2015 Apr, (- 1474-1784 (Electronic)): p. - 313-28.

149) AK, K., et al., - Human embryonic stem cell-derived test systems for developmental neurotoxicity: a. - Arch Toxicol. 2013 Jan;87(1):123-43. doi: 10.1007/s00204-012-0967-3. Epub 2012, (- 1432-0738 (Electronic)): p. - 123-43.

150) E, R., et al., - A transcriptome-based classifier to identify developmental toxicants by stem cell. - Arch Toxicol. 2015 Sep;89(9):1599-618. doi: 10.1007/s00204-015-1573-y. Epub 2015, (- 1432-0738 (Electronic)): p. - 1599-618.

151) V, S., et al., - Human Pluripotent Stem Cell Based Developmental Toxicity Assays for Chemical. - J Vis Exp. 2015 Jun 17;(100):e52333. doi: 10.3791/52333., (- 1940-087X (Electronic)): p. - e52333.

152) M, J., et al., - Focus on germ-layer markers: A human stem cell-based model for in vitro. - Reprod Toxicol. 2020 Dec;98:286-298. doi: 10.1016/j.reprotox.2020.10.011. Epub, (- 1873-1708 (Electronic)): p. - 286-298.

153) Lauschke, K., et al., A novel human pluripotent stem cell-based assay to predict developmental toxicity. Archives of Toxicology, 2020. 94: p. 3831-3846.

154) X, W., et al., - Cardiac Development in the Presence of Cadmium: An in Vitro Study Using Human. - Environ Health Perspect. 2022 Nov;130(11):117002. doi: 10.1289/EHP11208. Epub, (- 1552-9924 (Electronic)): p. - 117002.

155) S, G., et al., - The Human Induced Pluripotent Stem Cell Test as an Alternative Method for. - Int J Mol Sci. 2022 Mar 18;23(6):3295. doi: 10.3390/ijms23063295., (- 1422-0067 (Electronic)): p. T - epublish.

156) Jamalpoor, A., et al., A novel human stem cell-based biomarker assay for in vitro assessment of developmental toxicity. Birth Defects Research, 2022. 114(19): p. 1210-1228.

157) Q, L., et al., - Disruption of mesoderm formation during cardiac differentiation due to. - Sci Rep. 2018 Aug 28;8(1):12960. doi: 10.1038/s41598-018-31192-0., (- 2045-2322 (Electronic)): p. - 12960.

158) Ye, D., et al., Inhibition of cardiomyocyte differentiation of human induced pluripotent stem cells by Ribavirin: Implication for its cardiac developmental toxicity. Toxicology, 2020. 435: p. 152422.

159) GJ, M. and B. JT, - Cardiac developmental toxicity. - Birth Defects Res C Embryo Today. 2011 Dec;93(4):291-7. doi: 10.1002/bdrc.20219., (- 1542-9768 (Electronic)): p. - 291-7.

160) Ahmed, R.E., et al., - A Brief Review of Current Maturation Methods for Human Induced Pluripotent Stem Cells-Derived Cardiomyocytes. 2020. - 8.

161) Ingber, D.E., - Human organs-on-chips for disease modelling, drug development and personalized medicine. 2022. - 23(- 8): p. - 491.

162) Tadano, K., et al., 2021. - 22: p. - 349.

6 Appendix

6.1 Supplements

Table S1 Predicted probabilities for teratogenicity

Compounds	Predicted probability for teratogenicity[b] 1-fold C_{max} [a]	20-fold C_{max} [a]
Non-teratogens		
Ampicillin	0.04	0.00
Ascorbic acid	0.00	0.02
Buspirone	0.03	0.03
Chlorpheniramine	0.00	0.01
Dextromethorphan	0.00	0.01
Diphenhydramine	0.44	0.15
Doxylamine	0.08	0.00
Famotidine	0.05	0.02
Folic acid	0.00	0.00
Levothyroxine	0.00	0.00
Liothyronine	0.00	0.01
Magnesium chloride	0.00	0.02
Methicillin	0.02	0.01
Ranitidine	0.28	0.07
Retinol	0.23	0.38
Sucralose	0.77	1.00
Teratogens		
9-cis-retinoic acid	0.73	0.91
Acitretin	0.99	1.00
Actinomycin D	1.00	1.00
Atorvastatin	0.01	0.02
Carbamazepine	0.89	1.00[c]
Doxorubicin	1.00	1.00
Entinostat	1.00	1.00
Favipiravir	0.89	0.98
Isotretinoin	1.00	1.00
Leflunomide	1.00	---[c]
Lithium chloride	0.76	0.96
Methotrexate	0.98	0.85
Methylmercury	0.91	0.70
Panobinostat	1.00	1.00
Paroxetine	0.47	0.34
Phenytoin	0.37	---[c]
Teriflunomide	1.00	---[c]
Thalidomide	0.33	0.41
Trichostatin A	1.00	1.00
Valproic acid	1.00	1.00[e]
Vinblastine	1.00	1.00

TN = True Negative; FN = False Negative; FP = False Positive; TP = True Positive

Table S2: Classification of the in vitro test results in the two classifiers

	SPS-procedure		Top 1000-procedure	
	1-fold C_{max}[a]	20- old C_{max}[a]	1-fold C_{max}[a]	20-fold C_{max}[a]
Non-teratogens				
Ampicillin	TN	TN	TN	TN
Ascorbic acid	TN	FP	TN	TN
Buspirone	TN	TN	TN	TN
Chlorpheniramine	TN	TN	TN	TN
Dextromethorphan	TN	TN	TN	TN
Diphenhydramine	TN	TN	FP	TN
Doxylamine	TN	TN	TN	TN
Famotidine	TN	TN	TN	TN
Folic acid	TN	TN	TN	TN
Levothyroxine	TN	TN	TN	TN
Liothyronine	TN	TN	TN	TN
Magnesium (chloride)	TN	FP	TN	TN
Methicillin	TN	TN	TN	TN
Ranitidine	TN	TN	TN	TN
Retinol	TN	TN	TN	FP
Sucralose	TN	TN	FP	FP
Teratogens				
9-cis-retinoic acid	TP	TP	TP	TP
Acitretin	TP	TP	TP	TP
Actinomycin D	TP	TP	TP	TP
Atorvastatin	FN	TP	FN	FN
Carbamazepine	TP	TP[b]	TP	TP[b]
Doxorubicin	TP	TP	TP	TP
Entinostat	TP	TP	TP	TP
Favipiravir	FN	TP	TP	TP
Isotretinoin	TP	TP	TP	TP
Leflunomide	TP	--[b]	TP	--[b]
Lithium (chloride)	TP	TP	TP	TP
Methotrexate	TP	TP	TP	TP
Methylmercury	TP	FN	TP	TP
Panobinostat	TP	TP	TP	TP
Paroxetine	TP	TP	TP	TP
Phenytoin	FN	--[b]	TP	--[b]
Teriflunomide	TP	--[b]	TP	--[b]
Thalidomide	TP	TP	TP	TP

[a]Maximal plasma or blood concentrations which were usually observed in humans after the administration of therapeutic compound doses (Table S 2, Table S 3). Fetal enrichment was considered if relevant (Table S 4).

[b]Carbamazepine and VPA were tested at 10-fold and 1.67-fold C_{max}, respectively, instead of 20-fold C_{max}; leflunomide, phenytoin, teriflunomide and vismodegib were tested at 1-fold C_{max} due to lited solubility.

Table S3: The 31 genes and their descriptiony

Gene Symbol	Description
HOXA5	homeobox A5
HOXB2	homeobox B2
MEIS2	Meis homeobox 2
RBM20	RNA binding motif protein 20
TSHZ1	teashirt zinc finger homeobox 1
CYP26A1	cytochrome P450 family 26 subfamily A member 1
HOXD1	homeobox D1
GREB1L	GREB1 like retinoic acid receptor coactivator
MECOM	MDS1 and EVI1 complex locus
ID4	inhibitor of DNA binding 4
LOC100240734	uncharacterized LOC100240734
ZNF503	zinc finger protein 503
SKAP2	src kinase associated phosphoprotein 2
KRT19	keratin 19
LINC02381	long intergenic non-protein coding RNA 2381
HOTAIRM1	HOXA transcript antisense RNA, myeloid-specific 1
PRTG	protogenin
IFI16	interferon gamma inducible protein 16
ZNF703	zinc finger protein 703
LRATD1	LRAT domain containing 1
VIL1	villin 1
DHRS3	dehydrogenase/reductase 3
KRT38	keratin 38
HAGLR	HOXD antisense growth-associated long non-coding RNA
FBLN2	fibulin 2
RIN2	Ras and Rab interactor 2
DMRT1	doublesex and mab-3 related transcription factor 1
KDR	kinase insert domain receptor
EOMES	eomesodermin
ETS1	ETS proto-oncogene 1, transcription factor
HHEX	hematopoietically expressed homeobox
SOX9	SRY-box transcription factor 9

The 31 deregulated developmental related genes that have been utilized to define the CDI31g score (at least 2 fold up or down deregulation)

Biological interpretation of genes differentially expressed after exposure of hiPSC to teratogens and non-teratogens. The following combinations were investigated:

- Fig. S1: Only upregulated probe sets at 1-fold C_{max}
- Fig. S2: Only downregulated probe sets at 1-fold C_{max}
- Fig. S3: All deregulated probe sets at 20-fold C_{max}
- Fig. S4: Only upregulated probe sets at 20-fold C_{max}
- Fig. S5: Only downregulated probe sets at 20-fold C_{max}
- **(A)** Numbers of significant probe sets (log2 fold change >1; adjusted p-value <0.05) induced by non-teratogens and teratogens at the given concentration **(B)** Top genes in the gene sets of the overlap, teratogens and non-teratogens from (A). The numbers in the bars indicate how many compounds deregulated the specific genes. All differential genes are given in the SI "Top genes". **(C)** Numbers of significantly (adj. p-value <0.05) overrepresented GO groups in the overlap, teratogen and non-teratogen gene sets. **(D)** The ten GO-groups with the lowest adj. p-values in the overlap and teratogen gene sets. No significant GO-groups were obtained for the non-teratogen gene set. The names of the GO-groups were shortened. Full names and complete GO-group lists and in the SI "GO analysis". "Count": Number of significant genes from (A) linked to the GO group. "Hits": Percentage of significant genes compared to all genes assigned to the GO group. **(E)** KEGG pathway enrichment analyses of the overlap and teratogen gene sets. The ten KEGG pathways with the lowest adj. p-values are given. No significant KEGG pathways were obtained for the non-teratogen gene set. Full names and complete KEGG-pathway lists are given in the SI "KEGG pathways". "Count": Number of significant genes from (A) linked to the KEGG pathway. "Gene Ratio": Percentage of significant genes associated to the pathway compared to the number of all significant genes associated to any pathway.

Figure S1: Upregulated probe sets at 1-fold C_{max}

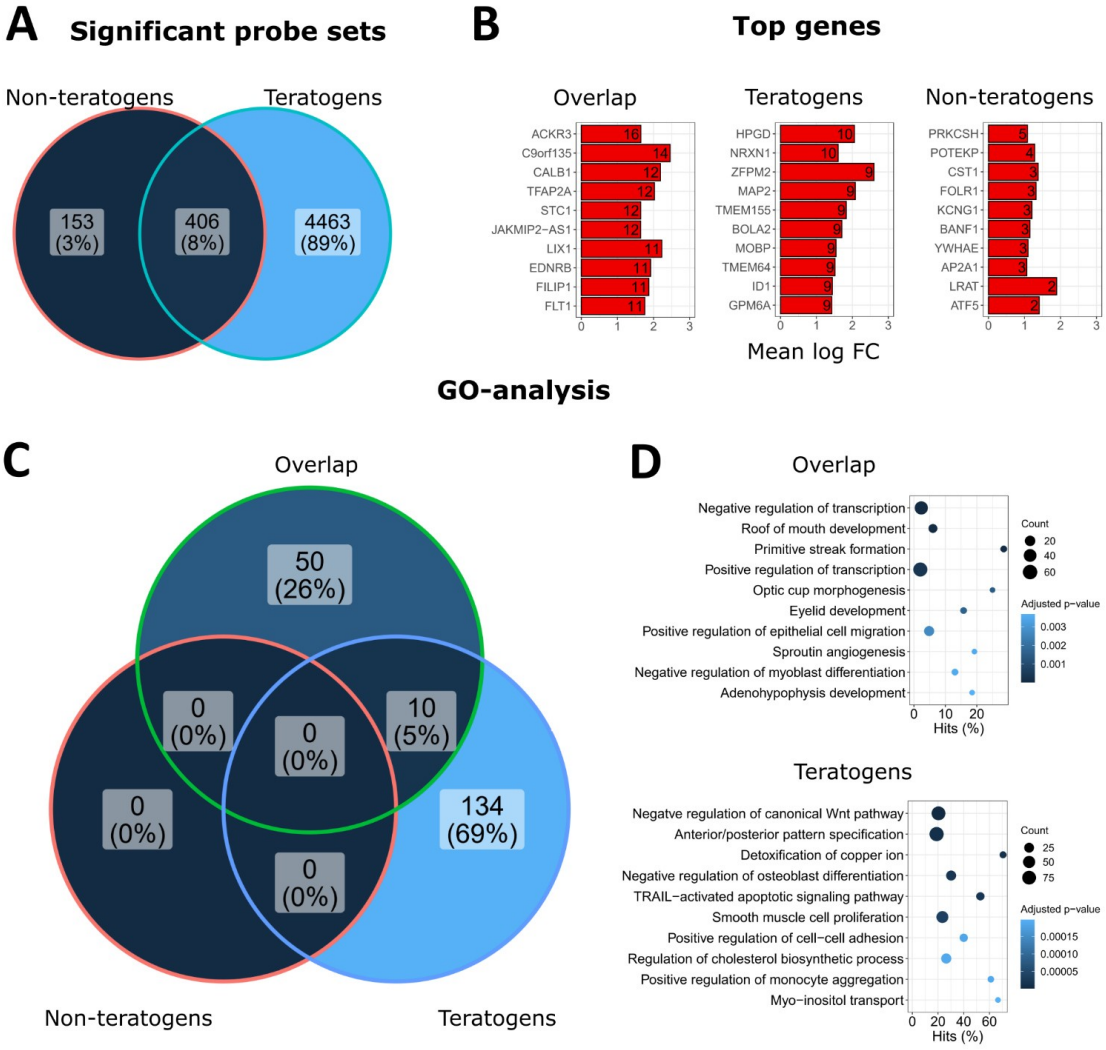

Figure S2: Downregulated probe sets at 1-fold C_{max}

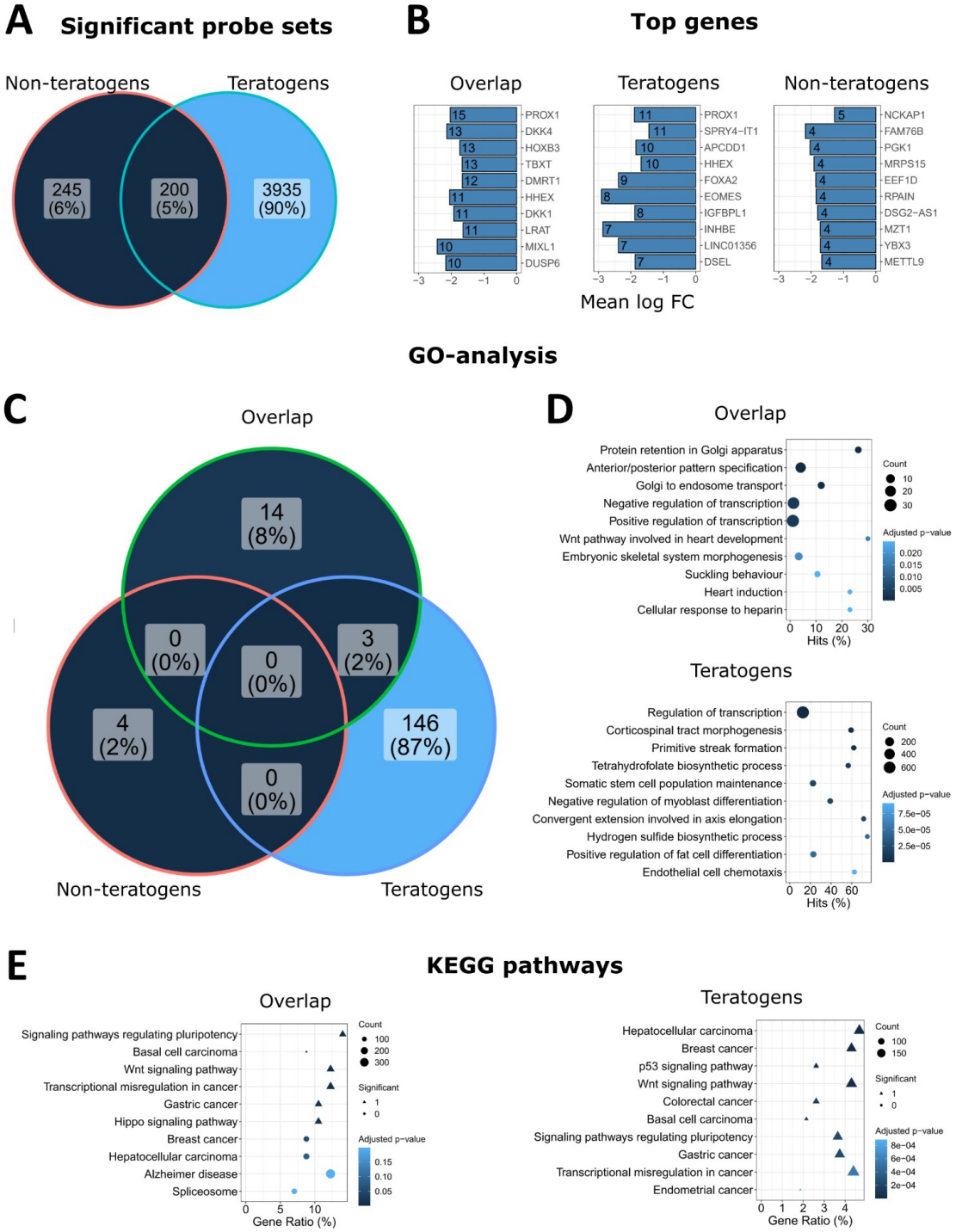

Figure S3: All deregulated probe sets at 20-fold C_{max}

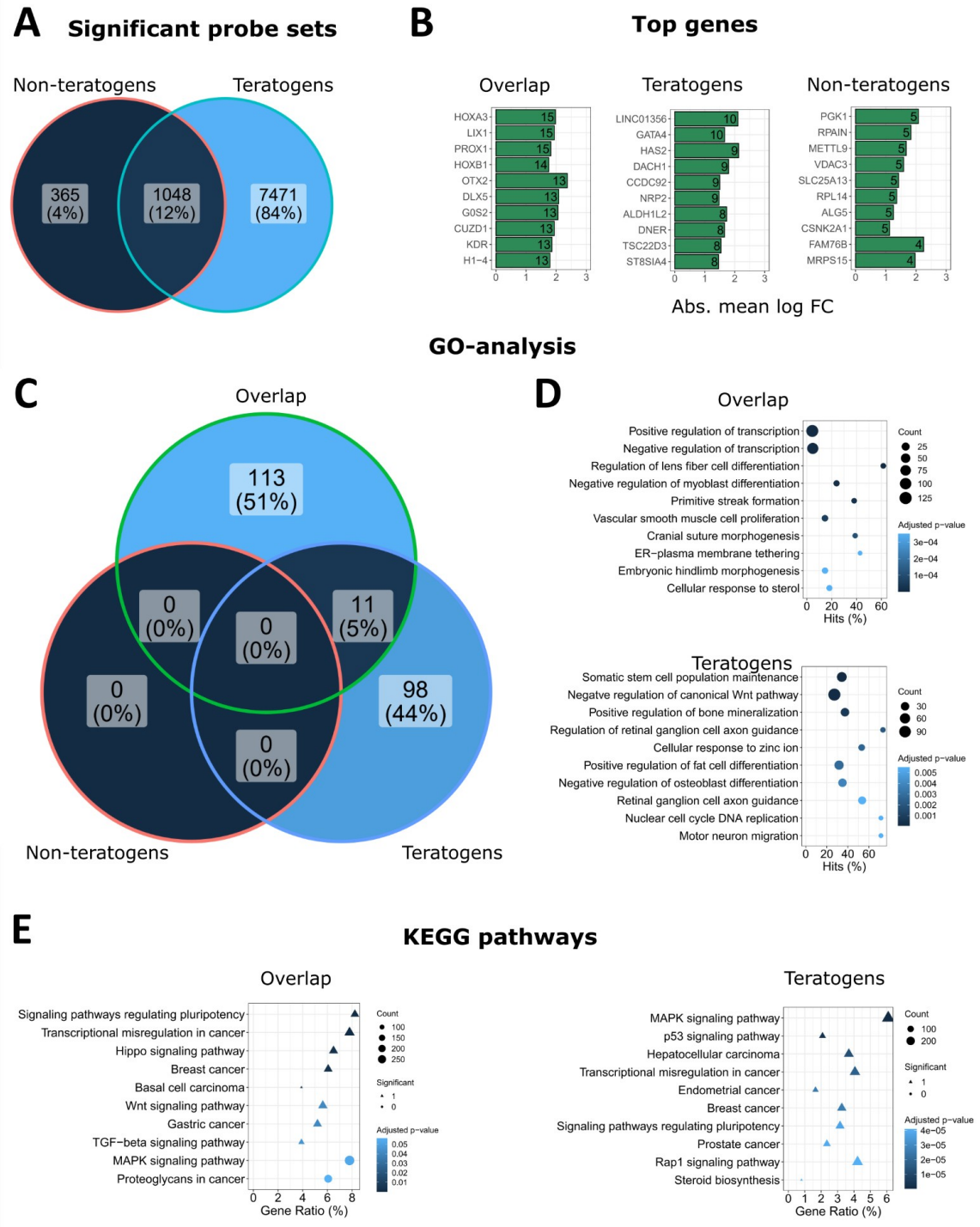

Figure S4: Pregulated probe sets at 20-fold C_{max}

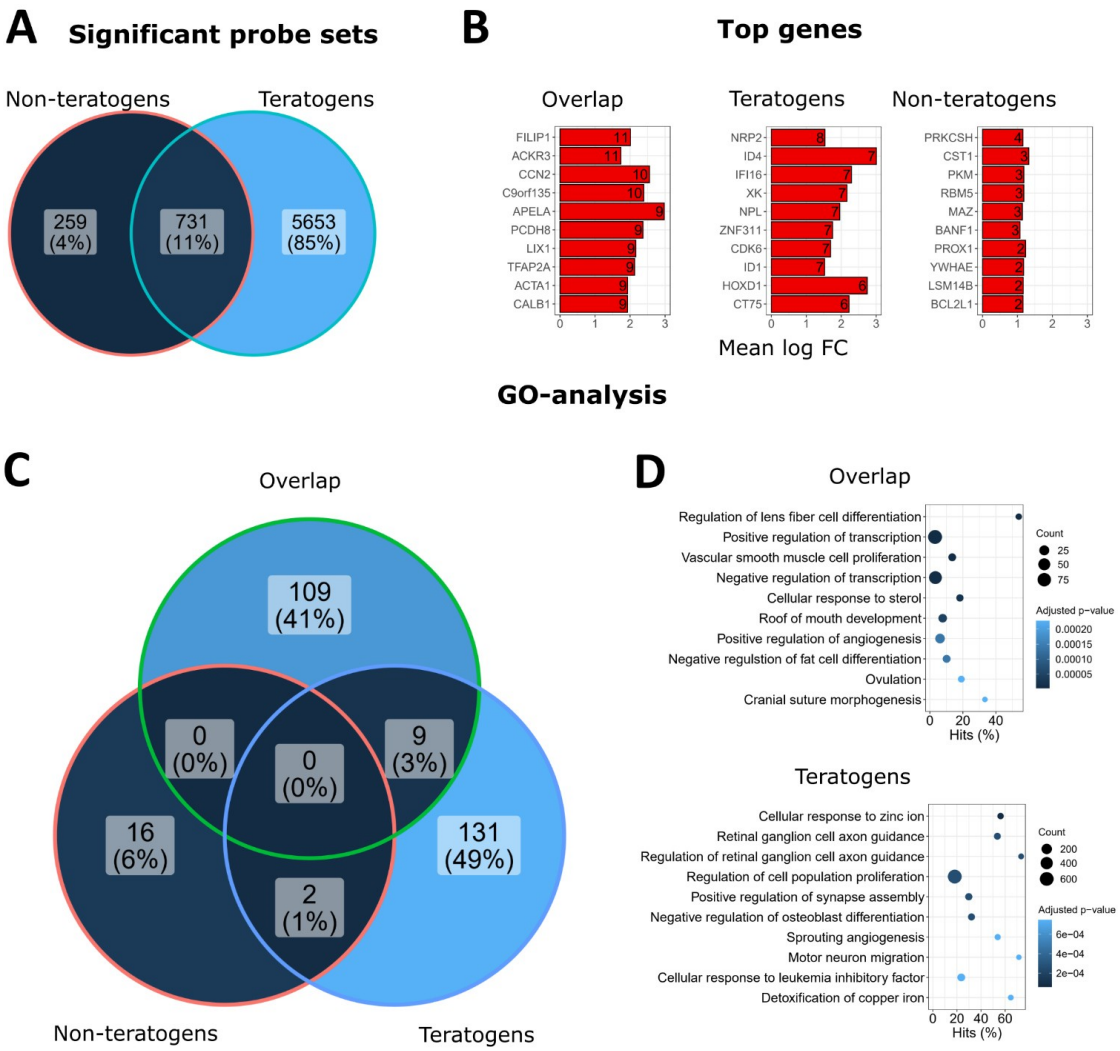

Figure S5: Downregulated probe sets at 20-fold C_{max}

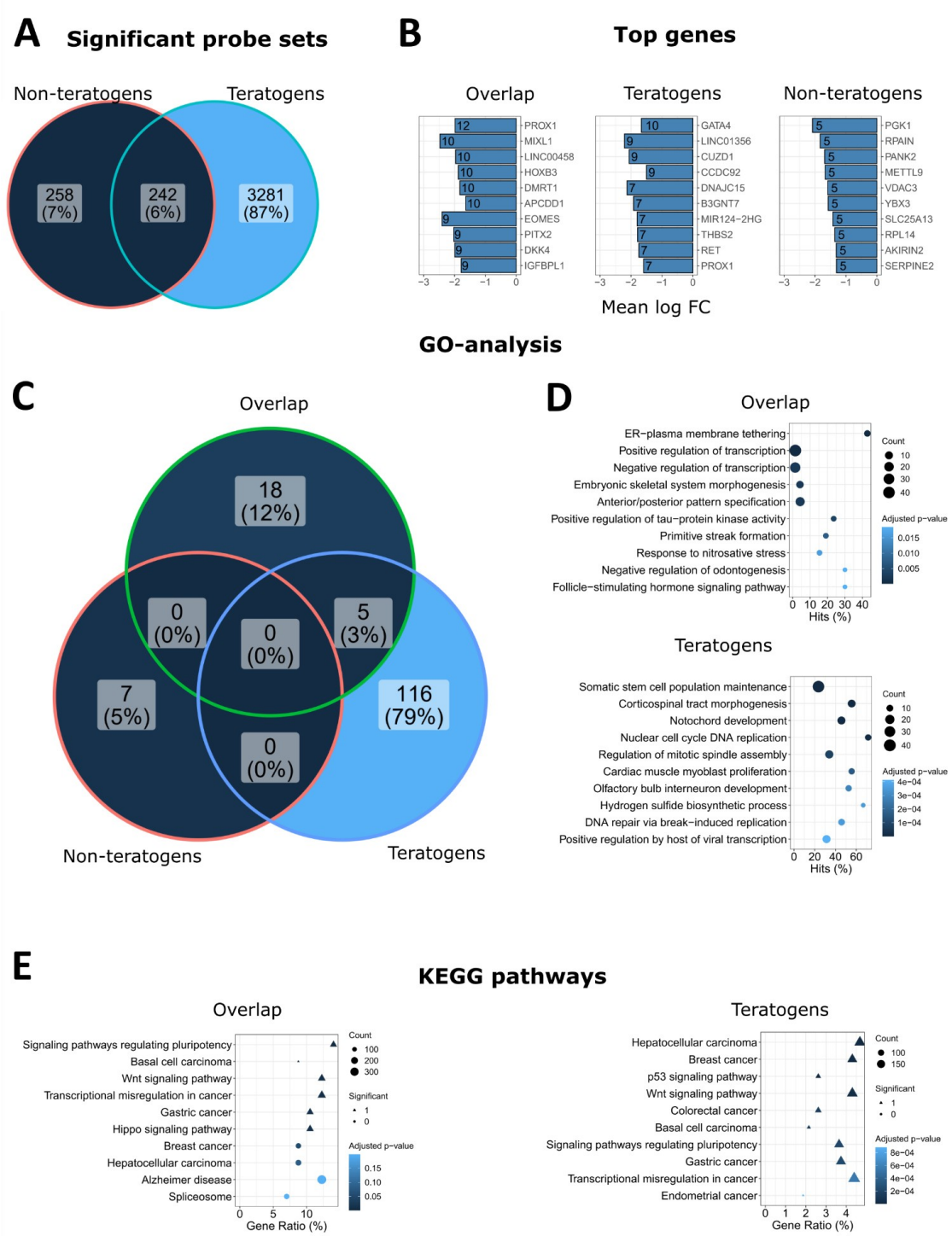

Figure S6

A Downregulated Enriched terms

Term	Description	LogP	Log(q-value)	Symbols
GO:0048729	tissue morphogenesis	-967,514	-5,325,671,589	BMP2,FGF8,GATA4,TNC,KDR,SNAI2,SOX9,EOMES,SLIT2,NTN1,HS3ST3A1,DKK1,FLRT3,LGR4,RSPO3,CAV1,ITGB8,TGFA,THY1,FAT4,TMEM231
GO:0002009	morphogenesis of an epithelium	-782,497	-4,293,523,867	BMP2,FGF8,GATA4,TNC,KDR,SOX9,SLIT2,NTN1,HS3ST3A1,FLRT3,LGR4,RSPO3
GO:0035239	tube morphogenesis	-773,991	-4,293,523,867	BMP2,CAV1,FGF8,GATA4,ITGB8,KDR,SOX9,TGFA,THY1,SLIT2,NTN1,HS3ST3A1,LGR4,RSPO3
GO:0048598	embryonic morphogenesis	-410,718	-1,887,048,514	FGF8,GATA4,SOX9,EOMES,NTN1,DKK1,FLRT3,TMEM231,RSPO3
GO:0003197	endocardial cushion development	-793,168	-4,293,523,867	BMP2,FGF8,GATA4,SNAI2,SOX9,DKK1,COL13A1,KDR,SLIT2,HS3ST3A1,RSPO3,LGR4,EDNRB,EOMES,FLRT3,DNAAF4,EGR2,ENPP1,TACR1,TNC,CAV1,TMEM231,P2RY1,NTN1,ETS1,FOS,IER3,CMKLR1,ITGB8,PTCHD1,G
GO:0001763	morphogenesis of a branching structure	-713,765	-3,934,308,405	BMP2,COL13A1,FGF8,KDR,SOX9,SLIT2,HS3ST3A1,RSPO3
GO:0003170	heart valve development	-697,975	-3,806,367,494	BMP2,GATA4,SNAI2,SOX9,SLIT2,DKK1
GO:0007507	heart development	-588,589	-3,041,568,983	BMP2,FGF8,GATA4,KDR,SNAI2,SOX9,EOMES,SLIT2,DKK1,FLRT3,DNAAF4
GO:0060070	canonical Wnt signaling pathway	-613,792	-3,150,178,166	CAV1,EDNRB,SOX9,DKK1,LGR4,RSPO3,BMP2,HHEX,SNAI2,EGR2,FOS,GAS1,ENPP1,FGF8,GNB4,EOMES,ALS2,TMEM231,LRAT

C Upregulated Enriched terms

Term	Description	LogP	Log(q-value)	Symbols
GO:0048568	embryonic organ development	-1,795,168,103	-1,380,054,186	ADM,PRDM1,BMP7,DLG1,DLX5,GLI3,HOXA2,HOXA5,HOXB1,HOXB2,HOXB3,HOXB8,HOXB9,HOXC4,HOXD4,KRT19,KMT2A,MMP16,PCSK5,RARB,TBX3,TWIST1,ZIC1,TSHZ1,HEY2,NIPBL
GO:0048706	embryonic skeletal system development	-1,784,793,357	-1,380,054,186	BMP7,DLG1,GLI3,HOXA2,HOXA5,HOXB1,HOXB2,HOXB3,HOXB8,HOXB9,HOXC4,HOXD1,HOXD4,MMP16,PCSK5,TWIST1,NIPBL
GO:0009952	anterior/posterior pattern specification	-1,444,303,026	-109,397,066	CDX1,GLI3,HOXA2,HOXA5,HOXB1,HOXB2,HOXB3,HOXB8,HOXB9,HOXC4,HOXD4,KMT2A,PCSK5,TBX3,TSHZ1,SEMA3C,HEY2
GO:0007389	pattern specification process	-127,585,786	-9,410,156,907	BMP7,CDX1,GLI3,HOXA2,HOXA5,HOXB1,HOXB2,HOXB3,HOXB8,HOXB9,HOXC4,HOXD4,MEIS1,MEIS2,KMT2A,PCSK5,TBX3,ZIC1,TSHZ1,SEMA3C,HEY2
GO:0007507	heart development	-601,996,227	-3,181,510,934	ADM,PRDM1,BMP7,GLI3,PCSK5,RARB,TBX3,TWIST1,DHRS3,SEMA3C,HEY2,NIPBL,GREB1L,RBM20,SYPL2
GO:0035239	tube morphogenesis	-7,919,582,782	-4,801,610,006	ADM,RHOB,PRDM1,BMP7,COL8A1,DLG1,GLI3,HOXA5,HOXB3,HPGD,MEIS1,RORA,TBX3,TWIST1,EDAR,HEY2,NIPBL,RGMA,GREB1L,SEMA3C
R-HSA-5617472	Activation of anterior HOX genes in hindbrain development during early	-7,451,977,236	-4,417,464,896	HOXA2,HOXB1,HOXB2,HOXB3,HOXC4,HOXD1,HOXD4,MEIS1,RARB,GLI3,BMP7,RORA,NANOS1,SYPL2

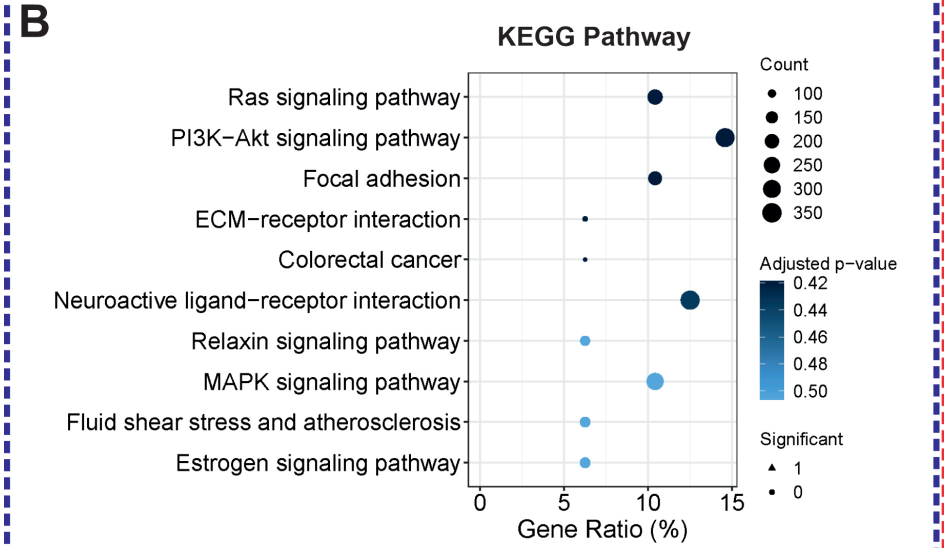

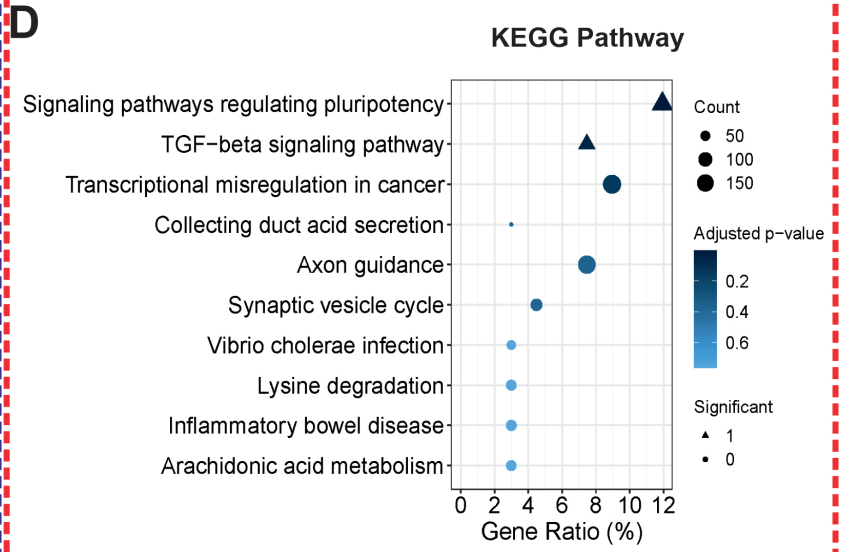

Metascape analysis of down-regulated (Fig. S6A) and up-regulated (Fig.S6C) enriched term of the SPS specific for ISO on day1 and the corresponding genes . ”Log10(P)” is the p-value in log base 10. ”Log10(q)” is the multi-test adjusted p-value in log base 10. KEGG pathway enrichment analysis of the down-regulated (Fig. S6B) and upregulated (Fig.S6D) SPS specific for ISO. The ten KEGG pathways with the lowest adj. p-values are given. ‘‘Count:’’ number of significant genes linked to the KEGG pathway. ‘‘Gene Ratio:’’ percentage of significant genes associated with the pathway compared to the number of all significant genes associated with any pathway.

Figure S7

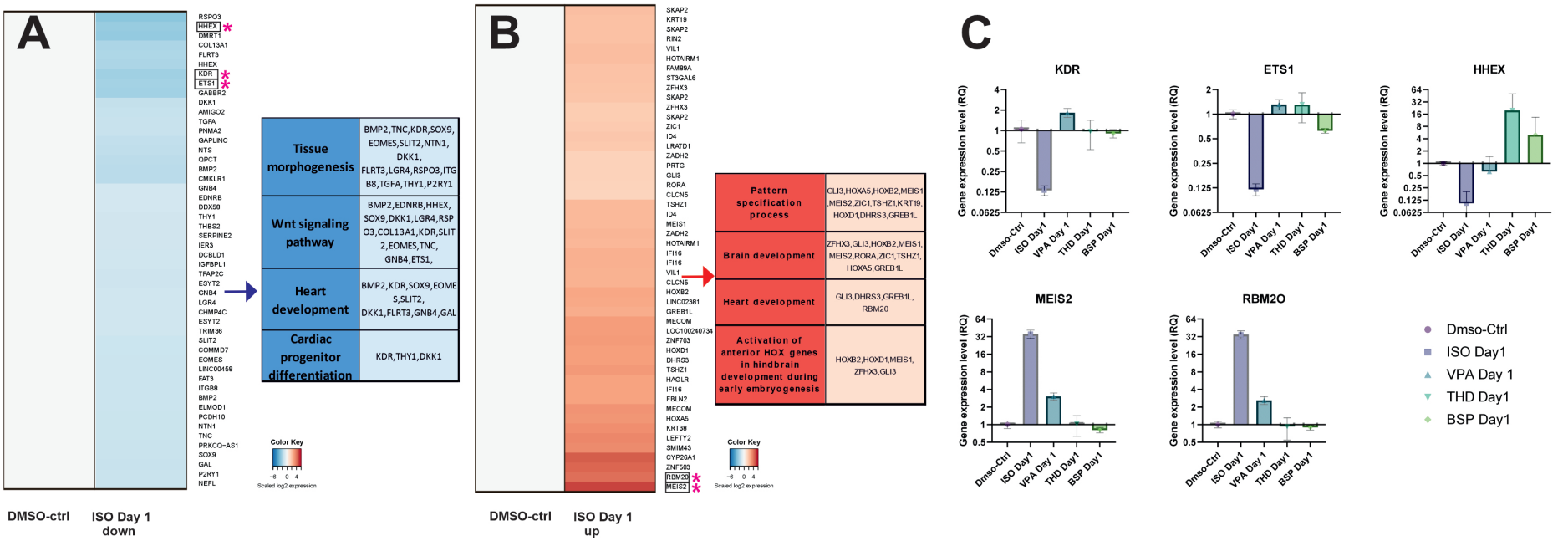

The heat map with the top 50 genes down-regulated (Fig.S7A) and upregulated (Fig.S7B) SPS specific for ISO, sorted according to their p-values. The heat map colour code indicates and down-regulation (blue) and up-regulation (red) of genes in comparison to control. The blue arrow showing a table with biological significant pathways that the top 50 deregulated genes belong to. Validation of deregulated genes by by qRT-PCR on day1 for all the test compounds (Fig.S7C).Data are shown as the mean ± SD; n = 3. Graphs represent 3 independent experiments (n = 3). Statistically significant results are presented with (*) as determined with t-test with $p < 0.05$.

Figure S8

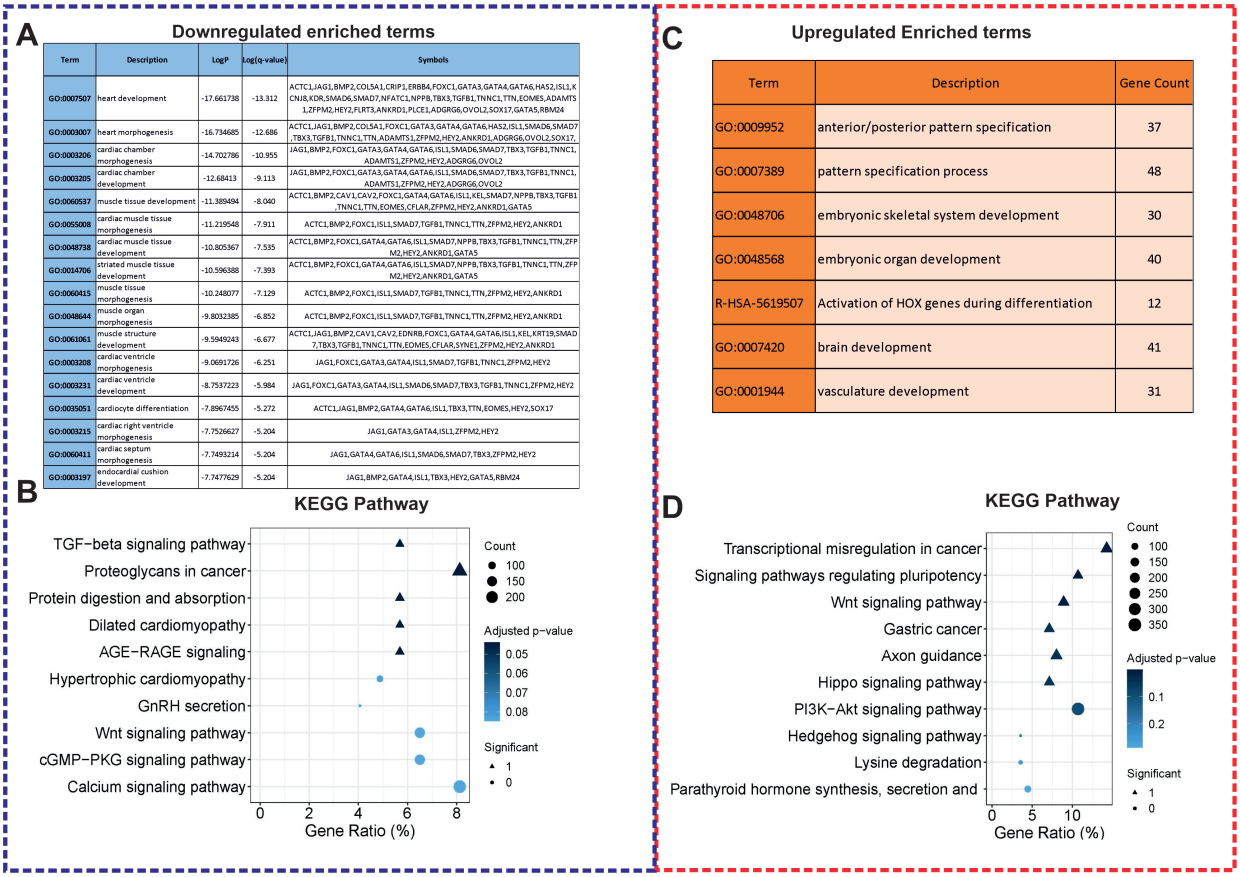

Term	Description	LogP	Log(q-value)	Symbols
GO:0007507	heart development	-17.661738	-13.312	ACTC1,JAG1,BMP2,COL5A1,CRIP1,ERBB4,FOXC1,GATA3,GATA4,GATA6,HAS2,ISL1,KCNJ8,KDR,SMAD6,SMAD7,NFATC1,NPPB,TBX3,TGFB1,TNNC1,TTN,EOMES,ADAMTS1,ZFPM2,HEY2,FLRT3,ANKRD1,PLCE1,ADGRG6,OVOL2,SOX17,GATA5,RBM24
GO:0003007	heart morphogenesis	-16.734685	-12.686	ACTC1,JAG1,BMP2,COL5A1,FOXC1,GATA3,GATA4,GATA6,HAS2,ISL1,SMAD6,SMAD7,TBX3,TGFB1,TNNC1,TTN,ADAMTS1,ZFPM2,HEY2,ANKRD1,ADGRG6,OVOL2,SOX17,
GO:0003206	cardiac chamber morphogenesis	-14.702786	-10.955	JAG1,BMP2,FOXC1,GATA3,GATA4,GATA6,ISL1,SMAD6,SMAD7,TBX3,TGFB1,TNNC1,ADAMTS1,ZFPM2,HEY2,ADGRG6,OVOL2
GO:0003205	cardiac chamber development	-12.68413	-9.113	JAG1,BMP2,FOXC1,GATA3,GATA4,GATA6,ISL1,SMAD6,SMAD7,TBX3,TGFB1,TNNC1,ADAMTS1,ZFPM2,HEY2,ADGRG6,OVOL2
GO:0060537	muscle tissue development	-11.389494	-8.040	ACTC1,BMP2,CAV1,CAV2,FOXC1,GATA4,GATA6,ISL1,KEL,SMAD7,NPPB,TBX3,TGFB1,TNNC1,TTN,EOMES,CFLAR,ZFPM2,HEY2,ANKRD1,GATA5
GO:0055008	cardiac muscle tissue morphogenesis	-11.219548	-7.911	ACTC1,BMP2,FOXC1,ISL1,SMAD7,TGFB1,TNNC1,TTN,ZFPM2,HEY2,ANKRD1
GO:0048738	cardiac muscle tissue development	-10.805367	-7.535	ACTC1,BMP2,FOXC1,GATA4,GATA6,ISL1,SMAD7,NPPB,TBX3,TGFB1,TNNC1,TTN,ZFPM2,HEY2,ANKRD1,GATA5
GO:0014706	striated muscle tissue development	-10.596388	-7.393	ACTC1,BMP2,FOXC1,GATA4,GATA6,ISL1,SMAD7,NPPB,TBX3,TGFB1,TNNC1,TTN,ZFPM2,HEY2,ANKRD1,GATA5
GO:0060415	muscle tissue morphogenesis	-10.248077	-7.129	ACTC1,BMP2,FOXC1,ISL1,SMAD7,TGFB1,TNNC1,TTN,ZFPM2,HEY2,ANKRD1
GO:0048644	muscle organ morphogenesis	-9.8032385	-6.852	ACTC1,BMP2,FOXC1,ISL1,SMAD7,TGFB1,TNNC1,TTN,ZFPM2,HEY2,ANKRD1
GO:0061061	muscle structure development	-9.5949243	-6.677	ACTC1,JAG1,BMP2,CAV1,CAV2,EDNRB,FOXC1,GATA4,GATA6,ISL1,KEL,KRT19,SMAD7,TBX3,TGFB1,TNNC1,TTN,EOMES,CFLAR,SYNE1,ZFPM2,HEY2,ANKRD1
GO:0003208	cardiac ventricle morphogenesis	-9.0691726	-6.251	JAG1,FOXC1,GATA3,GATA4,ISL1,SMAD7,TGFB1,TNNC1,ZFPM2,HEY2
GO:0003231	cardiac ventricle development	-8.7537223	-5.984	JAG1,FOXC1,GATA3,GATA4,ISL1,SMAD6,SMAD7,TBX3,TGFB1,TNNC1,ZFPM2,HEY2
GO:0035051	cardiocyte differentiation	-7.8967455	-5.272	ACTC1,JAG1,BMP2,GATA4,GATA6,ISL1,TBX3,TTN,EOMES,HEY2,SOX17
GO:0003215	cardiac right ventricle morphogenesis	-7.7526627	-5.204	JAG1,GATA3,GATA4,ISL1,ZFPM2,HEY2
GO:0060411	cardiac septum morphogenesis	-7.7493214	-5.204	JAG1,GATA4,GATA6,ISL1,SMAD6,SMAD7,TBX3,ZFPM2,HEY2
GO:0003197	endocardial cushion development	-7.7477629	-5.204	JAG1,BMP2,GATA4,ISL1,TBX3,HEY2,GATA5,RBM24

Term	Description	Gene Count
GO:0009952	anterior/posterior pattern specification	37
GO:0007389	pattern specification process	48
GO:0048706	embryonic skeletal system development	30
GO:0048568	embryonic organ development	40
R-HSA-5619507	Activation of HOX genes during differentiation	12
GO:0007420	brain development	41
GO:0001944	vasculature development	31

Metascape analysis of down-regulated (Fig. S8A) and up-regulated (Fig.S8C) enriched term of the SPS specific for ISO on day4 and the corresponding genes . ”Log10(P)” is the p-value in log base 10. ”Log10(q)” is the multi-test adjusted p-value in log base 10. KEGG pathway enrichment analysis of the down-regulated (Fig. S8B) and upregulated (Fig. S8D) SPS specific for ISO. The ten KEGG pathways with the lowest adj. p-values are given. ‘‘Count:’’ number of significant genes from to the KEGG pathway. ‘‘Gene Ratio:’’ percentage of significant genes associated with the pathway compared to the number of all significant genes associated with any pathway.

Figure S9

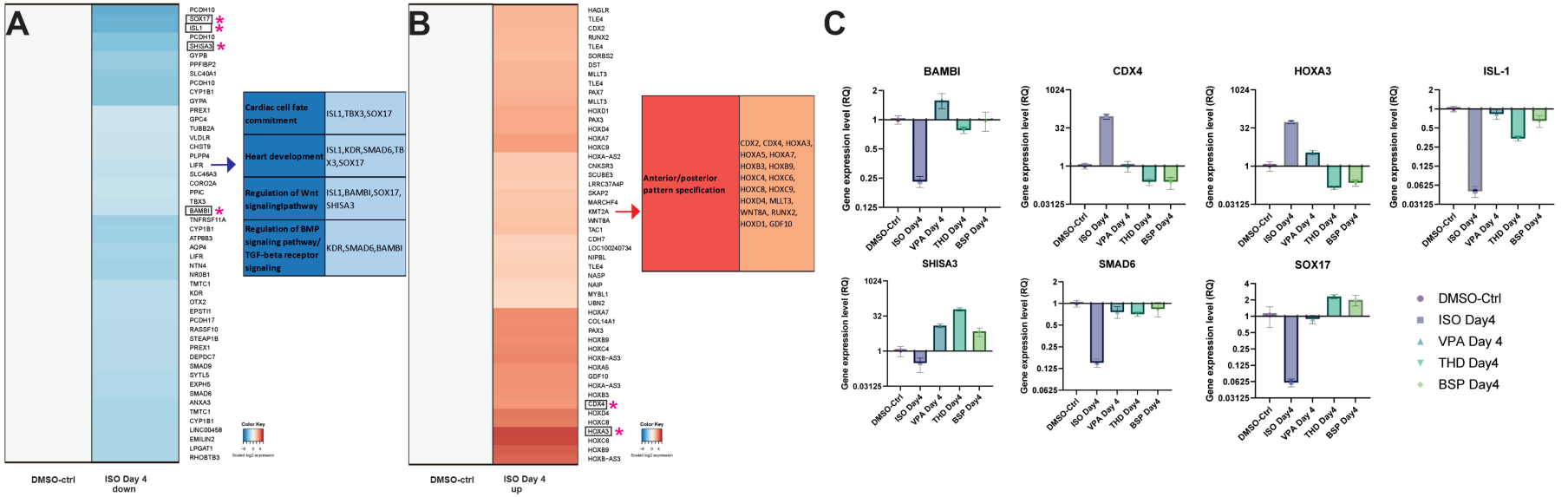

The heat map with the top 50 genes down-regulated (Fig. S9A) and upregulated (Fig. S9B) SPS specific for ISO, sorted according to their p-values. The heat map colour code indicates and down-regulation (blue) and up-regulation (red) of genes in comparison to control. The arrow showing a table with biological significant pathways that the top 50 deregulated genes belong to. Validation of deregulated genes by by qRT-PCR on day1 for all the test compounds (Fig.S9C).Data are shown as the mean ± SD; n = 3. Graphs represent 3 independent experiments (n = 3). Statistically significant results are presented with (*) as determined with t-test with $p < 0.05$.

Figure S10

A. The Venn diagrams shows the number of down-regulated SPS (log2 fold change > 1; adjusted p-value < 0.05), respectively induced by ISO, VPA and THD, at day1.
B. Metascape analysis for specific VPA-induced downregulated SPS at day1. Analysis shows the statistically enriched BPs and pathways as coloured by the p values.
C. VPA induced heart related down-regulated enriched GOs with their representative enriched terms, at day4. ”Log10(P)” is the p-value in log base 10. ”Log10(q)” is the multi-test adjusted p-value in log base 10.
D. The Venn diagrams shows the number of up-regulated SPS (log2 fold change > 1; adjusted p-value < 0.05), respectively induced by ISO, VPA and THD, at day1.
E. Metascape analysis for specific VPA-induced up-regulated SPS at day1. Analysis shows the statistically enriched BPs and pathways as coloured by the p values.
F. The Venn diagrams shows the number of down-regulated SPS (log2 fold change > 1; adjusted p-value < 0.05), respectively induced by ISO, VPA and THD, at day4.
G. Metascape analysis for specific THD-induced down-regulated SPS at day1. Analysis shows the statistically enriched BPs and pathways as coloured by the p values, at day4.
H. THD induced heart related down-regulated enriched GOs with their representative enriched terms, at day4.”Log10(P)” is the p-value in log base 10. ”Log10(q)” is the multi-test adjusted p-value in log base 10.
I. The Venn diagrams shows the number of up-regulated SPS (log2 fold change > 1; adjusted p-value < 0.05), respectively induced by ISO, VPA and THD, at day4.
J. THD induced heart related up-regulated enriched GOs with their representative enriched terms, at day4.”Log10(P)” is the p-value in log base 10. ”Log10(q)” is the multi-test adjusted p-value in log base 10.
K. THD induced heart related up-regulated enriched GOs with their representative enriched terms, at day4.”Log10(P)” is the p-value in log base 10. ”Log10(q)” is the multi-test adjusted p-value in log base 10.

A Day 1 downregulated SPS (analysis for VPA)

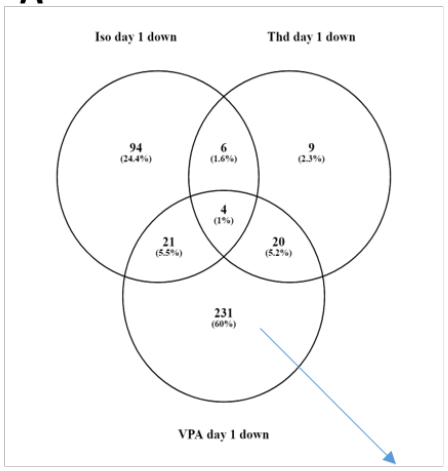

B VPA downregulated GOs day 1

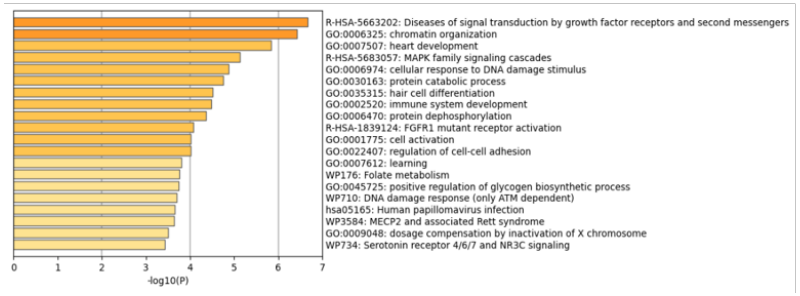

C

VPA down regulated heart related GOs

Term	Description	LogP	Log(q-value)	Symbols
GO:0007507	**heart development**	-5.84446	-1.97316	JAG1,FGF2,HNRNPU,MDM2,NF1,PITX2,PROX1,SOX11,TGFBR1,TTN,KDM6A,VEGFA,LMO4,FGF19,SMYD2,RBM15,ARID2
GO:0007423	sensory organ development	-5.22853	-1.54429	JAG1,DLG1,FBN2,FGF2,NF1,PDGFA,PITX2,PROX1,SOX11,TGFBR1,VEGFA,SLC4A7,RAB18,SLC7A11,MCOLN3,USP45
GO:0045596	negative regulation of cell differentiation	-5.03997	-1.54429	ABCA1,JAG1,DDX6,FGF13,FOXA2,HNRNPU,IFRD1,NF1,PROX1,SOX11,TGFBR1,VEGFA,FZD7,BCL11A,RBM15,JDP2,PRTG,EIF2AK4
GO:0060977	coronary vasculature morphogenesis	-4.95652	-1.54429	FGF2,TGFBR1,VEGFA,ARID2
GO:0048844	artery morphogenesis	-4.82784	-1.54429	JAG1,NF1,PROX1,TGFBR1,VEGFA,ARID2
GO:0001822	kidney development	-4.79186	-1.54429	JAG1,CYP26A1,DLG1,FGF2,GCNT1,NF1,PROX1,SOX11,TGFBR1,VEGFA,PCSK9
GO:0003279	cardiac septum development	-4.76696	-1.54429	JAG1,MDM2,PROX1,SOX11,TGFBR1,LMO4,RBM15
GO:0060411	cardiac septum morphogenesis	-4.75713	-1.54429	JAG1,MDM2,PROX1,SOX11,TGFBR1,RBM15
GO:0003281	ventricular septum development	-4.68859	-1.54429	MDM2,PROX1,SOX11,TGFBR1,LMO4,RBM15
GO:0072001	renal system development	-4.65829	-1.54031	JAG1,CYP26A1,DLG1,FGF2,GCNT1,NF1,PROX1,SOX11,TGFBR1,VEGFA,PCSK9
GO:0003007	heart morphogenesis	-4.54809	-1.49893	JAG1,MDM2,PITX2,PROX1,SOX11,TGFBR1,TTN,VEGFA,RBM15,ARID2
GO:0001654	eye development	-4.54184	-1.49893	JAG1,DLG1,FBN2,NF1,PITX2,PROX1,SOX11,TGFBR1,VEGFA,RAB18,SLC7A11,USP45
GO:0150063	visual system development	-4.49682	-1.49893	JAG1,DLG1,FBN2,NF1,PITX2,PROX1,SOX11,TGFBR1,VEGFA,RAB18,SLC7A11,USP45
GO:0001568	blood vessel development	-4.48116	-1.49893	JAG1,RHOB,FGF2,MDM2,NF1,PDGFA,PIK3CA,PROX1,TGFBR1,VEGFA,FOSL1,QKI,RBM15,ARID2
GO:0060982	coronary artery morphogenesis	-4.46714	-1.49893	TGFBR1,VEGFA,ARID2
GO:0048880	sensory system development	-4.43041	-1.47992	JAG1,DLG1,FBN2,NF1,PITX2,PROX1,SOX11,TGFBR1,VEGFA,RAB18,SLC7A11,USP45
GO:0043010	camera-type eye development	-4.38263	-1.45073	JAG1,DLG1,FBN2,NF1,PITX2,PROX1,SOX11,TGFBR1,VEGFA,SLC7A11,USP45
GO:0003231	cardiac ventricle development	-4.30905	-1.4284	JAG1,MDM2,PROX1,SOX11,TGFBR1,LMO4,RBM15
GO:0001944	vasculature development	-4.2997	-1.4284	JAG1,RHOB,FGF2,MDM2,NF1,PDGFA,PIK3CA,PROX1,TGFBR1,VEGFA,FOSL1,QKI,RBM15,ARID2
GO:0001935	endothelial cell proliferation	-4.07784	-1.28085	DLG1,FGF2,NF1,TGFBR1
GO:0048514	blood vessel morphogenesis	-4.02903	-1.27254	JAG1,RHOB,FGF2,NF1,PDGFA,PIK3CA,PROX1,TGFBR1,VEGFA,QKI,RBM15,ARID2
GO:0060840	artery development	-3.9747	-1.25975	JAG1,NF1,PROX1,TGFBR1,VEGFA,ARID2
GO:0010631	epithelial cell migration	-3.95053	-1.25049	ARSB,FGF2,PIK3CA,PROX1,TGFBR1,VEGFA
GO:0061061	muscle structure development	-3.89592	-1.21955	JAG1,ZFHX3,CHD2,HNRNPU,IFRD1,NF1,PROX1,SOX11,TGFBR1,TTN,VEGFA,QKI,MKX

D **Day 1 upregulated SPS (analysis for VPA)**

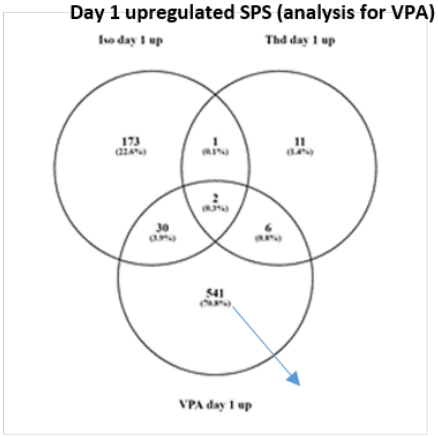

E **VPA upregulated GOs day 1**

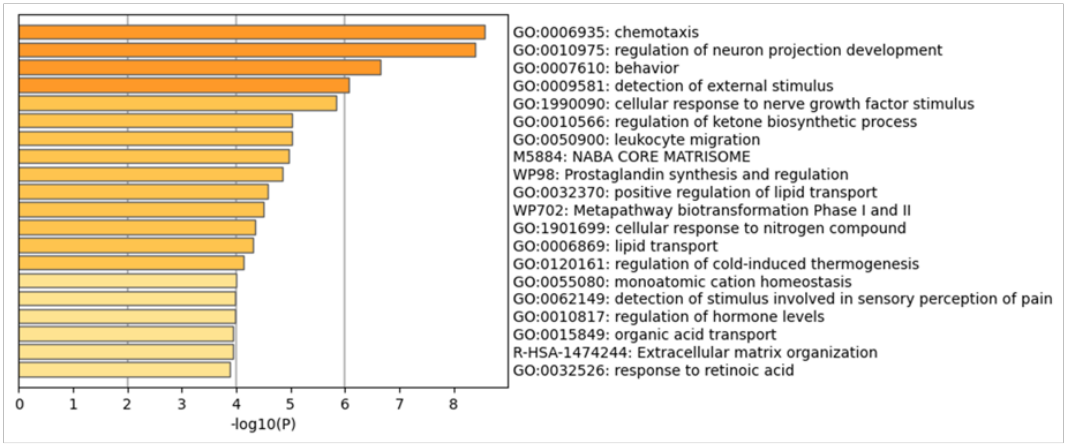

The significant VPA upregulated GOs and the corresponding genes are in supplementary xl sheet 1.

F **Day 4 downregulated SPS (analysis for THD)**

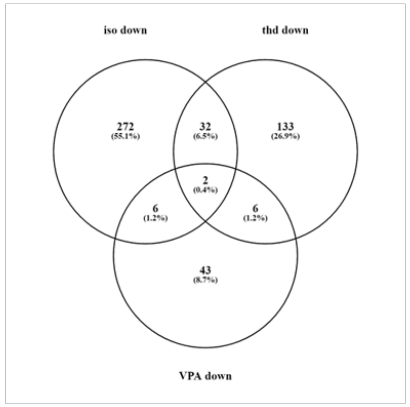

G **THD downregulated GOs day 4**

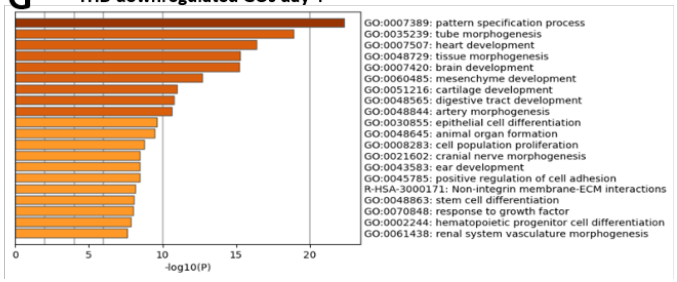

H **THD downregulated heart related GOs**

Term	Description	LogP	Log(q-value)	Symbols
GO:0007507	heart development	16.4092	-13.014	BMP4,BMP5,CDH11,COL2A1,COL3A1,COL11A1,EMP2,FOXF1,FN1,LRP2,MSX1,PDGFRA,PDGFRB,PKP2,PROX1,RARB,TNNI1,WNT5A,NRP1,ALDH1A2,MICAL2,DKK1,HEY1,RBM20
GO:0003007	heart morphogenesis	14.7373	-11.564	BMP4,BMP5,COL2A1,COL11A1,EMP2,FOXF1,LRP2,MSX1,PKP2,PROX1,TNNI1,WNT5A,NRP1,ALDH1A2,MICAL2,HEY1,RBM20
GO:0048738	cardiac muscle tissue development	12.9959	-9.947	BMP4,BMP5,COL11A1,LRP2,MSX1,PDGFRA,PDGFRB,PKP2,PROX1,RARB,TNNI1,WNT5A,ALDH1A2,HEY1
GO:0014706	striated muscle tissue development	12.8054	-9.778	BMP4,BMP5,COL11A1,LRP2,MSX1,PDGFRA,PDGFRB,PKP2,PROX1,RARB,TNNI1,WNT5A,ALDH1A2,HEY1
GO:0061061	muscle structure development	12.0559	-9.104	BMP4,COL3A1,COL11A1,FOXF1,LRP2,MSX1,PDGFRA,PDGFRB,PKP2,PROX1,RARB,NR2F2,TNNI1,WNT5A,DPF3,HEY1,SOX6,DISP1,TANC1
GO:0060537	muscle tissue development	11.7774	-8.843	BMP4,BMP5,COL3A1,COL11A1,LRP2,MSX1,PDGFRA,PDGFRB,PKP2,PROX1,RARB,NR2F2,TNNI1,WNT5A,ALDH1A2,HEY1
GO:0003206	cardiac chamber morphogenesis	11.0122	-8.094	BMP4,BMP5,COL11A1,FOXF1,LRP2,PKP2,PROX1,TNNI1,WNT5A,NRP1,HEY1
GO:0003205	cardiac chamber development	9.71107	-6.964	BMP4,BMP5,COL11A1,FOXF1,LRP2,PKP2,PROX1,TNNI1,WNT5A,NRP1,HEY1
GO:0003231	cardiac ventricle development	-8.3232	-5.752	BMP4,COL11A1,FOXF1,LRP2,PKP2,PROX1,TNNI1,WNT5A,HEY1
GO:0007517	muscle organ development	7.93389	-5.417	COL3A1,COL11A1,LRP2,MSX1,PKP2,PROX1,NR2F2,TNNI1,WNT5A,DPF3,SOX6,DISP1
GO:0003208	cardiac ventricle morphogenesis	7.56119	-5.109	COL11A1,FOXF1,LRP2,PKP2,PROX1,TNNI1,HEY1
GO:0060415	muscle tissue morphogenesis	7.47614	-5.053	COL3A1,COL11A1,LRP2,PKP2,PROX1,NR2F2,TNNI1,WNT5A
GO:0048644	muscle organ morphogenesis	-7.1972	-4.802	COL3A1,COL11A1,LRP2,PKP2,PROX1,TNNI1,WNT5A
GO:0055008	cardiac muscle tissue morphogenesis	6.58934	-4.269	COL11A1,LRP2,PKP2,PROX1,TNNI1,WNT5A
GO:0055010	ventricular cardiac muscle tissue morphogenesis	5.75451	-3.519	COL11A1,LRP2,PKP2,PROX1,TNNI1

I

Day 4 upregulated SPS (analysis for THD)

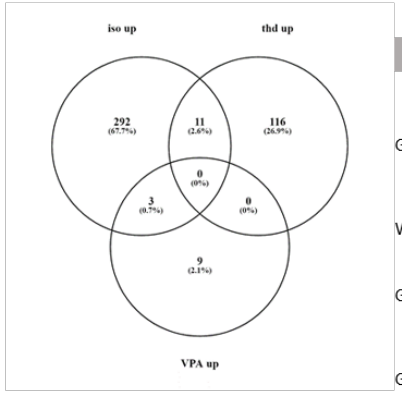

J

THD upregulated GOs day 4

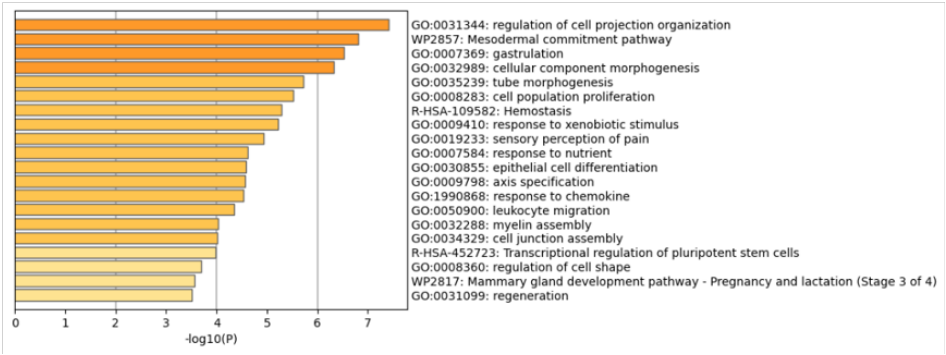

K

THD upregulated heart related GOs

Term	Description	LogP	Log(q-value)	Symbols
GO:0031344	regulation of cell projection organization	-7.41706	-3.068	KIF1A,KLF5,GAP43,GATA3,GPM6A,ITGA6,ITGA2,L1CAM,SFRP1,SFRP2,VIL1,FEZ1,TBR1,BCL11A,ARHGAP24,SIX3,ESRP1,IGFBP3,NPY1R,SOX17,FOXA2,FST,NMRK2
WP2857	Mesodermal commitment pathway	-6.8166	-2.834	KLF5,GATA3,FOXA2,FZD5,EOMES,FZD8,SOX17,NANOG,CD9,GNAS,HHEX,CXCL6,HDAC9,DOCK8,MEGF10,CCL2,ABCC4,SORCS1,PTPRZ1,SFRP1,SFRP2,TNFRSF11A,FST,ADM,FOXD3,POU5F1B,CNKSR2,BCL11A,ESRP1,ITGA2
GO:0007369	gastrulation	-6.52684	-2.779	FOXA2,ITGA2,OTX2,SFRP1,SFRP2,EOMES,SOX17,NANOG,ADM,GATA3,SIX3,FZD5,MAB21L2,GAP43,TBR1,HHEX,FST,NFIB
GO:0032989	cellular component morphogenesis	-6.3305	-2.759	CD9,GAP43,GATA3,GPM6A,L1CAM,MOBP,NFIB,OTX2,PTPRZ1,SH3GL2,UGT8,DCLK1,FEZ1,CXCL3,LOX,CCL2,CXCL6,TNFRSF11A,SOX17,ADM,EOMES
GO:0035239	tube morphogenesis	-5.7168	-2.53	ADM,KLF5,GATA3,LOX,NFIB,CCL2,SFRP1,SFRP2,FZD5,FZD8,SOX17,ARHGAP24,THSD7A,CD9,GAP43,GNAS,SH3GL2,DCLK1,TNFRSF11A,ITGA2,SIX3,EOMES,FST,FOXA2,HHEX,ESRP1,ITGA6,OTX2,PTPRZ1,GPM6A,PMAIP1,NPY1R,HDAC9,SHISA3,FOXD3,IGFBP3,APOA2,VIL1,USP44,BCL11A

Figure S11

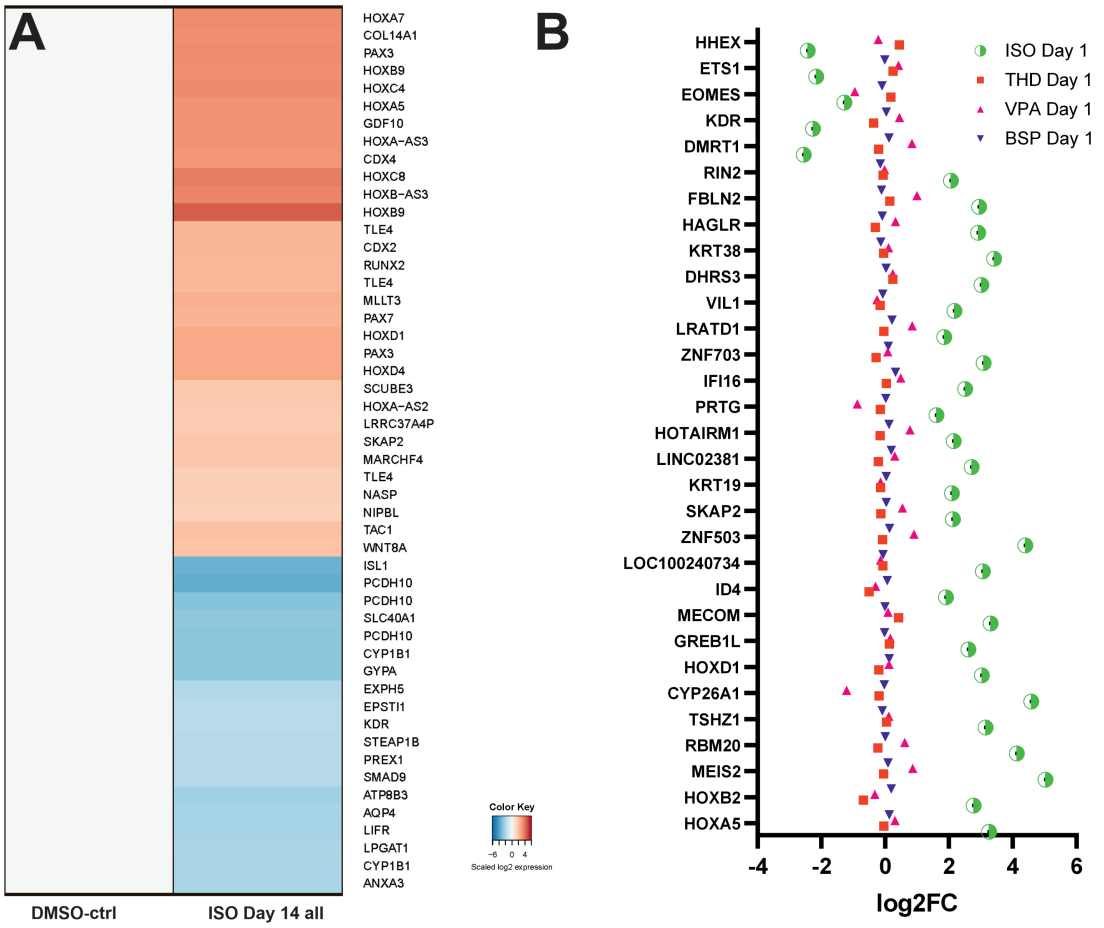

The heat map with the top 50 genes (Fig. S11A) de-regulated for SPS specific for ISO, sorted according to their p-values, on day14. The heat map colour code indicates the up (red) down-regulation (blue) of genes in comparison to control.B (Fig. S11B) The 31 common significantly deregulated genes from retinoids, in hiPSC-IMR90, on day1 among the test compounds (Iso, VPA, THD, BSP).

Figure S12

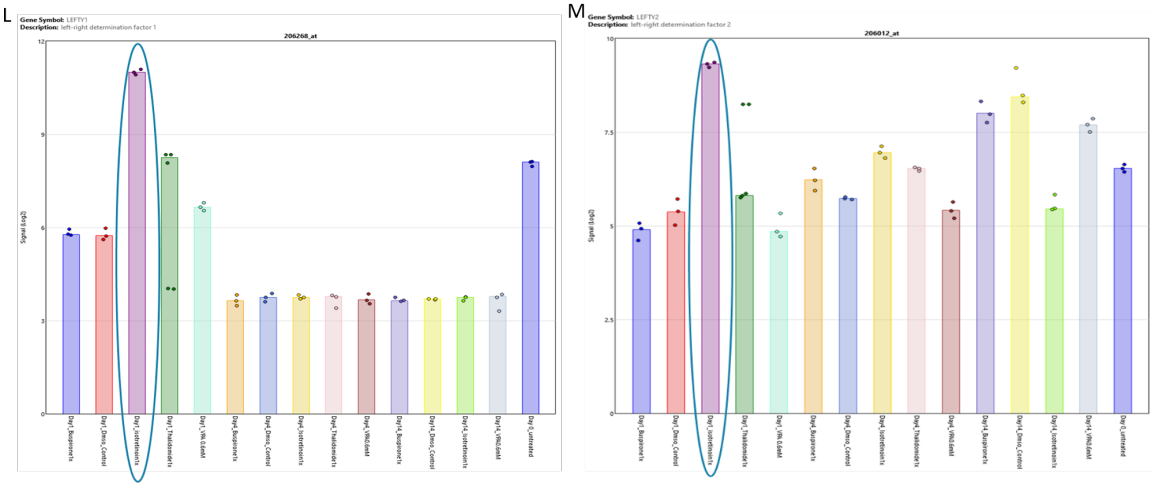

LEFTY 1 and LEFTY2 expression among all other probe sets. (Affymetrix value expression, Table is from TAC software)

6.2 Raw data

The microarray data is available in the Gene Expression Omnibus (GEO) (NCBI): GSE187001. The Supplementary Videos S1 and S2 can be found in digital files which were handed in along with this work.

6.3 List of figures

6.4 List of tables

6.5 Aknowledgements

I would like to express my deepest gratitude to Prof. Agapios Sachinidis for providing me with the exceptional opportunity to work under his supervision in the Neurophysiology department at Uniklinik of Cologne. Throughout this captivating project, Prof. Sachinidis entrusted me with his unwavering trust, and his guidance and remarkable expertise proved invaluable in navigating challenging situations and making crucial decisions. I am sincerely grateful for his mentorship, which has played a significant role in shaping me into a better scientist. I am also indebted to Professor Jan Hengstler for his outstanding guidance and supervision throughout the entirety of our project, as well as for offering the opportunity to collaborate with the Department of Toxicology at Ifado Dortmund.

I extend my sincere thanks to all the collaboration partners who were involved in this project. Prof. Marcel Leist, Dr. Nadine Dreser, and Dr. Tanja Waldman (former member) from the Department of In Vitro Toxicology and Biomedicine at the University of Konstanz, Dr. Florian Seidel from the Department of Toxicology at Ifado Dortmund (former member), Prof. Jörg Rahnenführer, Dr. Franziska Kappenberg, and Dr. Katrin Madjar (former member) from the Faculty of Statistics at the TU Dortmund, and Prof. Nils Blüthgen and Dr. Johannes Meisig from the Charité at the University of Berlin have all contributed significantly to the project's success. Our fruitful and enjoyable meetings and discussions exemplified the power of collaboration, ultimately leading us to achieve our objectives.

I would like to express my profound appreciation to all the members of the Neurophysiology department at Uniklinik of Cologne. You have all been exceptional colleagues, always ready to lend a helping hand, and spending time with you has been an absolute joy. I am especially grateful to Dr. Sureshkumar Perumal Srinivasan for his cheerful disposition, excellent communication skills, and consistent support as an office colleague. I am indebted to my brilliant friends and colleagues who have inspired me throughout the years. I extend my thanks to Dr. Harshal Nemade and Dr. Aviseka Acharya for their valuable discussions, insightful suggestions, and the ever-inspiring work environment. I would also like to acknowledge the assistance of Ms. Margit Henry, Mrs. Tamara Rotshteyn, and Mrs. Susan Rohani in the lab, as well as our dedicated secretaries, Mrs. Elke Lieske, Mrs. Suzan Wood, and Mrs. Aja Lens from CCB of TU Dortmund, for their invaluable support in material ordering, official documentation, and organization.

Finally, I am incredibly grateful to my family and friends who have been a constant source of support and understanding throughout the entirety of this project. Their unwavering belief in my abilities, encouragement during moments of self-doubt, and understanding of the sacrifices I had to make have been invaluable. Their love, patience, and unwavering support have provided me with the strength and motivation to persevere through the challenges and reach the culmination of this research journey. I am truly fortunate to have such remarkable individuals in my life, and I dedicate the successful completion of this thesis to them.